J.C. Walraven

AGGREGATE INTERLOCK:
A theoretical and experimental analysis

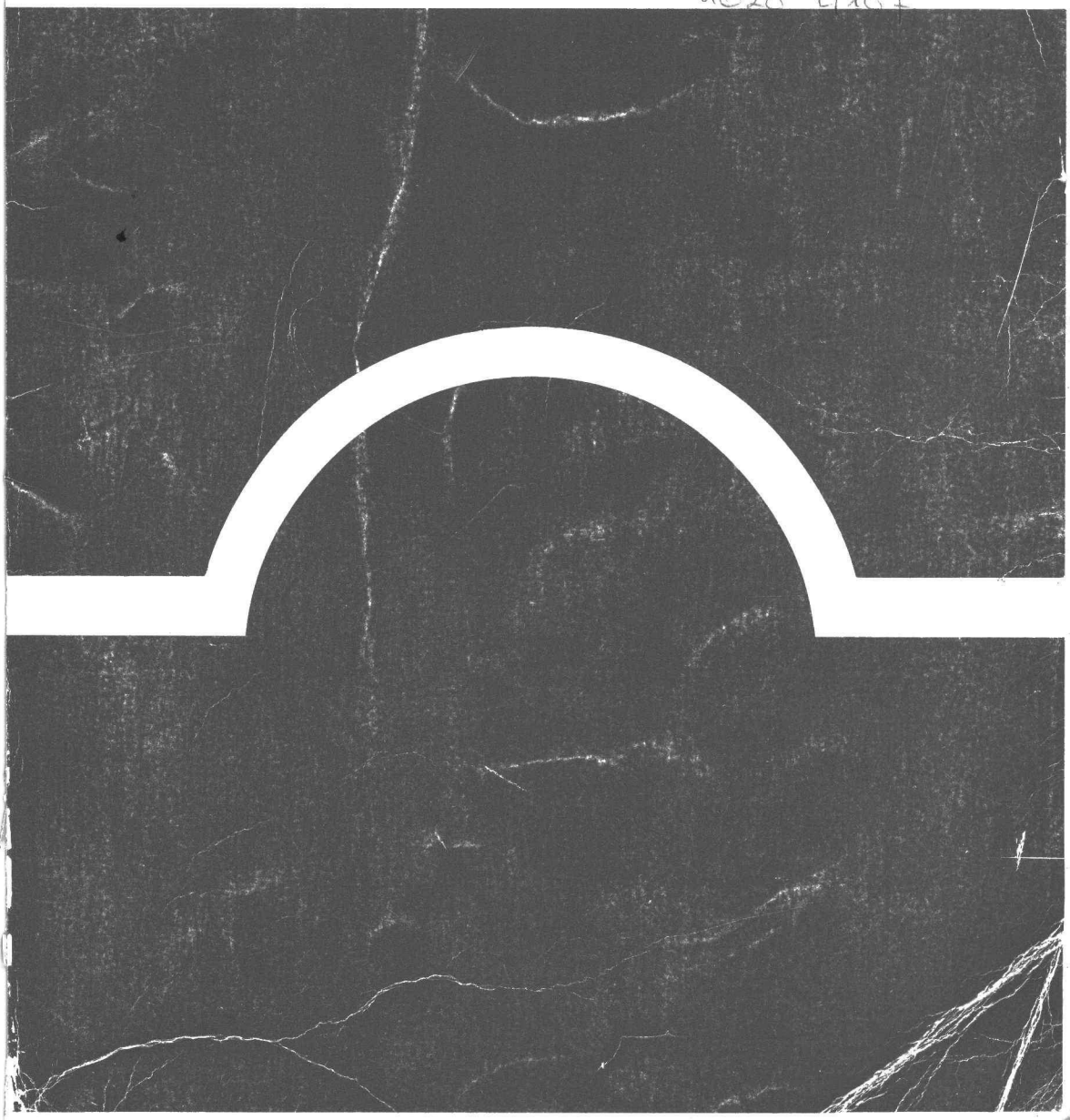

AGGREGATE INTERLOCK:
A theoretical and experimental analysis

AGGREGATE INTERLOCK:
A theoretical and experimental analysis

PROEFSCHRIFT ter verkrijging van
de graad van doctor in de
technische wetenschappen
aan de Technische Hogeschool Delft,
op gezag van de rector magnificus,
voor een commissie aangewezen
door het college van dekanen
te verdedigen op
woensdag 8 oktober 1980
te 16.00 uur door
JOOST CORNELIS WALRAVEN
civiel ingenieur
geboren te Breda

Delft University Press / 1980

Dit proefschrift is goedgekeurd door
de promotor: PROF.DR.IR. A.S.G. BRUGGELING

ACKNOWLEDGEMENT

The author wishes to record his thanks to all the members of the "Concrete Structures Group" of the Stevin Laboratory who have contributed to this research project, in particular Ir. E. Vos, who carried out the experimental part of the program, and Prof.Dr.-Ing. H.W. Reinhardt, for the discussions on the subject and his indications.

Furthermore the author is greatly indebted to the CUR, the Netherlands Committee for Concrete Research, for their financial support and encouragement.

The financial support of the "Stichting Professor Bakkerfonds" for this publication is greatly appreciated.

CONTENTS

1	INTRODUCTION	1
1.1	Motives and scope of the research	1
1.2	Some aspects of the role of the roughness of the cracks in concrete structures	3
1.3	The formulation of crack characteristics in existing numerical programs	11
1.4	Aim of the research program	17
2	STATE OF THE ART	19
2.1	Aggregate interlock	19
2.2	Dowel action	27
2.3	Axial restraint stiffness of the reinforcing steel	44
2.4	Interaction of components in cracks, crossed by reinforcement	49
2.5	Conclusions	52
3	A FUNDAMENTAL THEORY FOR AGGREGATE INTERLOCK	54
3.1	Basic assumptions	54
3.2	General considerations on the basic variables	60
3.3	Determination of the relation between the projected contact areas A_x and A_y for a unit crack area on the one hand and the displacements between the crack faces on the other hand	65
4	EXPERIMENTS	90
4.1	General	90
4.2	Pure aggregate interlock tests	90
4.2.1	Test specimens, instrumentation and testing procedures	90
4.2.2	Variables	92
4.2.3	Results	93
4.3	Tests on reinforced cracks	95
4.3.1	Specimens, instrumentation and testing procedures	95
4.3.2	Variables	97
4.3.3.	Results	99

5	INTERPRETATIONS AND FURTHER ANALYSIS	110
5.1	Aggregate interlock	110
5.1.1	Comparison of theory and results	110
5.1.2	Analysis of some aspects of aggregate interlock on the basis of the model developed	114
5.2	Transmission of forces across reinforced cracks	132
5.2.1	Components involved in the transmission of forces	132
5.2.2	Comparison between reinforced and unreinforced cracks	136
5.2.3	Quantitative analysis of the behaviour of reinforced cracks	143
5.2.4	Specimens with reinforcing bars inclined to the crack plane	151
5.2.5	Hypothesis for the behaviour of reinforced cracks subjected to general combinations of external loads or imposed displacements	155
6	A MATHEMATICAL FORMULATION OF THE RELATION BETWEEN STRESSES AND DEFORMATIONS OF CRACKED REINFORCED CONCRETE, TAKING INTO ACCOUNT THE CRACK PROPERTIES	159
6.1	The stress-displacement relation for a single crack	159
6.2	The relation between stresses and displacements in cracked reinforced concrete	162
7	RETROSPECTIVE VIEW	168
8	SUMMARY	171
9	REFERENCES	177
10	NOTATION	188
11	APPENDICES	191

1 INTRODUCTION

1.1 Motives and scope of the research

A fundamental demand in the design of structures is that sufficient safety against failure is obtained. With regard to concrete structures it can be stated that numerous experiments have been carried out in order to enable the ultimate resistance of many types of structural members under various loading configurations to be estimated. However, while it is true that at present many equations are available for predicting bearing capacities in adequate agreement with available test results, it cannot be claimed that the theories always truly explain the calculated strengths. Lack of fundamental knowledge in several respects means that it is often impossible to be confident in extending existing equations to structures with a more complex behaviour.
Particularly in the last decade an increase in scale and complexity of new structures has occurred. Problems encountered in the design of offshore structures subject to wind, waves, drifting ice and collisions with other floating objects go far beyond the level of the actually available experimental knowledge. The same can be said of the construction of reactor vessels, requiring a high degree of safety against any possible damage caused by earthquake motions or flying objects. Also sea resisting structures, such as the surge tide barrier in the Eastern Scheldt (Oosterschelde) in the Netherlands, which has to protect thousands of people from another flood disaster, confront the designer with problems which he cannot solve by simply consulting the literature. Small-scale tests on such structures could provide a better insight into these situations, but often the incomplete knowledge about scale laws, particularly for concrete structures, leads to new incertainties. There is evidently a need for improved methods of analysis.

Fortunately, also in the field of calculation techniques new perspectives were opened by the development of the computer. The introduction of the finite element method, by means of which the behav-

iour of complicated structural systems could be analysed, although initially only on the assumption of linear elastic material properties, was an important step forward. However, for concrete structures, which exhibit a strongly non-linear character due to the formation of cracks and plastification of materials, more sophisticated programs had to be developed, involving the possibility of redistribution of forces. Therefore not only the numerical programs had to be improved, but also close attention had to be paid to accurate formulation of the properties of the constituent materials. To give added impetus to further development in this direction, the research project "Concrete Mechanics" was started. It was expected that the best results would be obtained by a collaboration of investigators in the fields of computer analysis and material research. Participating in the project were on the one hand the Rijkswaterstaat, a division of the Netherlands Ministry of Transport and Public Works, concentrating on the numerical part of the research program, and on the other hand the Technological Universities of Delft and Eindhoven and the Institute for Applied Scientific Research on Building Materials and Building Structures (IBBC-TNO), focusing on the material aspects. The overall project "Concrete Mechanics" was financially supported and organized by the CUR, the research committee in the Netherlands Concrete Association. A survey of the structure of the project is presented in Fig. 1.1.

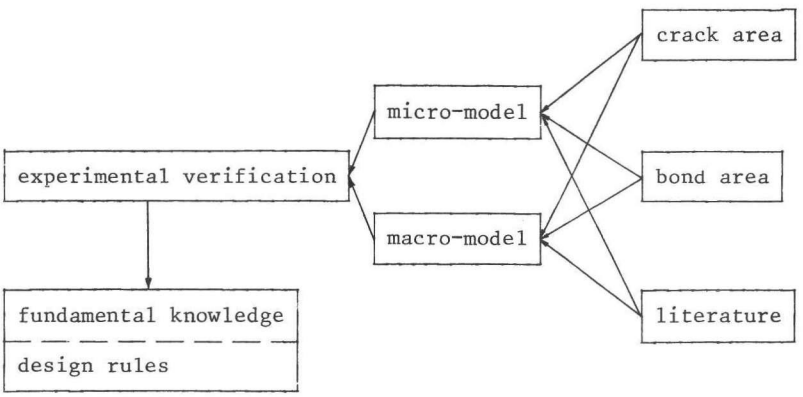

Fig. 1.1 Structure of the organization of the project "Concrete Mechanics"

The numerical part of the project has meanwhile resulted in two non-linear finite element programs, the micro and the macro-model. The micro-model is able to describe the formation of discrete cracks in a concrete structure. In this way the displacements at a crack can be determined and the effect of these displacements on the internal stresses can be taken into account. Since this model can make a dominant crack distinctly discernible, it is especially suitable for the analysis of complex structures and reinforcing details (Grootenboer [27]). The other model, the macro-model, is based on a different concept. To calculate the behaviour under loading a structure is divided into imaginary layers of concrete and steel, having different properties. The effect of cracking is taken into account by modifying the stiffness characteristics of a layer. The cracks are as such "smeared out" (Blaauwendraad et al. [6]). Both programs enable non-linear material properties to be inserted in an appropriate way.

The material research was subdivided into three parts: a study of the mechanisms directly related to the crack area, an analysis of the bond area and a study of literature to provide remaining characteristics, such as the behaviour of concrete under biaxial loading.

The part of the project reported in this document is concerned with the study of the crack area and was carried out at the Delft University of Technology. An adequate understanding and formulation of the transmission of forces across cracks in concrete is necessary to take full advantage of the possibility, included in the numerical programs, to describe redistributions of forces.

1.2 Some aspects of the role of the roughness of the cracks in concrete structures

Prior to discussing some examples illustrating the role of the roughness of the cracks, it may be useful to point out two important features inherent in the behaviour of cracks in reinforced and prestressed concrete.

a. Although cracks are generally formed perpendicularly to the

direction of the local principal tensile stresses in the concrete in the uncracked loading stage, they do not necessarily also open perpendicularly to their direction. This is mainly caused by the fact that the stress-strain relations of cracked reinforced or prestressed concrete differ essentially from those in the uncracked stage. Whereas in the uncracked stage the influence of the reinforcement on the stress-strain relations is small and the behaviour is not far from being isotropic (De Josselin de Jong [33] and Walraven [80]), in the cracked state generally an anisotropic type of behaviour is developed, resulting in shear stresses parallel to the cracks. In an earlier publication [81] this subject was discussed. Apart from this argument, it must also be noted that in non-prestressed concrete shrinkage and temperature stresses as well as previous loads may produce a crack of any direction, existing before the ultimate load is introduced. The existence of cracks in other directions than would directly result from the loads in the ultimate loading state itself, is sometimes even a necessary assumption for design: an example of this is that current design criteria in the United States for conventionally reinforced nuclear containment vessels [1] require that the structure be designed to withstand the simultaneous occurrence of internal pressure and the inertia forces generated by a strong motion earthquake. Crack planes form in the concrete wall in the horizontal and vertical directions (Fig. 1.2) due to internal pressure. The cyclic shearing forces due to a seismic excitation must then be transmitted along these planes (Laible et al. [40]).

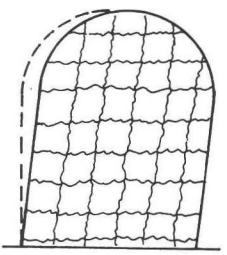

Fig. 1.2 Cracking of a vessel under internal pressure and seismic loading [40]

b. As a result of its rough structure the cracks can transmit forces in the normal and the parallel direction if the crack faces are shifted in opposite directions. Three mechanisms can contribute to this transmission:

- Aggregate interlock: this mechanism is directly related to the way in which a crack is formed in concrete. Because the strength of the hardened cement paste in most concretes is lower than the strength of the aggregate particles, cracks intersect the cement paste but run along the edges of the aggregate particles. So the aggregate particles, extending from one of the crack faces, "interlock" with the opposite face and resist shear displacements (Fig. 1.3.a).
- Dowel action: this term denotes the resistance of a reinforcing bar, crossing a crack, to shear displacement (Fig. 1.3.b). It is generally assumed that dowel action is inferior to aggregate interlock for the reinforcement ratios which are used in practice.
- Axial forces in reinforcing bars inclined to the crack plane (Fig. 1.3.c).

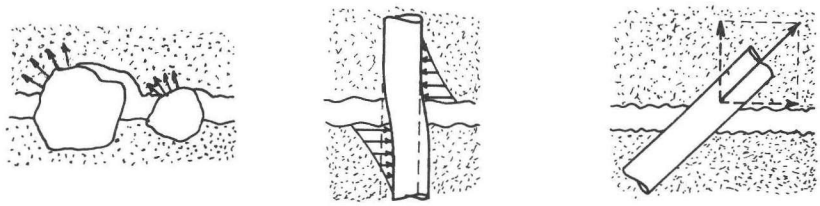

a b c

Fig. 1.3 Aggregate interlock (a), dowel action (b) and axial steel force (c)

In the following some examples are given, illustrating the role of the transmission of forces in cracks and emphasizing the need to have a better understanding of this phenomenon.

Fig. 1.4 shows the cracking pattern of a beam without shear reinforcement, subjected to a 4-point loading test, at about 80% of the ultimate load [82].

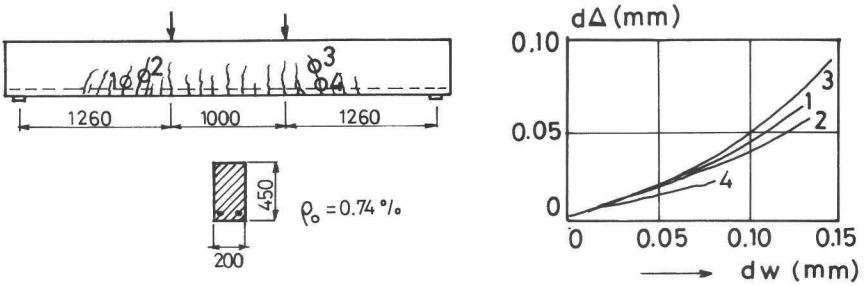

Fig. 1.4 Measurements on cracks in a beam without shear reinforcement [82]

During this test some strain gauge rosettes were stuck on the cracks, immediately after observation (at a crack width of w = 0.10 - 0.15 mm), so that the displacements could be measured. It is seen that an increasing amount of shear displacement was recorded, so that shear forces can be expected to be transmitted across the cracks (see also Fig. 1.3.a). Estimates of the contribution of aggregate interlock in the cracks on the basis of experiments conducted on single cracks (see section 2.1), varied between 40 and 90% (Taylor [75], Fenwick [18], Swamy [73]).
The research project from which the results presented in Fig. 1.4 were borrowed, refuted a persistent misunderstanding about aggregate interlock. A study of the phenomenon that the shear resistance of such types of beam does not increase linearly with the scale of the beam, but less, was undertaken. This was generally believed to be due to the fact that in experiments the size of the aggregate particles was the only variable that was not scaled properly, which would lead to differences in aggregate interlock. In the investigation a series of differently scaled beams, made of gravel concrete, was compared with an identical series, made of lightweight concrete. In spite of the fact that lightweight concrete can only

supply a very reduced aggregate interlock component, as a result of the low strength of the lightweight aggregate particles permitting the crack to run both through the hardened cement paste and the particles (Fig. 1.5), the sensitivity to the increase of the scale did not differ from that obtained for gravel concrete. Only the shear resistance was lower over the full range of tests. It was demonstrated that not aggregate interlock, but the influence of the strain gradient on the flexural tensile strength of the concrete, is responsible for the scale effect. This may illustrate that caution is necessary in testing structures on model scale if no full understanding of aggregate interlock is available.

Fig. 1.5 Aggregate interlock in gravel concrete (intermediate or low strength) and lightweight concrete

The capability of aggregate interlock to transmit shear forces was even more clearly demonstrated in an investigation into the influence of axial tensile forces on the shear resistance of symmetrically reinforced beams without shear reinforcement (Regan [61]). Prior to shear loading, the beams were subjected to axial tensile loads, producing cracks perpendicular to the beam axis. These tensile loads were kept constant during loading, at values between 0 and 130 kN. The loading arrangement is presented in Fig. 1.6.

The influence of axial loading on the shear strength was found to be very small. In all beams failure was caused by the formation of a single well-defined crack, with an inclination notably flatter than that of any earlier cracks.

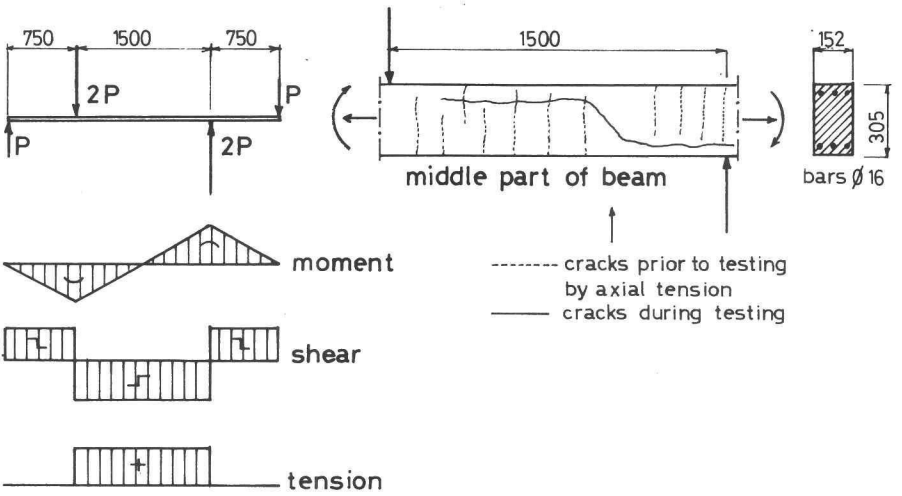

Fig. 1.6 Beam subjected to combined shear and axial loading [61]

It was apparent from the behaviour of beams containing vertical cracks over their whole depth that shear was being transmitted by aggregate interlock and dowel action, especially as such cracks near points of contraflexure were never even partially closed by the formation of compression zones due to bending. A special beam was tested to investigate the possible significance of dowel action. This beam had a smooth-sided crack preformed in it at the section of contraflexure. The crack was formed by a sheet of acetate paper. The beam failed at a very low load with the formation of dowel cracks at the levels of the top and bottom reinforcement.

High reliability is further imposed on the capacity of cracks to transmit shear forces in the application of theories based on the principle of plastic behaviour. In these theories it is assumed that shear displacements of the crack faces are completely prevented by aggregate interlock, implying that the cracks can open only in the perpendicular direction. With regard to beams with shear reinforcement, it is assumed that there is an upper and a lower stringer, which are both infinitely stiff in the axial direction and have no flexural stiffness at all: as a result the flexural moment is fully resisted by these stringers and the shear

force is fully carried by the web of the beam. Due to these conditions shear stresses are provoked in the cracks, resulting in compression diagonals with a flatter inclination than the cracks themselves. The "plastic truss" leads to a more economical design of the shear reinforcement than the original Mörsch truss (Fig. 1.7), which has compression diagonals, by definition inclined at 45 degrees to the beam axis, and which is generally known to overestimate the forces in the shear reinforcement considerably.

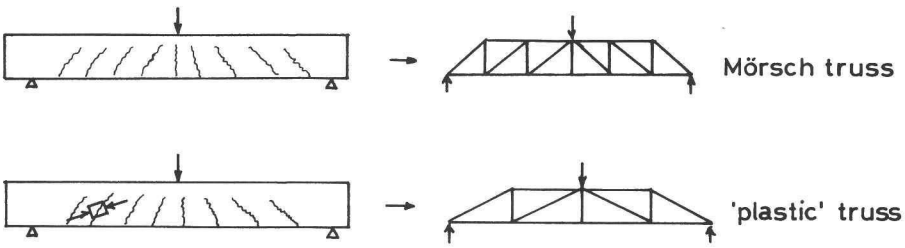

Fig. 1.7 Mörsch truss analogy and plastic truss analogy

However, to get good agreement between the prediction of the plastic theory and the results of experiments, mostly correction coefficients are necessary, which are not the same for all cases of loading and cannot be physically explained in a satisfactory way. To obtain a better idea of the merits and limitations of the plastic theory and the way in which improvements could be achieved, it is necessary to have a better understanding of the most fundamental assumption of the theory: the full prevention of shear displacements in cracks by aggregate interlock. Fig. 1.8 shows some measurements of the opening direction of cracks in a partially prestressed beam, tested in an earlier investigation (Bruggeling et al. [8]). It is seen that the assumption of fully prevented shear displacement does not hold true. However, it is felt that the occurrence of shear displacements is a better argument for the presence of shear stresses in the cracks than an observation of perpendicular

crack opening would be (see also Fig. 1.3.a).

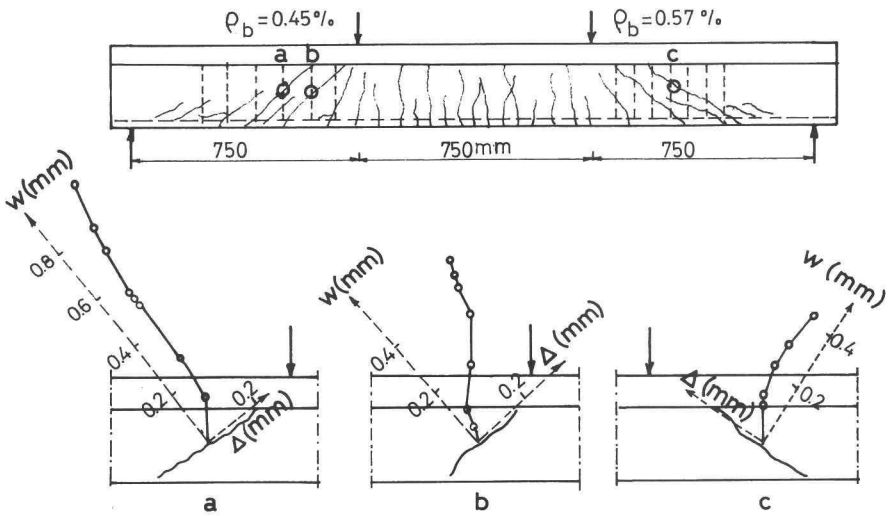

Fig. 1.8 Measurements on cracks in a partially prestressed beam without shear reinforcement [8].

The last example is concerned with the generally underestimated role that aggregate interlock plays in the design of mesh reinforcing systems, which is a fundamental problem for concrete shells, shear walls, box girders and vessels, prestressed as well as unprestressed, and has been studied intensively ([2, 7, 39, 41]). Generally, the role of aggregate interlock has been disregarded, arguing that the friction is highly variable and, to be on the safe side, should be neglected. Recently Bažant [4] pointed out, that this argument is false. The reason is that during subsequent tangential displacement the wedging effect of surface asperities in contact causes further relative normal displacements, which is manifested by an overall volume increase due to shear (dilatancy) (Fig. 1.9).

Due to this dilatancy the reinforcement crossing the crack is tensioned. If this effect is not taken into account, it may happen that tensile yielding of the reinforcement occurs before the applied load component normal to the crack alone is great enough for

achieving it. Furthermore it may occur that the crack width in the serviceability state is greater than expected (Fig. 1.9), which would be rather undesirable in, for instance, bridges or nuclear structures. Consequently, taking aggregate interlock into account generally leads to heavier rather than lighter reinforcement and thus a neglect of this mechanism is seen to be generally on the unsafe side.

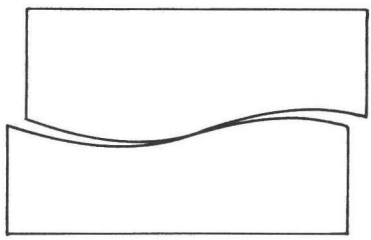

Fig. 1.9 Shear dilatancy in cracks

1.3 The formulation of crack characteristics in existing numerical programs

Earlier numerical programs display a great variety of properties, attributed to the cracks.
Ngo/Scordelis [54], Nilson [55] and Stauder [71] introduced cracks in their non-linear finite element programs by disconnecting the nodes between the elements. In this way discrete cracks were obtained, each side of which was considered to be an independent external boundary, unable to transmit shear stresses (Fig. 1.10). The disadvantage of this method is that the crack directions are restricted to the direction of the element edges. Another, more generally applied method, which is not subject to this restriction, is to "smear out" the effect of cracking over the elements: it is then assumed that, if the tensile strength of the concrete in an element is reached, an infinite number of identical cracks with the same direction is formed (Fig. 1.11).

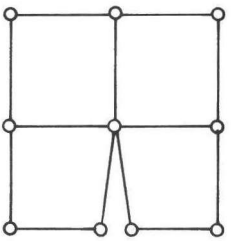

Fig. 1.10 Crack representation by means of disconnecting nodes [54, 55, 71]

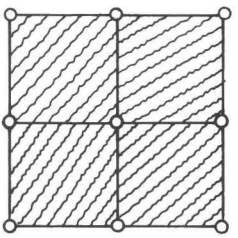

Fig. 1.11 Crack representation by means of smeared-out crack fields

The cracked elements are considered as continua with an anisotropic behaviour. The assumption that these cracks behave as smooth surfaces, unable to transmit shear stresses, was made by Cervenka [13] and Loov [46]. Inherent in this assumption is that the principal stress directions after cracking are fixed in, and perpendicular to, the direction of the cracks: as a result a redistribution of forces after cracking was impossible. The shear stiffness modulus, denoted by G in the uncracked state, was reduced to zero immediately after cracking (Fig. 1.12).

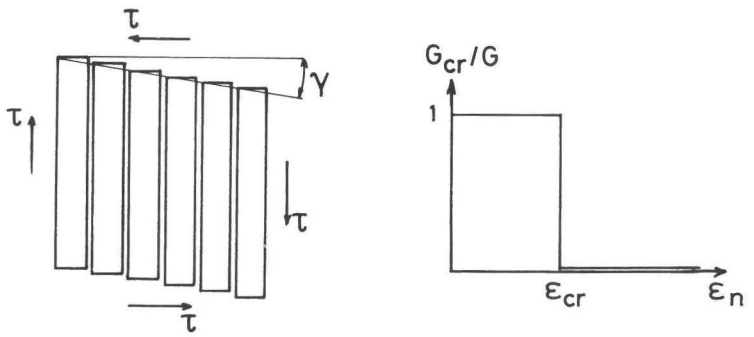

Fig. 1.12 Shear modulus of cracked concrete according to [13, 46]

Maintainance of the full shear resistance after cracking was supposed in the non-linear finite element programs developed by

Franklin [21], Isenberg/Adham [31], Zienkiewics/Phillips/Owen [92], Swoboda [74] and Müller [52] (Fig. 1.13). As was mentioned already in section 1.2, this assumption was also used in the analytical methods based on the theory of plasticity (Braestrup/Nielsen [5], Thürlimann [78], CEB-Model Code [10]).

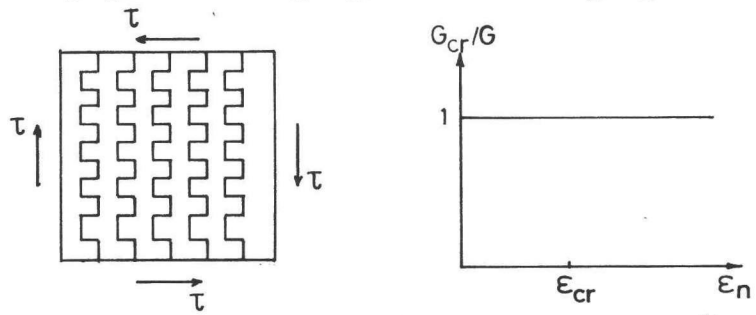

Fig. 1.13 Shear modulus of cracked concrete according to [5, 10, 31, 52, 53, 74, 78, 92]

Also Ebbinghaus [15] took a fully maintained G-value after cracking into account, but added the condition that this value is reduced to zero, if the shear stress in the cracks exceeds a certain limit. This limit was defined to decrease for increasing strain normal to the crack direction (or, formulated differently, for increasing crack widths) (Fig. 1.14).

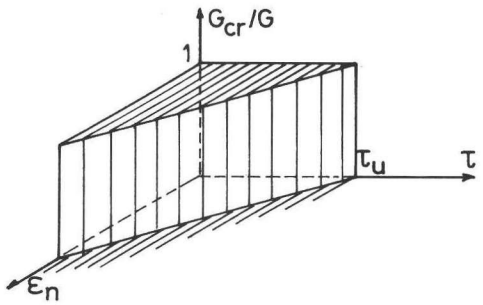

Fig. 1.14 Shear modulus of cracked concrete according to [15]

A formulation which is still generally used, implies that the shear stiffness of an element after cracking is reduced to a lower value,

but remains greater than zero, according to the equation:

$$\tau = \alpha.G.\gamma$$

in which α is a predetermined constant, with $0 < \alpha < 1$ (Fig. 1.15).

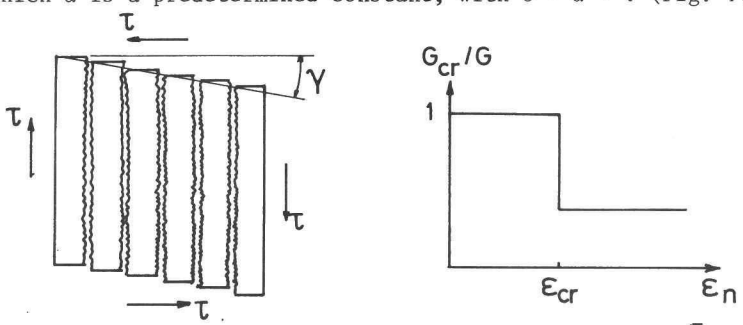

Fig. 1.15 Shear modulus of cracked concrete according to [11, 28, 37, 43, 72, 91]

This type of formulation was used by Hand/Pecknold/Schnobrich [28] ($\alpha = 0.4$), Yuzugullu/Schnobrich [91] ($\alpha = 0.2$), Suidan/Schnobrich [72] ($\alpha = 0.5$), Lin/Scordelis [43], Cedolin/Dei Poli [11] and Krisnamoorthy/Paneerselvam [37]. In a later publication Cedolin and Dei Poli improved this formulation, relating α to the strain normal to the direction of the cracks (Fig. 1.16) [12].

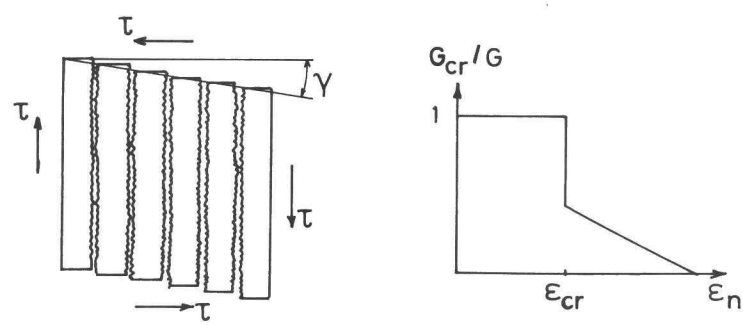

Fig. 1.16 Shear modulus of cracked concrete according to [12]

The suggested expression for G was:

$$G_{cr}/G = C\ (1 - \frac{\varepsilon_n}{\varepsilon_p}) \qquad \text{if } \varepsilon_{cr} < \varepsilon_n < \varepsilon_p$$

$$G_{cr}/G = 0 \qquad \text{if } \varepsilon_n > \varepsilon_p$$

in which C is a numerical constant (suggested value 0.1 E_c), ε_n is the fictitious strain (the contribution of the concrete to the strain was neglected) in the direction normal to the crack and ε_p is a limit value beyond which no shear transmission across the cracks is supposed to be possible ($0.0035 < \varepsilon_p < 0.0045$). Schimmelpfennig [67] used a reduction factor α which was defined to decrease as a function of increasing strain normal to the crack direction, but was also related to the level of the shear stress in the cracks (Fig. 1.17).

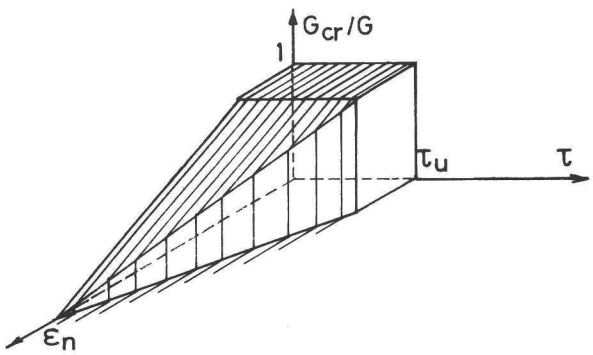

Fig. 1.17 Shear modulus of cracked concrete according to [67]

However, although relating the value α to the development of the strain normal to the cracks results in an improved expression for α, this formulation, too, has to be regarded as rather provisional, since it is obvious that other factors may influence the shear stiffness as well, such as the distribution of crack widths and distances, the concrete quality, the value of the shear displacement and the load history. These aspects were taken into account by Schäfer [65], who assumed that the initial resistance of two

crack faces against shear displacement can by neglected over a certain distance, while after this "free sliding range" a linear relation between shear stress and shear displacement can be assumed (Fig. 1.18). The length of the free sliding range was theoretically derived, while the linear relation was subsequently based on test results ([30], see also section 2.2). In combination with formulas for the average crack width and distance, a relation was derived which related α both to the strain normal to the crack direction and to the shear deformation (Fig. 1.19).

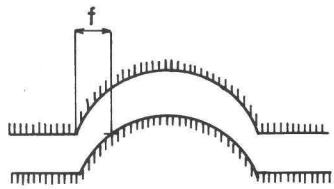

Fig. 1.18 Free sliding range according to [65]

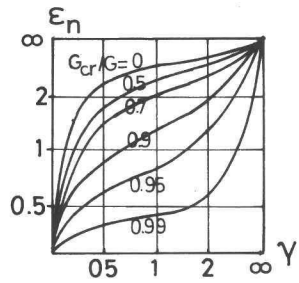

Fig. 1.19 Shear modulus of cracked concrete, according to [65]

Geistefeld [24] dealt, in his two-dimensional tension stiffening model, with the shear stiffness in a similar way, but did not take into account the free sliding range.

It is obvious that the formulation of characteristics representing the transfer of stresses across cracks is generally rather provisional. A great number of variables which may reasonably be expected to influence the behaviour is not taken into account. In none of the programs was the possibility of shear dilatancy due to wedging action of the cracks implemented. Since up to now the numerical programs have predominantly been used to investigate relatively uncomplicated structures subjected to simple loading conditions in which shear generally played a subordinate role, the rele-

vance of transfer of stresses in cracks has only partially been recognized. Only in [12], in which beams without shear reinforcement subjected to shear forces were numerically investigated, it was pointed out that there was a strict relationship between the inserted characteristics regarding aggregate interlock and the results of the calculations. Since calculation programs are bound to be applied to structures and loading types of greater complexity, a good formulation of these material properties is also becoming more important.

1.4 Aim of the research program

The aim of the research program is to establish the relation between stresses and displacements between crack faces. In the first instance the behaviour under monotonic increased loading will be studied. In the previous part it has already been pointed out that the relation which is generally employed up to now and which is represented by

$$d\tau = C_{tt} . d\Delta \tag{1.1}$$

is not the basic equation describing the transfer of stresses across cracks, but that this relation has to be represented by (see also Fig. 1.20)

$$\begin{Bmatrix} d\sigma \\ d\tau \end{Bmatrix} = \begin{bmatrix} C_{nn} & C_{nt} \\ C_{tn} & C_{tt} \end{bmatrix} \begin{Bmatrix} dw \\ d\Delta \end{Bmatrix} \tag{1.2}$$

The coefficients C_{nn}, C_{nt}, C_{tn} and C_{tt} depend on the interaction between the mechanisms of aggreate interlock, dowel action and axial restraint forces in the reinforcing steel. Firstly, it has to be assessed how these individual components are influenced by technological factors. Secondly, it has to be established how the interactions between the components are achieved.

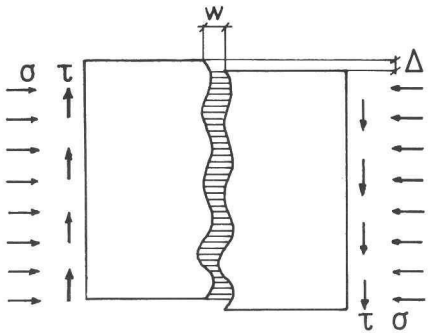

Fig. 1.20 Stresses and displacements in a crack

It is important that not merely empirical relations for the coefficients of equation (1.2) are provided, but also that an insight into the fundamental behaviour of the mechanism is obtained. This would not only give information over a wider range of values than covered by the experimental results alone, but would also give some idea of the behaviour under other types of loading (cyclic loading or long-term constant loading). In extending the investigation, at a later stage, to the effect of such types of loading conditions, a fundamental insight could contribute considerably to an efficient design of new test series. It will be investigated what information is already available in the literature and where new research is necessary.

2 STATE OF THE ART

The mechanisms involved in the transmission of forces across cracks are, as mentioned before, aggregate interlock, dowel action and axial restraint stiffness of reinforcing bars (see also Fig. 1.3). These components will first be dealt with separately. Then the available information on the interaction of these components in cracks crossed by reinforcement is reviewed. Topics are discussed only as far as they supply information which is directly concerned with the subject to be studied. An extended review of the whole field of available information, focusing also on cyclic and impact loading, was published earlier (Walraven [83]).

2.1 Aggregate interlock

In order to avoid confusion when talking about crack width, it is emphasized, before dealing with the phenomenon of aggregate interlock, that the crack width is defined as the displacement that the crack faces have undergone in the normal direction in relation to each other. This definition is necessary because on the micro scale the local crack widths vary considerably when a shear displacement has occurred (Fig. 2.1). As defined here, the crack width is independent of the shear displacement.

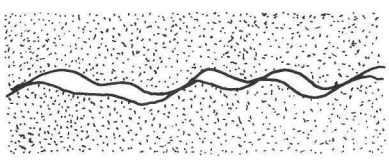

Fig. 2.1 Local variation of "crack width" on the micro scale

Fenwick [18] conducted tests on specimens as represented in Fig. 2.2. The specimens were cracked prior to testing by an external tensile force. The crack plane was predetermined by a groove along the outline of the specimen. After cracking, the crack width

was kept constant at values ranging from 0.06 to 0.38 mm. To obtain a constant crack width during a test, after every load increment the crack width was adjusted by means of an external force, normal to the crack plane. Values for this force were not given. All the specimens failed as a result of flexural tensile cracking at an early stage of loading (Fig. 2.2.a).

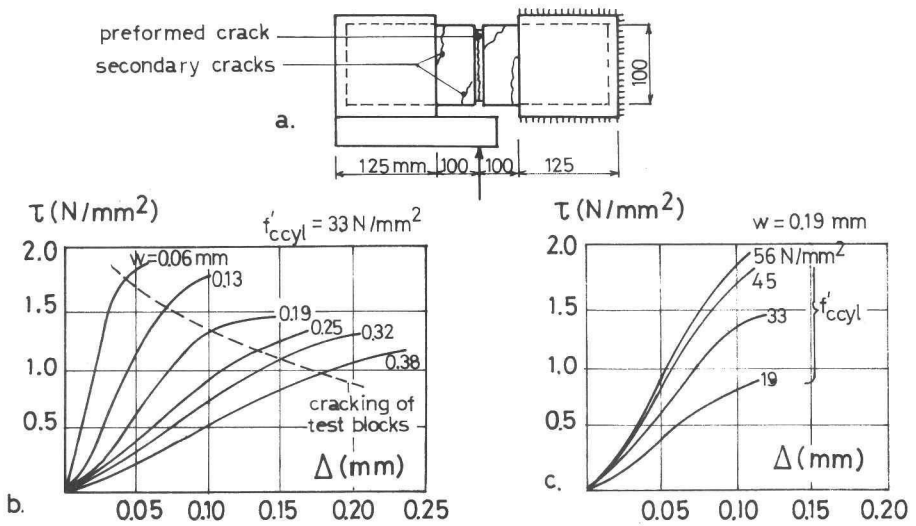

Fig. 2.2 Test equipment and results of Fenwick/Paulay [18]

Fig. 2.2.b shows the development of the shear stress acting on the crack plane as a function of the shear displacement for various constant crack widths, the concrete strength being constant. Fig, 2.2.c shows the influence of the concrete strength on this relation for a constant crack width: before tensile cracking the crack stiffness with regard to shear loading appeared to be an increasing function of the concrete strength.

Figures like 2.2.b and 2.2.c represent average shear stresses. It must be realized that the shear stresses are generally not uniformly distributed, but vary along the length of the crack plane. This variation is a function of the geometry of the specimens (as demon-

strated by Schwing [69]) and of the method of introducing the loads. This effect has always to be taken into account when interpreting test results.
An investigation, based on the same testing concept as used in [18], was carried out by Houde and Mirza [30]. The results of this investigation did not differ very much from those obtained in [18].
Paulay and Loeber [60] conducted other constant crack width tests, using a different test set-up and larger specimens, in order to avoid early flexural tensile cracking. The type of specimen used in their tests is represented in Fig. 2.3.

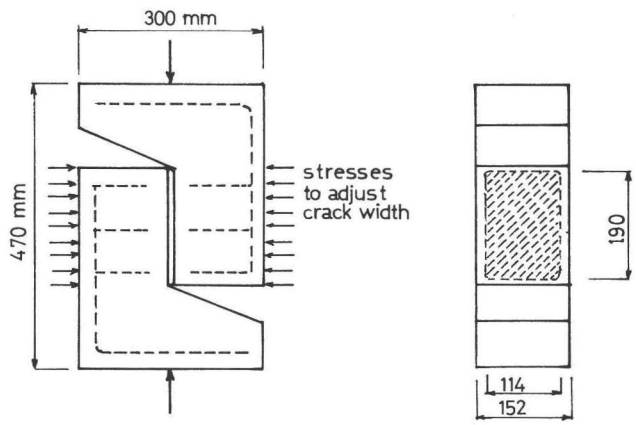

Fig. 2.3 Test arrangement according to [60]

The lower part of the specimen was completely fixed, while the upper part could move freely. The crack width could be adjusted with an accuracy of 2%. Crack width and shear displacement were measured on both sides of the specimen. The test results were not influenced by the development of secondary cracks in the specimens. The tests were carried out with a constant concrete strength equal to $f'_{ccyl} = 37\ N/mm^2$. Objects of investigation were the influence of the crack width, the effect of aggregate size and shape, and the effect of load history. The maximum values of the shear stresses

were much higher than obtained in the tests of [18, 30]. The upper limit of shear transfer at $\tau = 7$ N/mm^2 was not reached as a result of aggregate interlock in the crack. Either failure occurred as a result of local crushing of the concrete in the top or bottom section of the specimens, or further increase of load was not possible with the loading arrangement used. It was observed also by Paulay and Loeber [60] that the shear stress-displacement relation is essentially dependent on the crack width. Shape and size of the aggregate particles had no noticeable influence in the range tested (D_{max} = 9.5 - 19 mm, round and crushed). The relation between shear stresses and displacements is represented in Fig. 2.4, and the stresses normal to the crack plane, necessary to keep the crack width constant, are represented as a function of the shear stress in Fig. 2.5.

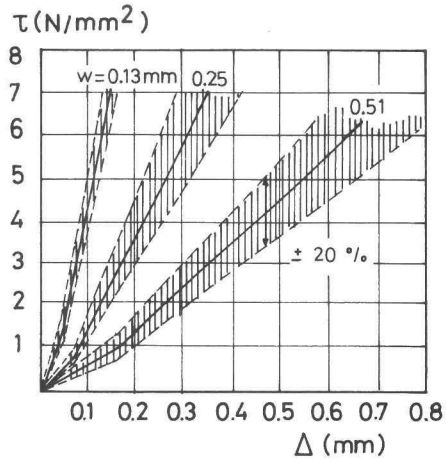

Fig. 2.4 Shear stress-shear displacement relation for constant crack widths, according to [60]

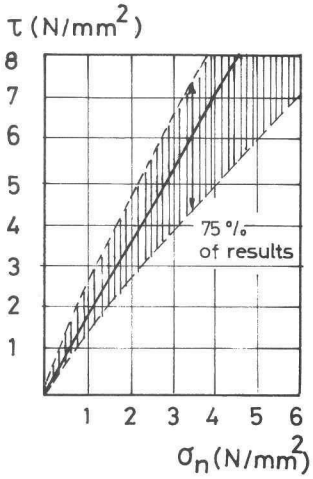

Fig. 2.5 Average shear stress-restraining normal stress relations for crack widths 0.25 - 0.51 mm

For these last-mentioned curves no significant influence of aggre-

gate type or crack width was observed. It is seen in Fig. 2.4 that the shear stress-shear displacement relations have a "hardening" character. This can be explained by the physical nature of the mechanism, since an increase of shear displacement must result in an increase of the total contact area between the crack faces (due to crushing of hardened cement paste), which results in increasing resistance to shear displacement. The influence of load history is shown in Fig. 2.6. In this diagram the mean experimental curve obtained in separate tests, carried out with a constant ratio between shear stress and crack width, is given, with on both sides the interval of scatter of 13% (shaded area). Upon this curve the results from the previous "constant crack width tests" (Fig. 2.4) have been superimposed to enable a comparison to be made. The dotted line connects the appropriate stress values for the three distinct crack widths used in the tests. It reveals the same form as the relationship obtained from the "variable crack width tests".

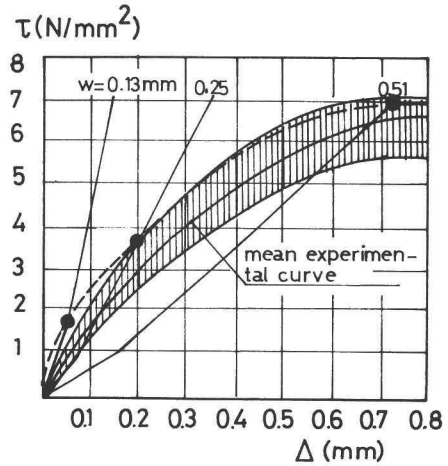

Fig. 2.6 Mean experimental curve for shear stress-displacement relationship with constant shear stress to crack width ratio, according to [60]

Taylor [75] carried out an investigation into the fundamental

behaviour of beams without shear reinforcement, in which it was demonstrated how the behaviour of the structure as a whole can be explained as an interaction of a number of basic mechanisms. One of these mechanisms was aggregate interlock. Measurements on beams showed that cracks do not open to their final width and shear then, but open and shear simultaneously. Therefore it was doubted whether the results obtained in [18, 30, 60] are immediately applicable to the analysis of actual beam behaviour. Observations on the beams without shear reinforcement appeared to show a constant ratio of crack width to shear displacement during crack opening. Therefore aggregate interlock tests were carried out, not with constant crack widths as in [18, 30, 60], but with constant crack width to shear displacement ratios (Fig. 2.7).

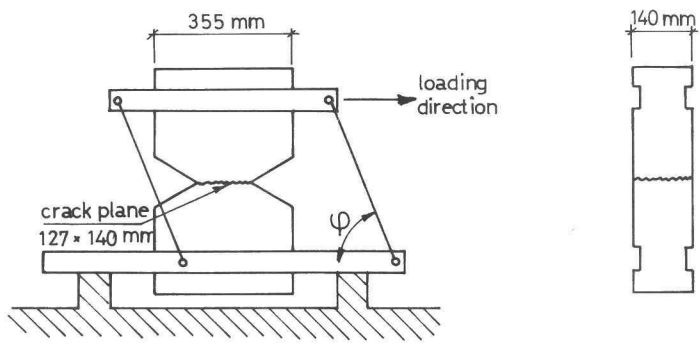

Fig. 2.7 Schematic illustration of test equipment, used in [75]

The ratio of normal to shear displacement could be changed between tests but was constant during a test. This ratio was introduced by means of a parallel ruler system. However, although a good approximation of real crack behaviour in constructional situations seemed to be obtained, it is felt that also objections could be raised, due to which no general validity can be attributed to the results. At first only the normal displacements at the crack were measured:

hence it is not certain that the ratio of normal to shear displacement, which was supposed to be introduced by the test arrangement, was also obtained at the level of the crack. This may only be considered to be true if it were certain that the crack faces have no resistance against the imposed displacements, so that no preference for any direction of crack opening would exist. Further, the observations that there is a linear proportionality between normal and shear displacements in beams without shear reinforcement were based on measurements by means of strain gauges which were stuck on the beam after the cracks had formed, so that a certain interval of displacement was not measured. Experiments in which the measurements on similar type of beams were carried out from the beginning of loading, thus providing a complete picture of the behaviour after cracking, revealed an increasing ratio between shear and normal displacements of the crack faces [82].

Important information about the way in which the stresses are actually transferred from one crack face to the other can be derived from cyclic loading tests. Tests by Laible et al. [40], which were aimed at studying the effect of seismic loading on the behaviour of cracks in reinforced concrete, therefore claimed attention. These tests were carried out on specimens as represented in Fig. 2.8.

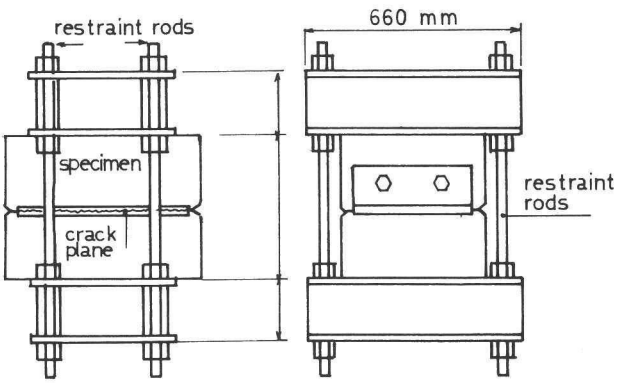

Fig. 2.8 Test specimen used in [40]

Dowel action was excluded by using external restraint bars. These

bars had a negligible shear stiffness but acted to hold the specimen halves together when shearing and overriding occurred. The specimens were cracked at mid-depth, prior to testing, by forcing cracking wedges into the sides of the specimen. The desired initial crack width was then set by positioning the upper half of the specimen with respect to the lower half by adjustment of the nuts on the restraint rods that passed through the upper restraint beams. The horizontal shearing surface had a net cross-sectional area of 194000 mm^2. Fully reversing cyclic shear stresses of about 1.24 N/mm^2 were applied across initial crack widths of 0.25, 0.51 and 0.76 mm by hydraulic rams. A result obtained on a specimen with an initial crack width of 0.76 mm and a restraint stiffness of 600 kN/mm is represented in Fig. 2.9.

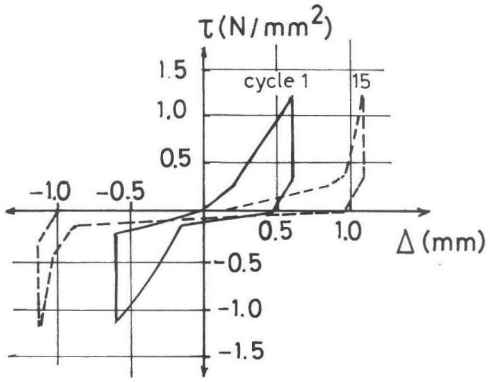

Fig. 2.9 Shear stress-shear displacement curve for cyclic loading, according to [40]
(f'_{ccyl} = 21 N/mm^2, D_{max} = 38 mm, w_o = 0.75 mm, restraint stiffness $\Delta\sigma$ = 0.3 N/mm^2 for Δw = 0.1 mm)

The result may be considered to be representative of the generally observed behaviour. Although the loading portion of the load-shear displacement curve during the first cycle is nearly linear, the very next cycle of all specimens demonstrated a marked degree of non-linearity similar to the results for cycle 15 in Fig. 2.9. In only a few cases did the shear displacement freely return to

as little as 50% of the maximum value. Usually the return shear displacement was in the range of 0 - 20% of this value. This is believed not to be caused by a type of "locking effect" between particles, since hardly any shear stress was necessary to return the specimen to its neutral position. It therefore appears obvious that this irreversibility is due to local deformation of the matrix (hardened cement paste). This feature is important as a basic property in further analysis of the mechanism.

Summarizing the available information on aggregate interlock, it is obvious that there is a serious lack of information. Experiments have generally been carried out disregarding the effect of shear dilatancy. Only in [60] a rather wide range of values has been indicated for the stress normal to the crack plane, necessary to adjust the crack width to its original value after every load increment. However, it is not only uncertain whether a constant crack width test is representative of the behaviour of a crack in a structure, but also it is questionable whether this normal stress itself is a realistic value, since it has to exceed the internal friction between the crack faces before being able to adjust the crack width: hence it may overestimate the stress that really occurs due to the shear dilatancy in a crack (compare also active and passive soil pressure). Tendencies revealed by the available test data are that the shear resistance increases with increasing concrete strength and increasing shear displacement, and decreases with increasing crack width. Furthermore it is apparent that irreversible deformation of matrix material is directly related to the overall observed behaviour. No reliable information was found about the role of the scale of the aggregate (D_{max}), the particle size distribution (grading curve) and the influence of the crack opening path. It is obvious that in order to define appropriate material properties concerning aggregate interlock it will be necessary to obtain more information.

2.2 Dowel action

Dowel action is defined as the capacity of reinforcing bars to

transfer forces perpendicular to their axis (Fig. 1.3.b). The effect of dowel action depends essentially on the constructional circumstances. This can be explained by considering the stresses around a bar, loaded by a dowel force, and the consequences of a tensile crack.

For a thin slice of an elastic material, loaded as indicated in Fig. 2.10, the stresses in the material can be determined by using plane stress elasticity methods [70, 90].

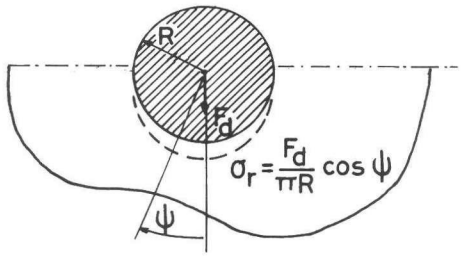

Fig. 2.10 Thin slice of an elastic material, loaded by a dowel force

In this way it was found that the radial stresses are equal to:

$$\sigma_r = \frac{F_d}{\pi R} \cos \psi \qquad (2.1)$$

Values of the circumferential tensile stresses in the concrete are:

$$\sigma_\psi = 0.344 \frac{2F_d}{\pi R} \qquad \psi = 0 \qquad (2.2)$$

$$\sigma_\psi = 0.637 \frac{2F_d}{\pi R} \qquad \psi = \frac{\pi}{2} \qquad (2.3)$$

Thus the tensile stress in the direction of the dowel action force is highest and the tensile stress normal to the dowel force, which tends to produce a wedging splitting action is only 54% of the maximum. This trend was experimentally confirmed by Weaver and Clark [86]. When the tensile strength of the concrete is reached

and a crack is formed, an adjustment in the load carrying system may be expected.
In an in-plane loaded planar element a redistribution of stresses occurs, resulting in higher stresses under the bar (Fig. 2.11.a). When the dowel load is increased, a progressive deterioration of the concrete under the bar occurs, resulting in a gradual decrease in stiffness till the ultimate load is reached (curve a in Fig. 2.11.c).

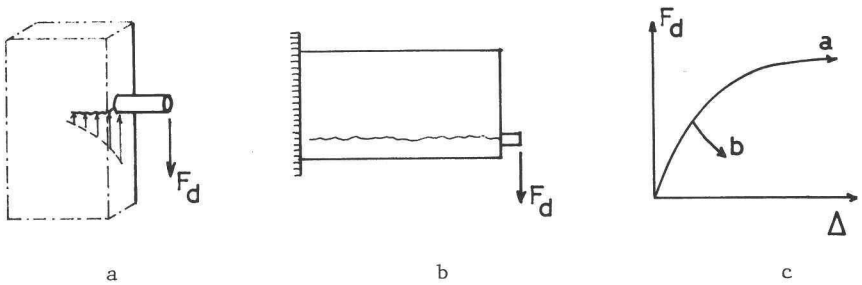

a b c

Fig. 2.11 a,b: Dowel cracking in a planar structure and in a beam
c : Load-deflection curves for both cases

In a beam, however, after the formation of a crack generally no redistribution of stresses is possible, and a rigorous extension of the crack along the bar axis, resulting in failure must be expected; only if the beam is reinforced with stirrups, the dowel crack may be stopped and a completely different mechanism is activated to transfer dowel forces.
This study focuses on dowel action in cracks in planar elements, in which particularly the relation between forces and displacements between the crack faces is considered. An extended review of available knowledge about dowel action in beams, before and after dowel cracking, the determination of ultimate bearing capacities at large deformations and the behaviour under cyclic loading has been represented in [83].

The deflection of the dowel will be defined as the total distance

between the axes of the undeformed parts of the bars on both sides of the crack (Fig. 2.12).

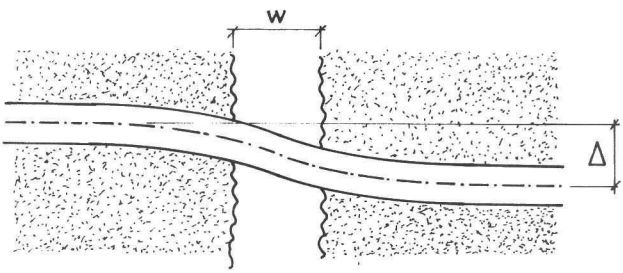

Fig. 2.12 Deflection of a bar subjected to a dowel force

As has been indicated, the total deflection is both a result of the deformation of the part of the bar embedded in the concrete and the part which is free over a certain length.
For the deformation over the free length, Paulay [59] distinguished three mechanisms (Fig. 2.13):

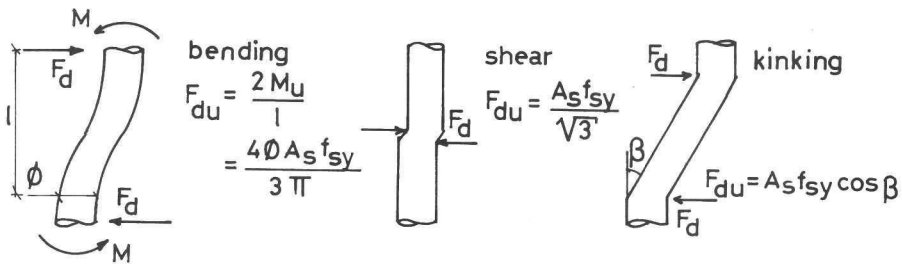

Fig. 2.13 Mechanisms of shear transfer over the free length according to [59]

- Load transfer by bending: the capacity of this mechanism is limited by the formation of plastic hinges in the bar.
- Load transfer by pure shear.
- Load transfer by kinking: if there is a considerable shift between the two main bar axes, for instance as a result of plastic

deformations, the axial force in the local deviation results in a component perpendicular to the main axis. There has been much discussion on this subject. It was often stated that this contribution could not be great, since the bar diameter is normally very large in relation to the crack width (Fig. 2.14).

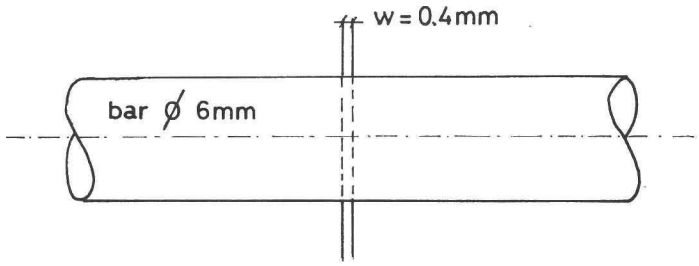

Fig. 2.14 Representation of a ratio bar diameter - crack width

However, it has to be realized that, because of crushing of the concrete, large deformations can occur, resulting in a considerable kinking effect. Especially for thin bars an important increase in load can be achieved after the formation of plastic hinges. The deformations necessary to develop this force are relatively large, so that kinking may play a role in parts of structures in which the bearing capacity is directly related to dowel action, such as some types of joints.
Later on it will further be shown that the free length can be greater than the crack width as a result of several effects, so that it is worthwile to take this length into account in a basic derivation of the dowel force - displacement relation.

The description of the dowel load-displacement relation can be based on the theory of beams on an elastic foundation, as published by Timoshenko and Lessels [79] (Fig. 2.15).
The first known application of this principle to the mechanism of dowel action is a publication of Friberg [22], who tried to calculate the loadbearing capacity of steel dowels in joints in concrete pavements.

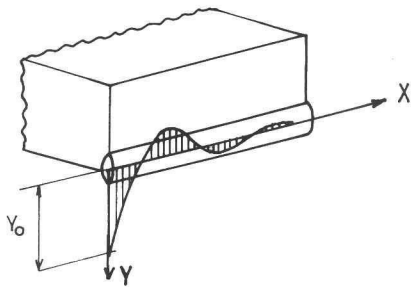

Fig. 2.15 Dowel considered as a beam on an elastic foundation

The derivation of the load-displacement relation, taking into account the deformations both in the concrete and in the steel, is given, based on the publications mentioned before. The model and the different partial displacements associated with it are represented in Fig. 2.16.

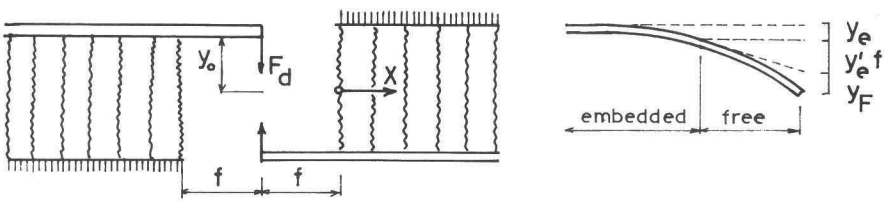

Fig. 2.16 Calculation model and partial displacements

The total deflection at the centre is the sum of three components:

$$y_o = y_e + y'_e\ (-\ f) + y_F \qquad (2.4)$$

According to Finney [19], y_e can be expressed as:

$$y_e = F_d \frac{1}{2\beta^3 EI} (1 + \beta f) \qquad (2.5)$$

in which

$$\beta = \sqrt[4]{\frac{G_f \cdot \phi}{4\ EI}}$$

$EI = E_s \frac{\pi \phi^4}{64}$ (flexural stiffness of the bar)

G_f = foundation modulus of concrete

$$y'_e = - F_d \frac{1}{2\beta^3 EI} \beta(1 + 2\beta f) \qquad (2.6)$$

y_F is the deflection of a bar which is fixed (restrained) at x = 0 and subjected to a load F_d at x = -f:

$$y_F = \frac{F_d \cdot f^3}{3\ EI} \qquad (2.7)$$

The relation between the dowel force F_d and the total deflection y_o is:

$$y_o = \frac{F_d}{6\beta^3 EI} \{3 + 6\beta f + 6\beta^2 f^2 + 2\beta^3 f^3\} \qquad (2.8)$$

The shear deformation of the steel over the free length is neglected in this formulation. Stanton [70] demonstrated that this contribution to the total displacement is always < 4%, independent of the bar diameter. The relation between the dowel force and the total dowel deflection, which is equal to the total shift between the two parallel bar axes ($\Delta = 2\ y_o$), is then:

$$F_d = \frac{3\beta^3 EI\ \Delta}{3 + 6\beta f + 6(\beta f)^2 + 2(\beta f)^3} \qquad (2.9)$$

The validity of this model is restricted to the elastic range. A prediction of the ultimate bearing capacity on the basis of constant elastic material properties is doomed to fail. Marcus [48] demonstrated with the results of his experiments that, if the elastic model were valid, the concrete stress under the bars in the ultimate loading stage would reach values up to 2.6 times the concrete compression strength. Between the initial (elastic) loading range and the ultimate (plastic) loading range a transition range with changing material properties exists. Attention must be paid

to two important variables used in formulation (2.9): the value G_f, involved in the foundation modulus of the concrete, and the value of the free length f.
For the foundation modulus of the concrete G_f many different values are encountered in literature. A survey of values given by Finney [19] is represented in Table 2.I.

Table 2.I Values for G_f according to a survey by Finney [19]

G_f Range, N/mm	Average N/mm	Source	Remarks	Literature
834 - 417	-	Grinter	Estimation	[26]
max. 695	19.7 f'_c	Friberg	Tests on embedded dowels - 1938	[22, 23]
198 - 325	256	MSHD *	Load-deflection test 1947	[20]
217 - 1637	639	MSHD *	Tests on embedded dowels	Not published
247 - 2307	712	Marcus	Dowels with uniform bearing pressure	[48]
Not known	681	Loe	Load-deflection tests 1952	[45]
250 - 2391	695	MSHD *	Tests on embedded dowels	Not published

* Michigan State Highway Department

There are several reasons which can be advanced in order to explain the scatter in the values.

At first the value G_f is strongly related to the quality of the concrete immediately under the bar. So, even when the same concrete

composition is used, a scatter is obtained, depending on the position of the bar during casting. When the direction of the bar is parallel to the direction of casting (Fig. 2.17.a) a higher value of G_f can be expected than in the case of a bar perpendicular to this direction (Fig. 2.17.b), since during the vibration a local segregation of water under the bar can be expected, resulting in lower concrete quality. Also for bars situated nearer to the bottom of the structure (Fig. 2.17.c) a higher value for G_f may be expected, since the density of the concrete increases from top to bottom.

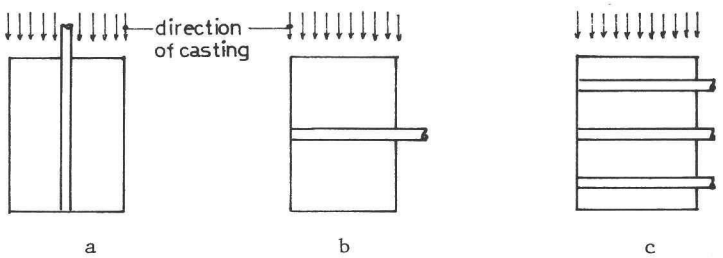

Fig. 2.17 Various positions of bars, influencing the value of G_f

Next, it is obvious that the value of G_f must decrease with increasing dowel force. As was stated earlier, at first small cracks will occur, parallel to the bar axis (Fig. 2.11.a). As a result, the concrete compressive stresses under the bars increase. For a higher degree of loading crushing of the concrete under the bars also occurs. A gradually decreasing value of G_f for increasing dowel action may be expected as a result of this. This is confirmed by a comparison between the theoretical values obtained from eq. (2.9) and the experimental values obtained in the tests of Paulay, Park and Phillips [59] (Fig. 2.18).
These tests were carried out by applying a transverse load to a corbel which was connected to the rest of the specimen by reinforcing bars, crossing a smooth contact area, excluding all possible loadbearing components, except dowel action.

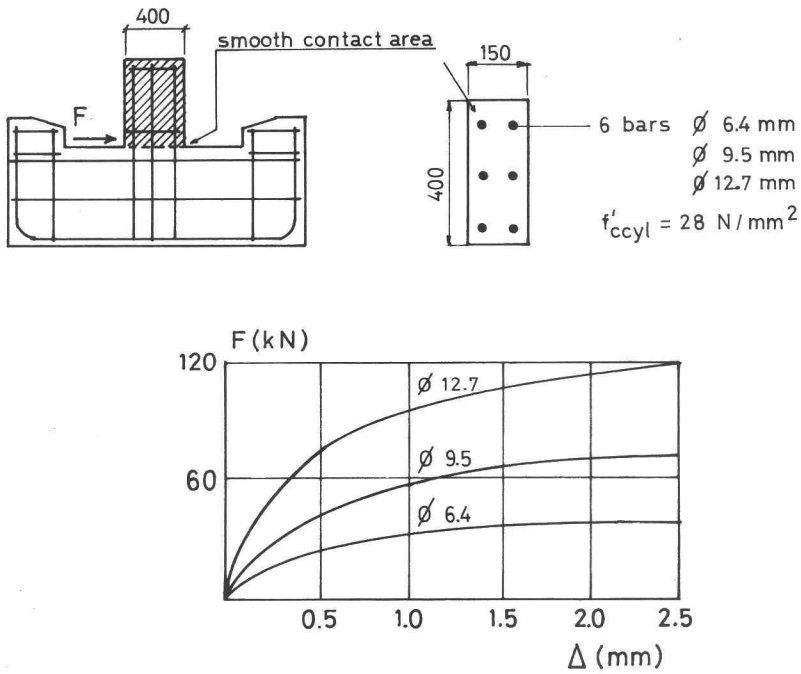

Fig. 2.18 Dowel tests carried out by Paulay, Park, Phillips [59]

To get agreement between (2.9) and these experiments, G_f must decrease as a function of the increasing dowel displacement: the result of this calculation is represented in Fig. 2.19. Apparently the bar diameter is not a significant parameter in this respect. This agrees with observations by Marcus [48] and Eleiott [17].

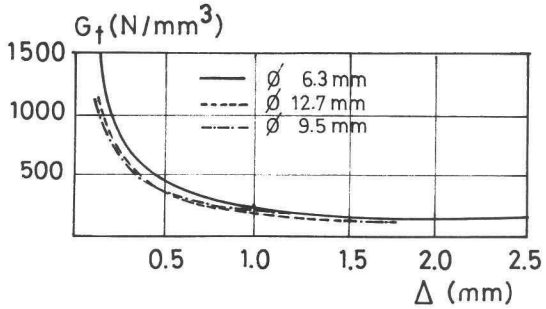

Fig. 2.19 G_f as a function of the dowel displacement, deduced from the experiments described in [59]

The value of G_f obtained in this way is in fact a function both of changes in material properties and of redistribution of stresses. G_f may be considered only as the value which has to be inserted in (2.9) to get the same load-deflection curve as is experimentally obtained due to a complex physical mechanism (Fig. 2.20).

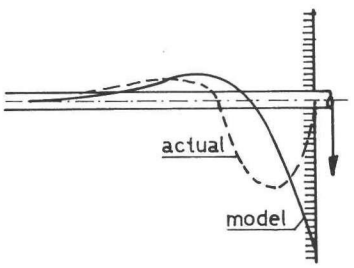

Fig. 2.20 Stress distribution, actual and modelled

Summarizing, it is obvious that G_f must not be considered as a uniform value, only depending on the concrete quality, but that further considerations have to be taken into account. Therefore, it is not surprising that the values for G_f represented in Table 2.I scatter over a wide range.

The second variable in the formulation (2.9) which has to be treated with caution is the free length f. At first sight it appears logical to insert for this variable the crack or joint width. However, there are circumstances that may lead to free lengths which are considerably greater.

- When bars cross a crack not perpendicularly, the concrete adjacent to the bars may locally crack off (Fig. 2.21).
  The free length which is caused in this way must depend on the angle θ and the bar diameter ϕ. Schäfer [65] suggested the relation:

$$f = C_r.\phi.\tan\theta \qquad (2.10)$$

in which C_r is a constant. This relation gives $f = 0$ for $\theta = 0^o$ and $f = \infty$ for $\theta = 90^o$.

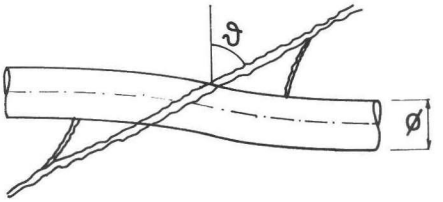

Fig. 2.21 Increase in free length for bars inclined to a crack

- An important other cause for an increased free length is the presence of an axial tensile force in the bar. As a result of this force large bond stresses occur, causing microcracks to form (Fig. 2.22).

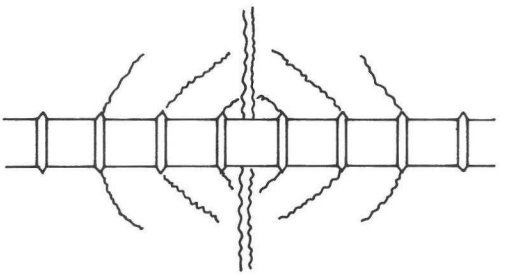

Fig. 2.22 Microcracks according to [25]

The existence of these cracks was first experimentally proved by Goto [25]. Due to this crack development, cone-shaped concrete elements are extracted, resulting in an increase of the free length. This increase (= 2f-w) depends on the value $\Delta\sigma_s$, which is the difference between the steel stress in the crack and in the undisturbed area, the bond properties and the diameter of the bar. Leonhardt [42] gave as an approximation for deformed bars (estimation on basis of centric tensile tests):

$$f = \frac{\Delta\sigma_s}{45}\,\phi \qquad (N/mm^2 \text{ and } mm) \tag{2.11}$$

See also Fig. 2.23.

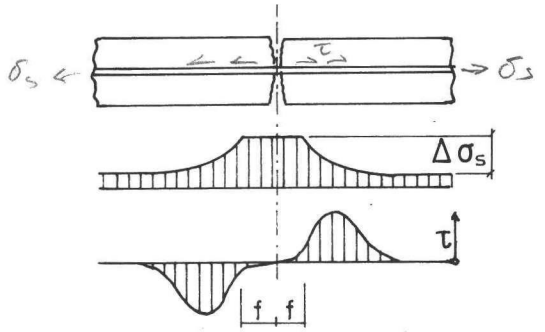

Fig. 2.23 Distribution of steel stresses and bond stresses over and beside the free lengths

It must furthermore be pointed out that an axial tensile force not only increases the free length, but also, because of microcracking, reduces the value of the foundation modulus G_f in the area where contact is still maintained. However, both developments lead to a decrease in dowel stiffness. The influence of the axial tensile force was experimentally confirmed by Eleiott [17]. His tests on pure dowel action were carried out with embedded bars of different sizes, stressed to different levels of axial stress. The tests were principally intended for studying the behaviour under cyclic loading. However, already during the first cycles a pronounced influence of the axial stress level was observed. Fig. 2.24 shows the load-deflection curves for the first load cycle for two tests on bars with a diameter of 12.8 mm: one test was carried out without an axial tensile stress, the other with an axial stress of 175 N/mm^2. The great loss of stiffness due to an increased axial stress is manifest.

In the same investigation a comparison was made between the effect of dowel action alone and the effect of aggregate interlock and dowel action together. The reinforcement in both cases was the same

(1 bar ϕ 12.8 mm), just as the axial tensile stress ($\sigma_s = 175\ N/mm^2$). The concrete area was 9525 mm^2. The results are given in Fig. 2.25.

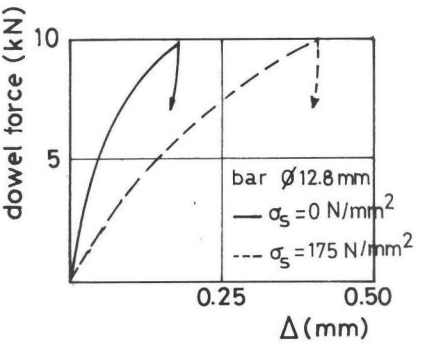

Fig. 2.24 Test results of [17] for a stressed and an unstressed dowel

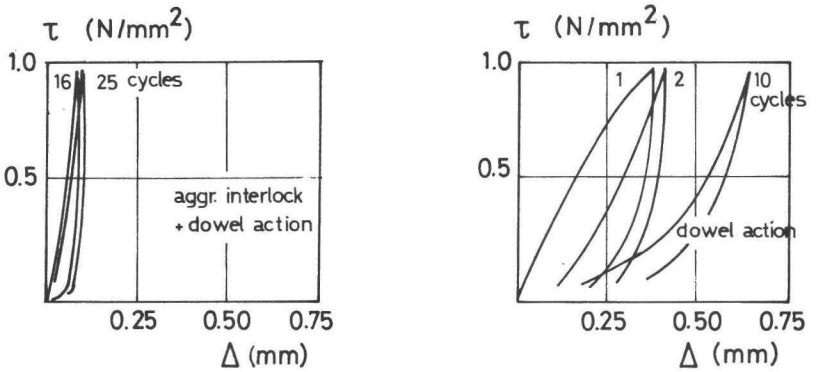

Fig. 2.25 Comparison between a test on combined aggregate interlock and dowel action (left) and a test on dowel action alone [17, 32, 89]

A comparison of the stiffnesses for this case showed that about 12% of the shear stiffness was provided by dowel action and about 88% by aggregate interlock.

Recapitulating, it may be stated that the deflection of a bar, subjected to a dowel force, is partially a result of the deformation

of the concrete around the bar and partially of the deformation of the steel over a free length. When the theory of a beam on an elastic foundation is used to calculate the load-deflection relation, some parameters have to be handled with caution. The value G_f, necessary to calculate the deformations in the concrete is not a constant, but decreases with increasing deflection. The position of the bar in the structure and the bond stresses, if any, may have an influence on G_f; the bar diameter has apparently no significant influence on this value. The free length of the steel, and therefore the contribution of this part to the total dowel deflection, increases if the axial tensile stress increases; also for bars inclined to the crack (joint) plane an increase in the free length is possible, this being due to the local spalling of the concrete. For relatively small deflections the deformation of the steel over the free length is mainly attributable to bending action: shear deformations may be neglected. Kinking of the bars can only occur for relatively large deflections. A prediction of the load-deflection relation only as a function of the deformations in the steel is an unrealistic approach, despite arguments, sometimes encountered in literature, which seem to confirm the opposite. This will be demonstrated, investigating a statement found in [59], in which it was concluded that dowel action is approximately proportional to the reinforcement ratio, irrespective of the bar diameters. This conclusion was based on a diagram in which dowel force-displacement relations were constructed for equal reinforcement ratios on the basis of tests on single bars with different diameters (Fig. 2.26). Comparing this result with the three mechanisms for the shear transfer, being possible for the steel over the free length (Fig. 2.13), it was concluded that shear and kinking would predominantly be responsible for the behaviour. This would be contrary to the tendendies emerging from other tests and theories treated in this chapter. However, it can be demonstrated that these results do not violate the assumption of behaviour according to the model of a beam on an elastic foundation. According to formula (2.9) for a free length f = 0 the dowel action of one bar can be written as:

$$F_d = \beta^3.EI.2\,y_o = \beta^3.EI.\Delta \quad \text{with } \beta = \sqrt[4]{\frac{\phi\, G_f}{4\, EI}} \tag{2.12}$$

Substitution of $\frac{\pi\phi^4}{64}$ for I results in the relation

$$F_d = 3.56\ \phi^{1.75}\ .\ G_f^{0.75}\ .\ \Delta \tag{2.13}$$

so that a proportionallity with $\phi^{1.75}$ is obtained.
If a number of n_1 bars with a diameter ϕ_1 in a joint results in a reinforcement ratio ρ, this can be written as:

$$n_1.\tfrac{1}{4}\pi\phi_1^2 = \rho bd \tag{2.14}$$

If a number of n_2 ($< n_1$) bars with a larger diameter $\phi_2 = \alpha\phi_1$ ($\alpha > 1$) results in the same reinforcement ratio, this can be written as:

$$n_2.\tfrac{1}{4}\pi(\alpha\phi_1)^2 = \rho bd \tag{2.15}$$

From (2.14) and (2.15) it is seen that

$$n_2 = \frac{n_1}{\alpha^2} \tag{2.16}$$

According to (2.13) the total dowel force for the bars with the smaller diameter is

$$\Sigma F_{d_1} = n_1\ .\ 3.56\ .\ \phi_1^{1.75}\ .\ G_f^{0.75}\ .\ \Delta \tag{2.17}$$

and for the bars with the larger diameter, with equal reinforcement ratio:

$$\Sigma F_{d_2} = n_2\ .\ 3.56\ (\alpha\phi_1)^{1.75}\ .\ G_f^{0.75}\ .\ \Delta =$$

$$= \alpha^{-0.25}\ (n_1\ .\ 3.56\ .\ \phi_1^{1.75}\ .\ G_f^{0.75}\ .\ \Delta) \tag{2.18}$$

Comparing (2.17) with (2.18) it is found that

$$\Sigma F_{d_2} = \alpha^{-0.25} \cdot \Sigma F_{d_1} \qquad (2.19)$$

This implies that, if the reinforcement ratio is the same, for equal values of Δ (and as a result of G_f), larger bars ought to give a slightly lower total dowel force than smaller bars (since $\alpha > 1$). This is indeed confirmed by Fig. 2.26.

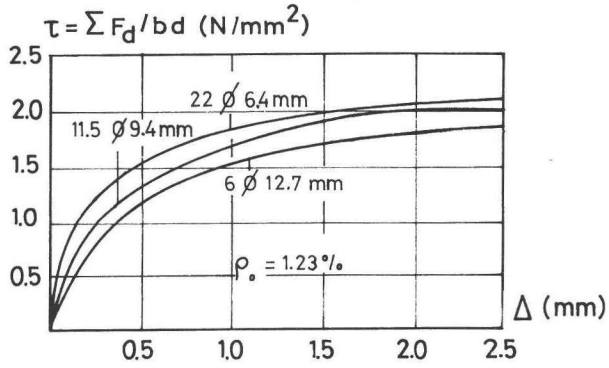

Fig. 2.26 Total dowel force for a joint with bars of several diameters, but the same reinforcement ratio, according to tests of [59]

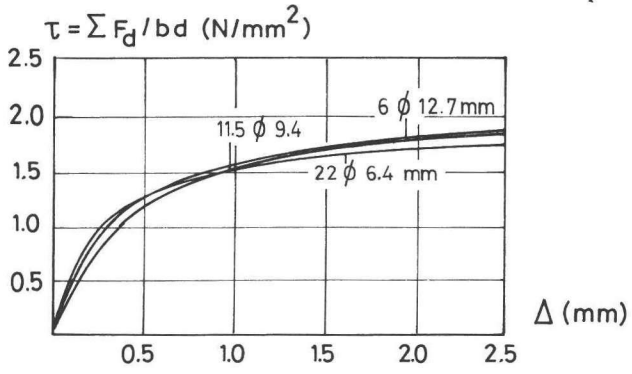

Fig. 2.27 The same curves after a correction on the basis of the model of a beam on an elastic foundation. (According to this theory the curves must coincide)

If these curves (from [59]) are "corrected" by means of a reduction factor $\alpha^{0.25} = (\frac{\phi_2}{\phi_1})^{0.25}$, related to the line for 6 ϕ 12.7 mm, it appears that a comparison on the basis of the model of a beam on an elastic foundation gives a surprisingly good result (Fig. 2.27).

Regarding dowel action in general it is apparent, that the influence of most parameters can adequately be described by the model of a beam on an elastic foundation. Since furthermore the contribution of dowel action in practical circumstances is greatly inferior to that of aggregate interlock, and a very accurate estimation is not possible due to the scatter in G_f, further experimental work on this subject would appear hardly to deserve high priority.

2.3 Axial restraint stiffness of reinforcing steel

In reinforced concrete the axial force in the reinforcing bars, whether inclined or not, is also a component which has to be considered when equilibrium of forces in a crack is analysed. The relation between the axial force in the bars and the slip at the crack is mainly a function of the bond between steel and concrete. Bond between steel bars and surrounding concrete depends predominantly on the profiling of the reinforcing bar, characterized by the ratio between the area of the ribs F_R and the shear area F_s: the related rib area f_R (Rehm [62, 63], Martin [49], Noakowski [56], Fig. 2.28).

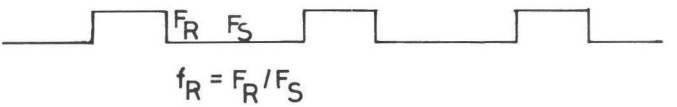

Fig. 2.28 Definition of related rib area f_R

How these f_R values are determined has been described in [9]. Average values for conventional steel bars are (Koch [35]):

$$f_R \approx 0.045 \rightarrow 0.060 \qquad \text{for } \phi = 4 \rightarrow 11 \text{ mm}$$

$$f_R \approx 0.065 \qquad \text{for } \phi > 12 \text{ mm}$$

Tests on reinforcing bars, embedded over a short length, demonstrated that for a wide range of slip values a proportionality between the bond stress and the concrete strength f'_{cc} exists. In order to find functions describing the relation between the pull-out force and the slip of a bar, it therefore appeared appropriate to base oneself on the value $\frac{\tau}{f'_{cc}}$. Experiments showed that the basic relation between $\frac{\tau}{f'_{cc}}$ and the slip Δ_s can be represented by

$$\frac{\tau}{f'_{cc}} = a_o + b_o \, \Delta_s^{\frac{1}{\beta}} \text{(cm)} \tag{2.20}$$

(a_o, b_o and β are constants).

However, this equation results in a complicated differential equation. Martin [49] showed that an approximate solution can be obtained by a difference calculation. The reinforcing bar is accordingly divided into elements with a length Δx. Besides equation (2.20), for all the elements two other conditions have to be fulfilled:

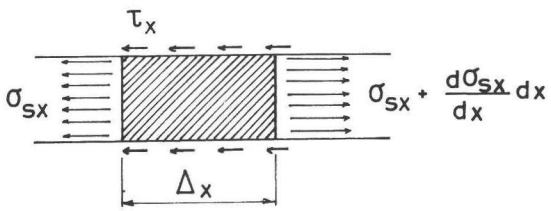

Fig. 2.29 Equilibrium of forces on a bar element

Equilibrium of forces (Fig. 2.29)

$$\frac{d\sigma_s}{dx} = \frac{U}{A_s} \cdot \tau_x \qquad (2.21)$$

In this equation is U = the circumference of the reinforcing bar and A_s is the cross-sectional area.

Compatibility of deformations

$$\frac{d\Delta x}{dx} = \frac{\sigma_{sx}}{E_s} \left(1 - \frac{\sigma_{cx}}{\sigma_{sx}} \cdot \frac{E_s}{E_c}\right) \qquad (2.22)$$

In words: the difference in strain between steel and concrete over the length of the element has to result in a slip d(Δx). Schiessl [66] demonstrated that the concrete strain is of minor influence and can be neglected without committing a significant error.
If the constants in equation (2.20) are known, a difference calculation on the basis of the equation (2.20 - 2.23) can provide a sufficiently accurate estimation of the steel stress, bond stress and the steel strain over the length of the bars, starting from initial values for σ_{so}, τ_{so} and Δ_{so}, on condition that the length of the elements is small enough. Calculations with a variable value of Δx demonstrated that a length equal to the distance between the ribs offers a fair degree of accuracy.
Martin [49] carried out tests in which the bar was embedded in the concrete over a length of 7 - 10 ϕ; on the basis of measurements of the bar slip in these tests and the equations (2.20, 2.21, 2.22) he determined by an iterative procedure the basic constants of equation (2.20). The values resulting from this calculation are represented in Table 2.II.
A result of a difference calculation for a bar with ϕ 8 mm and $f_R = 0.050$ is presented in Fig. 2.30. Detailed information on this type of calculations is given in [85, pp. 81].
It must be realized that the constants a_o, b_o and β are unreservedly valid only for the loading conditions as used in Martin's tests, in which no stresses transverse to the bar axis were acting (Fig. 2.31.a).

Table 2.II Constants in basic bond stress - slip relation (2.20), according to [49]

f_R	a_o	b_o	β
0.005	0.0320	0.129	2.34
0.010	0.0317	0.300	2.00
0.025	0.0317	0.680	1.85
0.050	0.0314	0.872	2.10
0.100	0.0315	1.135	2.31
0.200	0.0322	1,353	2.53
0.400	0.0316	1.308	2.85

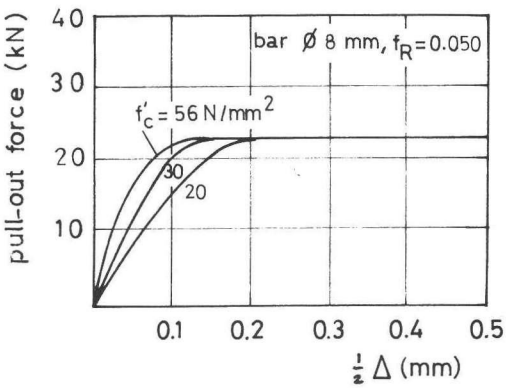

Fig. 2.30 Pull-out characteristic, calculated with the difference method

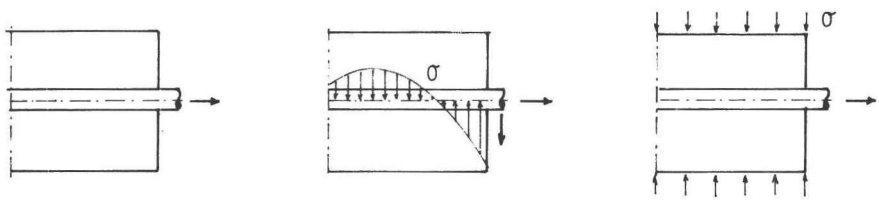

Fig. 2.31 Various stress conditions for reinforcing bars

It may for instance be asked how concentrated transverse stresses, due to dowel action, affect the basic bond slip relation (Fig. 2.31.b). This was investigated by Klein et. al. [34], who carried out tests on specimens as represented in Fig. 2.32. The specimens were reinforced with bars ϕ 10 and ϕ 16 mm, inclined at angles of $\theta = 45^{o}$, 60^{o} and 90^{o}.

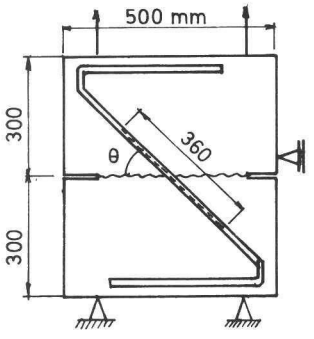

Fig. 2.32 Test specimen as used in [34]

All the tests were repeated several times in order to obtain representative results. Since the results of the investigation were principally intended to be applied to reinforced slabs in which the cracked parts are connected over the uncracked compression area, only displacements normal to the crack plane were imposed. Strain gauges were stuck to the bars over a length of 360 mm. For the ϕ 16 mm bars this length appeared to be insufficient, so that some extrapolation of the measurements was necessary. The results of the measurements were used to reconstruct the bond stress distribution over the length of the bars. It was also possible to deduce the basic bond-slip relation for each reinforcement geometry. These relations are represented in Fig. 2.33 for all angles and for both diameters. It is seen that in the case of ϕ 10 mm bars no systematic variation with the angle of inclination could be observed. An upper limit to the validity of the measurements was obtained because of yielding at one end of the bar. In the

case of ϕ 16 mm bars a deterioration of bond quality with decreasing angle of inclination (greater stress concentrations) was observed, which probably has to be attributed to the formation of longitudinal and transverse cracks, which were not observed in the specimens with the ϕ 10 mm bars.

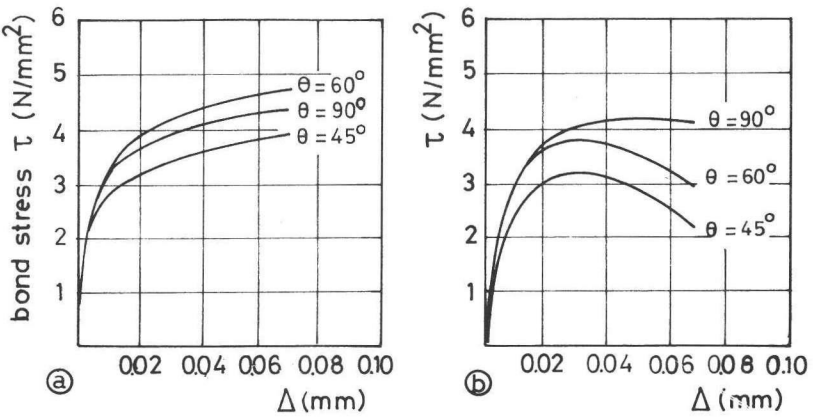

Fig. 2.33 Basic bond-slip curves for several angles of inclination for bars ϕ 10 mm (a) and ϕ 16 mm (b), deduced from tests conducted by Klein et al. [34]

Another possible loading condition, which frequently occurs in biaxially loaded structures, is that compressive stresses are applied in a direction transverse to the bar axis over its full length (Fig. 2.31.c). There are at present no known test results for this case. This phenomenon is studied in another part of the project "Concrete Mechanics" (Fig. 1.1).

2.4 Interaction of components in cracks crossed by reinforcement

The resistance of a "reinforced crack" to imposed displacements is the result of the interaction of the components dealt with earlier in this chapter in the sections 2.1 - 2.3: aggregate interlock, dowel action and axial steel forces. A schematic representation of

this interaction for the case where the reinforcing bars cross the crack perpendicularly is given in Fig. 2.34.

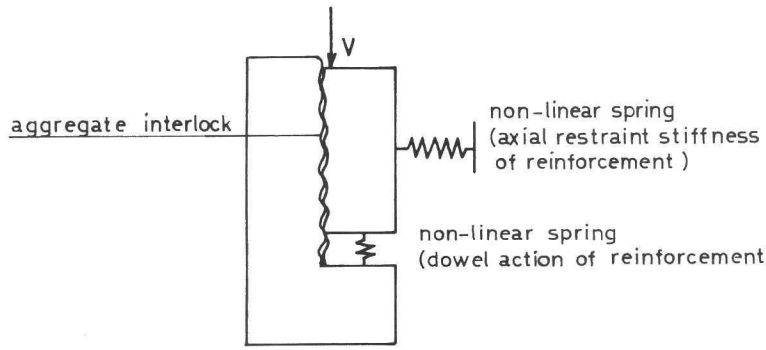

Fig. 2.34 Schematic representation of interaction of single components in a crack

Increased interest in the interdependence of stresses and displacements in cracks has developed only in recent years, and in most of the experiments on "reinforced cracks" attention has been confined to the ultimate bearing capacity under shear loading, while the relation between stresses and displacements has been disregarded [83]. An exception is an investigation conducted by Mattock [51], who tested specimens as shown in Fig. 2.35. The specimens were reinforced with varying numbers of closed stirrups, so that reinforcement percentages of 0.4 - 2.3% were obtained. The specimens were cracked prior to testing, which resulted in an average initial crack width of 0.25 mm (the scatter was not indicated). The displacements of the crack faces normal to the crack were measured by a gauge located at the middle of the length of the shear plane and the shear displacement by a gauge 50 mm below it (only on one side of the specimen). Fig. 2.35 further shows an example of a family of shear stress - shear displacement curves for one of the series.

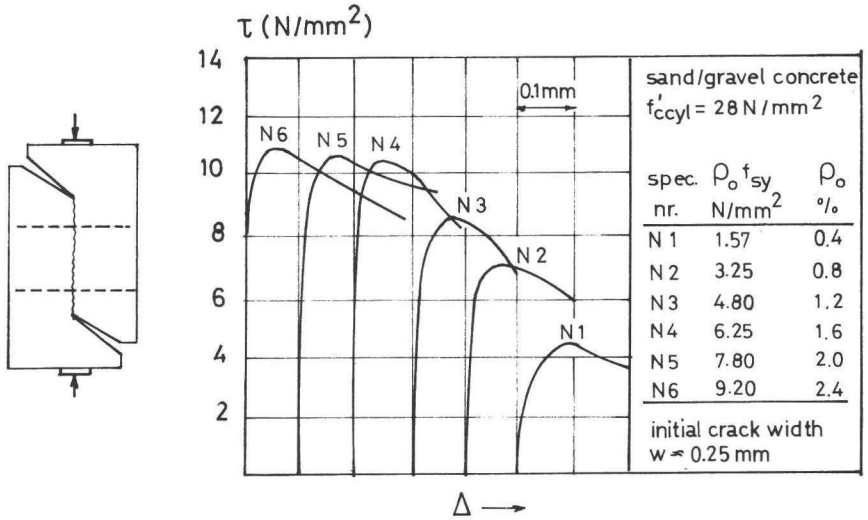

Fig. 2.35 Test specimen and some results of [51]

Fig. 2.36 shows the crack opening paths for two series. Both diagrams contain a family of curves for different reinforcement ratios, which are shifted in relation to one another for better comparison.

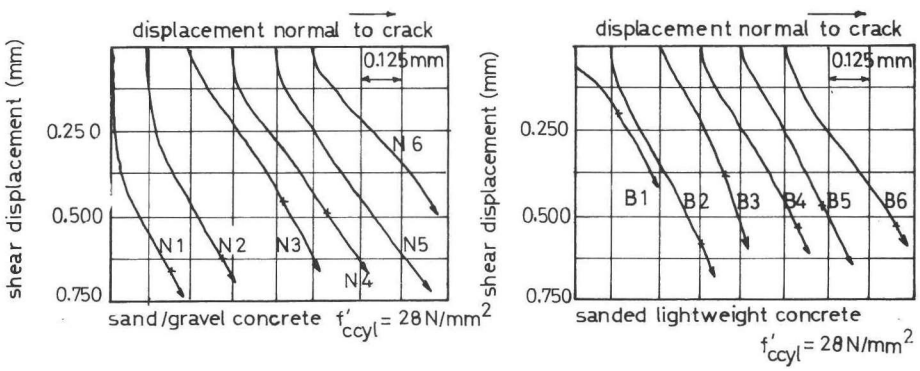

Fig. 2.36 Crack opening paths for precracked specimens with different reinforcement ratios, made of two types of concrete, according to [51]

Apparently the reinforcement ratio had no significant influence on

the crack opening direction, while also the fact that the lightweight particles of mix B are intersected by the crack had no noticeable influence. Since other series, made entirely of lightweight concrete, exhibited slightly steeper crack opening paths, it was believed that the behaviour could be explained by overriding of sand particles. If the sand particles are idealized as spheres (Fig. 2.37), the direction of motion due to overriding would be 30 degrees to the line of the crack, which corresponds closely to the average measured values of crack opening in Fig. 2.36.

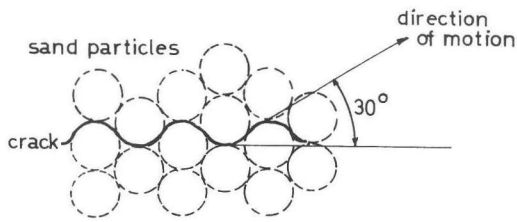

Fig. 2.37 Overriding of sand particles according to [51]

However, from a physical point of view it is not clear why only a certain sand fraction should predominantly govern the behaviour and how it could be explained that fractions with larger particles would be inactive. Furthermore, if overriding of particles were the essential mechanism, it is hard to explain why in "constant crack width tests" gradually increasing shear stress - shear displacement lines occur, without failure of the specimen due to secondary cracks (Fig. 2.3 and 2.4).

2.5 Conclusions

Considering the available knowledge, it is evident that in carrying out further study in this field, emphasis has to be placed on aggregate interlock. Not only is there a great lack of information on the relation between stresses and displacements, but also merely

speculations exist concerning the physical background of the phenomenon. If adequate knowledge of aggregate interlock were available, all the basic components acting in the transmission of forces across cracks would be sufficiently well known to enable the behaviour of "reinforced cracks" to be analysed. It must be investigated whether this behaviour can be explained on the basis of the individual components, or whether these components tend to interfere and a deviating mechanism is obtained. Accurate experimental data are required in this field anyway.

3 A FUNDAMENTAL THEORY FOR AGGREGATE INTERLOCK

3.1 Basic assumptions

To explain certain properties of concrete, this material is sometimes represented as a two-phase system: in a matrix (phase I) a collection of aggregate particles (phase II) are embedded. It is a matter of definition from which diameter the particles form part of the matrix. In the following, 0.25 mm is adopted as the limit between the phases I and II. For the crack widths to be considered in this study, the particles with a diameter smaller than 0.25 mm may practically be disregarded as far as their contribution to aggregate interlock between the crack faces is concerned. The properties of the matrix are, however, not very much influenced by the exact choice of this value, but are mainly governed by the properties of the hardened cement paste (Wischers [87]).
In general, the strength and stiffness of the aggregate particles are higher than those of the matrix. However, the contact area between the two materials, the bond zone, is the weakest link of the system. Hence, cracking occurs commonly through the matrix, but along the circumference of the aggregate particles. Only in the case of high-strength concretes (with high matrix strength) and lightweight concretes (with low particle strength) are cracks observed running both through the matrix and the particles. Generally crack faces are encountered which have a structure as indicated in Fig. 3.1.

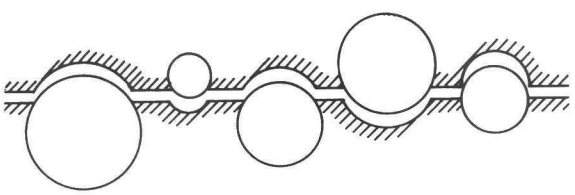

Fig. 3.1 Generally observed structure of crack planes

Considering such a crack structure, a number of trends emerging from earlier tests can be explained. The steady increase of the shear stress as a function of the shear displacement (Paulay/Loeber [60], Fig. 2.4) can be attributed to the growing contact area during shear displacement. The fact that the stiffness against shear displacement is smaller for larger crack widths, (see also Fig. 2.4) is due to the fact that the potential contact area between the opposite crack faces is reduced. Also an explanation can be given for the observed difference between the first and the subsequent loading cycles manifest in the tests, conducted by Laible et al.([40], Fig. 2.9): the concentrated stresses, occurring during the first loading cycle, result in local irreversible deformation of the matrix material, so that, during the subsequent cycle, the opposite crack faces have to travel a longer distance before touching each other. The increase in stiffness versus shear displacement with higher concrete strength, observed in the constant crack width tests of Fenwick et al. [18], can be attributed to the fact that high concrete strength is generally attended with high matrix strength, so that also a high resistance of the matrix to deformation is obtained.

Natural aggregate particles have an irregular shape. For the model to be developed, it is assumed that these particles are randomly orientated, so that no preferred directions exist. Furthermore the particles are simplified to spheres, for which it is supposed that they can be intersected by the crack plane at all depths with the same probability. Next, considering Fig. 3.1, it can be concluded that the "micro-roughness" of the crack, caused by the aggregate particles projecting from the crack faces, must dominate the effect of "macro-roughness", due to general undulations of the crack plane. Therefore the overall crack plane is considered to be a flat plane.

Hardened cement paste is a visco-elastic material: the deformations provoked by stresses are only partially elastic, for the other part plastic (Locher [44]). Under multi-axial stresses, as in the area between the aggregate particles in concrete, large plastic defor-

mations can occur as a result of pore-volume reduction. Since the plastic deformations are expected to dominate the elastic deformations, the stress-strain relation of the matrix material, consisting of hardened cement paste with aggregate particles smaller than 0.25 mm, is assumed to be rigid-plastic, as represented in Fig. 3.2. The stress at which yielding occurs is denoted as σ_{pu}.

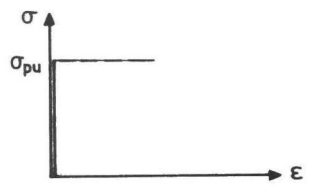

Fig. 3.2 Rigid-plastic stress-strain relation of the matrix material

Hence it can be expected that, during shear displacement of the crack faces, contact areas develop on the surface of the particles, interlocking between the crack faces, due to plastic deformation of the matrix. Fig. 3.3 shows the formation of this type of areas as a result of a shear displacement in the direction of the X-axis.

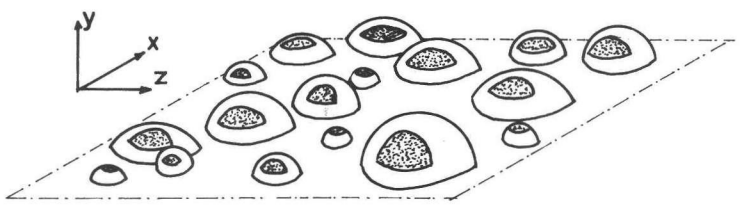

Fig. 3.3 Contact areas due to a shear displacement

The stresses at these contact areas produce reactions in the directions of all principal axes. However, if the crack area under consideration is not too small, it can reasonably be expected that the sum of all the components in the positive and the sum of all the components in the negative Z-direction are equal, so that equilibrium in that direction is automatically obtained without the action of external forces.
Furthermore it is assumed that the reactions in the positive and the negative Z-direction are uniformly distributed along the X-axis, so that no torsional moments with respect to the Y-axis are developed. These assumptions reduce the three-dimensional problem to a two-dimensional one. As a result it is possible to consider a cracked concrete body, as represented in Fig. 3.4.a, as an assembly of a large number of slices, each of finite width (Fig. 3.4.c), and it is possible to derive the overall behaviour of the crack by first studying the properties of this thin slice.

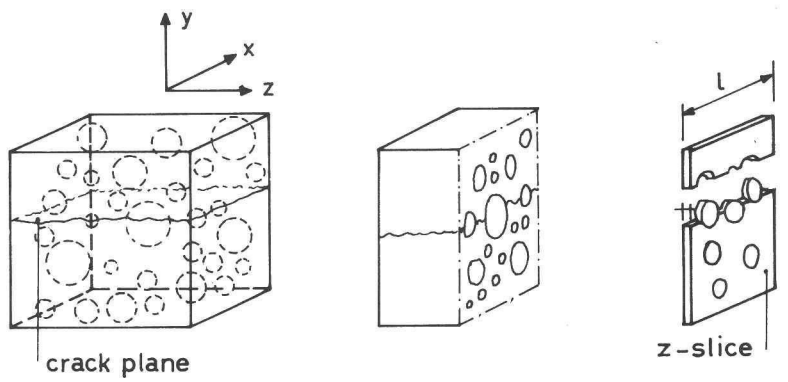

Fig. 3.4 Cracked concrete body (a), intersected by a Z-plane (b), and a representative slice (c)

Fig. 3.5 shows a cross-section through a particle lying in a Z-plane (see also Fig. 3.4.b and 3.4.c) in which there is a line of contact between the opposite crack faces. The projections of

this line of contact on the X- and Y- directions are a_x and a_y. The shaded area represents that part of the matrix which has disappeared due to plastic deformation of the matrix.

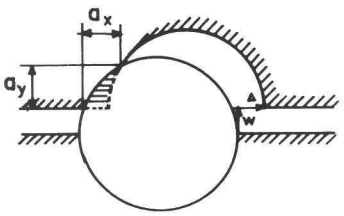

Fig. 3.5 Development of a contact area between matrix and aggregate

If the shear load on the plane of cracking is increased and crack opening is counteracted by restraining forces, for instance due to reinforcement, a mechanism will develop which can be described as follows: The contact areas tend initially to slide: as a result of this sliding, the contact area is reduced, which results in too high contact stresses. Hence, further yielding occurs, until equilibrium of forces is obtained in the X- and Y-directions. The stresses at the contact area are resolved into a stress σ_{pu}, normal to the contact area and a stress τ_{pu}, tangential to this area. The stresses σ_{pu} and τ_{pu} are interrelated by the condition that the contact areas are about to slide. Therefore the equilibrium conditions are formulated, based on a uniform critical stress combination (σ_{pu}, τ_{pu}), with $\tau_{pu} = \mu.\sigma_{pu}$ (Fig. 3.6).

Next, the components of the contact forces in the X- and Y-directions are derived, based on the previous assumptions. The circle in Fig. 3.7 represents the intersection of a particle by an arbitrary Z-slice (Fig. 3.4.c).

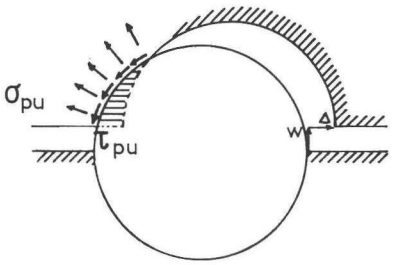

Fig. 3.6 Contact stresses on a particle

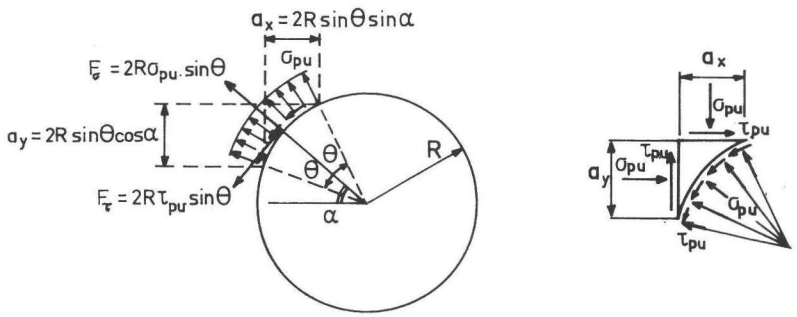

a b

Fig. 3.7 Equilibrium conditions

The radial stresses σ_{pu} are compounded to a force $F_\sigma = 2\ \sigma_{pu}\ R \sin\theta$. The component of this force in the direction of the Y-axis is $F_{\sigma y} = 2\ \sigma_{pu}\ R \sin\theta \sin\alpha$ and the component in the direction of the X-axis is $F_{\sigma x} = 2\ \sigma_{pu}\ R \sin\theta \cos\alpha$. The stresses τ_{pu} are compounded to a force $F_\tau = 2\ \tau_{pu}\ R \sin\theta$. The Y-component of this force is $F_{\tau y} = -2\ \tau_{pu}\ R \sin\theta \cos\alpha$ and the X-component is $F_{\tau x} = 2\ \tau_{pu}\ R \sin\theta \sin\alpha$.
The projection of the contact area on the X-axis is equal to $a_x = 2\ R \sin\theta \sin\alpha$ and on the Y-axis $a_y = 2\ R \sin\theta \cos\alpha$.
The resulting reactions in the X- and Y-directions can then be

formulated as

$$F_x = \sigma_{pu} \cdot a_y + \tau_{pu} \cdot a_x$$
$$F_y = \sigma_{pu} \cdot a_x - \tau_{pu} \cdot a_y \qquad (3.1)$$

Since $\tau_{pu} = \mu . \sigma_{pu}$ this is simplified to the final relations

$$F_x = \sigma_{pu}(a_y + \mu . a_x)$$
$$F_y = \sigma_{pu}(a_x - \mu . a_y) \qquad (3.2)$$

The total resistance of the crack area under consideration, of unit width and length 1, according to Fig. 3.4.c, is the sum of the contributions of all particles in that area:

$$\Sigma F_x = \sigma_{pu}(\Sigma a_y + \mu . \Sigma a_x)$$
$$\Sigma F_y = \sigma_{pu}(\Sigma a_x - \mu . \Sigma a_y) \qquad (3.3)$$

If also a unit length is considered, the projected contact areas are related to a unit surface area of the crack, so that (3.3) is modified to

$$\tau = \sigma_{pu}(A_y + \mu . A_x)$$
$$\sigma = \sigma_{pu}(A_x - \mu . A_y) \qquad (3.4)$$

in which τ and σ are the shear stress and normal stress, and A_x and A_y are the projected contact areas for a unit crack area.

3.2 General considerations on the basic variables

The equations (3.4) represent the contact forces in the X- and Y-directions for a crack area of predefined dimensions, expressed as functions of the projected contact areas A_x and A_y. These values

themselves are functions of the crack width w and and the shear displacement Δ, as seen in Fig. 3.6. So the relations between stresses and displacements are known, assuming that suitable values for the parameters σ_{pu} and μ can be inserted.

The projected contact areas A_x and A_y increase with decreasing values of the crack width w and increasing values of Δ. Other influencing factors are the relative volume of the aggregate and the distribution of the particle diameters (grading curve). The values A_x and A_y are stochastic variables. On the basis of assumptions for the relative volume, the distribution and the shape of the particles (assumed to be spherical) it must be possible to establish the expected average values of A_x and A_y by means of a statistical analysis. This analysis, which relates the stresses to the displacements, is carried out in section 3.3.

The matrix yielding strength σ_{pu} is representative of the average strength of the inhomogeneous matrix material subjected to locally differing multiaxial stress combinations. One aspect of inhomogeneity which is important for shear transfer in cracks is that during hardening of the concrete some segregation of water can occur in the contact zones between matrix and particles, due to which the matrix in the immediate vicinity of the particles may have a lower strength. These layers of lower matrix quality around the particles have no uniform thickness, so that, during shear displacement of the crack faces, the particles penetrate partially into soft and partially into strong matrix material. Furthermore the matrix is enclosed in small areas between the aggregate particles, so that the stresses around the individual aggregate particles mutually interfere and the stress conditions vary from point to point, resulting in strength values which are also subject to local variations.
Since at present no satisfactory model exists which describes the behaviour of the concrete on the basis of an interaction between the constituent components (Lüsche [47]), no appropriate values for the average yielding strength σ_{pu} are available. However, it

is possible to detect tendencies for this value by analysing the results of experiments on multiaxially loaded concrete. The matrix strength can be expected to exceed the uniaxial concrete compressive strength. The strength of the concrete is largely governed by the quality of the bond between matrix and aggregate particles, which is generally considered to be the weakest link of the loadbearing mechanism. In general the deterioration of the concrete under uniaxial loading starts with microcracking in this bond zone. Shah and Chandra [68] injected loaded concrete specimens with a fluorescent substance to facilitate the observation of microcracks. At about 50% of the failure load the number of microcracks around the particles, some of which cracks were already present before loading, began to increase significantly. At about 70% of the failure load these cracks began to intersect the matrix. If the formation of microcracks in the bond zone is delayed, for instance by a lateral confining pressure, the strength of the concrete is significantly increased (Fig. 3.8). If the matrix strength were smaller than the concrete strength, such an increase could never occur. For concretes subjected to lateral confining pressures ($\sigma_3 \geq \sigma_1 = \sigma_2 \geq 0$) Hobbs [29] gave as an approximate expression for the failure stress σ_{3u}, in terms of the compressive strength at atmospheric pressure f'_{cyl}, and the confining pressure, σ_{1u}, an equation of the form

$$\sigma_{3u} = f'_{cyl} + k_1 \sigma_{1u}$$

with k_1 ranging from about 5.7 for conventional concrete with a w/c ratio of 0.35 to about 4.5 for a conventional concrete with a w/c ratio of 0.71.
Writing this expression in an other form:

$$\frac{\sigma_{3u}}{f'_{cyl}} = 1 + \frac{\sigma_{1u}}{f'_{cyl}} k_1$$

it is seen that the relative strength $\frac{\sigma_{3u}}{f'_{cyl}}$ is a function of the uniaxial concrete strength: decreasing values are obtained for concretes with higher strengths.

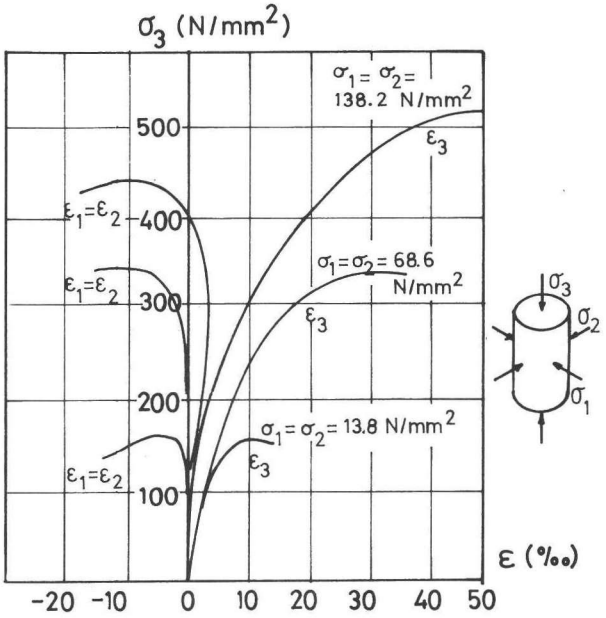

Fig. 3.8 Stress-strain curves for concrete cylinders subjected to different lateral confining stresses, according to tests of Newmann and Newmann [16]

Reinhardt [64] pointed out that this tendency is attributable to the more brittle behaviour of the matrix in high-strength concretes, giving rise to higher stress concentrations and as a result earlier formation of microcracks and accelerated deterioration of the load-bearing mechanism. This has also consequences for the yielding stress of the matrix σ_{pu}: if in places where high stress concentrations occur the strength of the matrix is exceeded, this has a reducing influence on the value σ_{pu}, since this is an average value for stresses of varying intensity.
Also under other loading conditions, such as biaxial tension-compression tests (Kupfer [38]), the relative strength values (referred to the uniaxial strength), increase for lower concrete qualities: also in such a case the relatively higher strength of the matrix in the lower-strength concrete must be responsible for

this tendency.

Summarizing, it can be stated that the matrix yielding strength σ_{pu} is higher than the uniaxial concrete strength f'_c, whereas the value $\frac{\sigma_{pu}}{f'_c}$ must be expected to decrease for increasing values of this uniaxial strength.

For the coefficient of friction μ between the matrix and the aggregate particles no adequate data are found in the literature either. An indication of the order of μ is found in the results of tests carried out by Weiss [88], who investigated the coefficient of friction between square concrete slices with sides of 100 mm and a thickness of 20 mm, the surfaces of which were always ground off in the same way. In these tests, performed on a large number of specimens in a so-called tribometer (Fig. 3.9), a coefficient of friction for concrete of $\mu = 0.52$ was found. If the surfaces were treated with hydrochloric acid, removing a small layer of the matrix, so that only the particle area remained, the value obtained was $\mu = 0.41$. Tests on specimens made of mortar (1 cement, 3 sand, w/c ratio = 0.5) yielded a value of $\mu = 0.47$, lying between the values for concrete and aggregate.

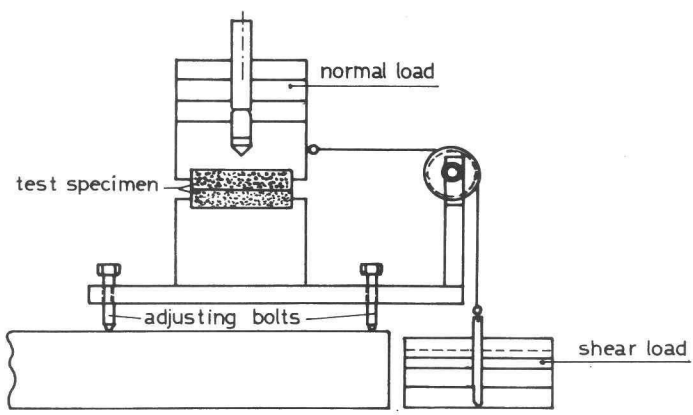

Fig. 3.9 Tribometer to establish the coefficient of friction between two solid bodies, according to Weiss [88]

Summarizing, it must be possible to express the values A_x and A_y in equation (3.4) as functions of the displacements w and Δ, on the basis of a given concrete mix composition (aggregate content, grading curve, particle shape).
For the values σ_{pu} and μ only tendencies are known. It would be too hypothetical to engage in further speculations about these values. Therefore the most suitable procedure seems to be to establish, first, the relations between A_x and A_y on the one hand and w and Δ on the other hand; next, to insert these expressions into the equation (3.4), and then to find the values σ_{pu} and μ indirectly, as the values which give the theoretical curves which best fit the results of experiments on cracks. If the model is realistic, this procedure ought to give values of σ_{pu} and μ which are in agreement with the tendencies previously outlined.

3.3 Determination of the relation between the projected contact areas A_x and A_y for a unit crack area on the one hand and the displacements between the crack faces on the other hand

Before dealing with the details of the analysis, the general concept of the calculation is schematically represented. The calculation is carried out in a number of steps.

a. An arbitrary Z-plane, intersecting the concrete body, is considered. Assuming a certain grading curve for the distribution of the particles in the mix, first, the most probable distribution of the diameters of the intersection circles in the Z-plane is derived (Fig. 3.10.a). Next, the most probable number of intersection circles with an arbitrary diameter D_o, which are also intersected by the crack over a length l, is calculated (Fig. 3.10.b). Then also for a unit crack length the most probable number of particles with a diameter D_o intersected by the crack is known (Fig. 3.10.c). Since the distribution of aggregate particles in a concrete is substantially a continuous function, it is not possible to give a most probable discrete number: probability density functions have to be used.

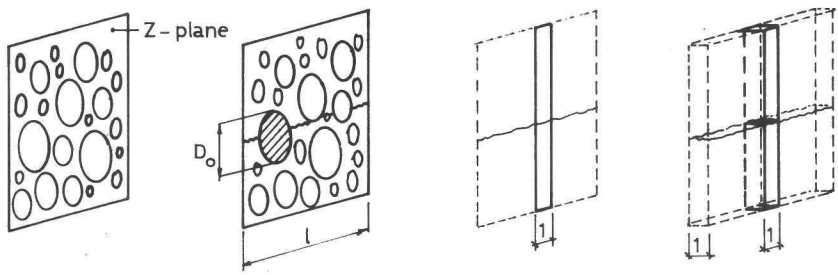

Fig. 3.10

b. In a second step of the calculation an answer is given to the question: "What are the average projected contact lengths a_x and a_y for an intersection circle with a diameter D_o, for an arbitrary displacement combination (w, Δ)?" In this calculation the variable position of the circle with regard to the central crack line (u) is taken into account (Fig. 3.11).

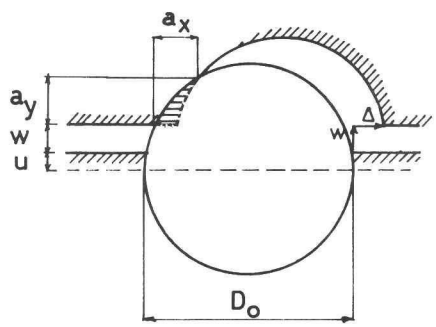

Fig. 3.11

c. If the density function of the most probable number of intersection circles with a diameter D_o is known from (a) and the average contact lengths a_x and a_y, provided by such a circle, are known from (b), the total contributions of the circles with a diameter D_o to the total contact lengths Σa_x and Σa_y are

known. The most probable total contact lengths, taking into account all possible circle diameters, are then found by integration over the full range of diameters, the distribution of which is known from (a).

Since the calculations have been carried out for an arbitrary Z-plane, and the same considerations are valid for all Z-planes, the projected contact areas A_x and A_y, for a crack area with a unit length and a unit width (Fig. 3.10.d), are obtained by multiplying the contact lengths Σa_x and Σa_y by that unit width.

3.3.a Determination of the most probable distribution of the diameters of the intersection circles, which are located in a Z-plane and are crossed by the crack

To be able to calculate the distribution of the diameters of the intersected circles in the Z-plane, an assumption has to be made for the distribution of the aggregate particles in the concrete mix. For this distribution a Fuller curve has been choosen. This curve represents a grading of aggregate particles which results in optimum density and strength and is therefore often used in practice. Besides, the curve is described by a simple and handy mathematical formula:

$$p = 100\sqrt{\frac{D}{D_{max}}} \qquad (3.5)$$

in which p denotes the percentage by weight passing a sieve with aperture diameter D, and D_{max} is the diameter of the largest aggregate particle. This relation is used as the cumulative distribution function of spherical aggregate particles with a diameter D (Fig. 3.12).

The probability that an arbitrary point in the concrete is located inside an aggregate particle is denoted by $p = p_k$. Actually p_k is the ratio of the total volume of the aggregate to the concrete volume. The probability that a point, if located inside a particle, also lies in a particle with a diameter smaller than an arbitrary chosen value D_*, can be expressed, using equation (3.5), as follows:

$$p\ (D < D_{*}) = p_k\ (\frac{D_{*}}{D_{max}})^{\frac{1}{2}} \tag{3.6}$$

By differentiation of this function the probability density function $p'(D_{*})$ is obtained:

$$p'(D_{*}) = p_k \frac{\partial\, p(D < D_{*})}{\partial\, D_{*}} = \tfrac{1}{2}\, p_k (\frac{D_{*}}{D_{max}})^{-\frac{1}{2}} \cdot \frac{1}{D_{max}} = C.D_{*}^{-\frac{1}{2}} \tag{3.7}$$

with

$$C = \tfrac{1}{2}.p_k.D_{max}^{-\frac{1}{2}}$$

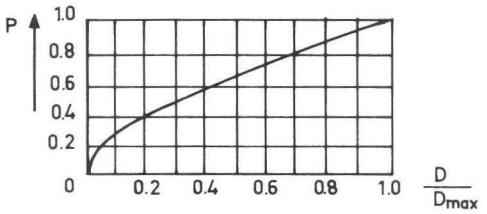

Fig. 3.12 Cumulative distribution function for spherical aggregate particles according to Fuller

Next, the probability that an arbitrary point, located in a Z-plane intersecting the concrete body, lies also in an intersection circle with a diameter D_o is analysed. The probability that a point, if located in a particle with a diameter D_{*}, lies also in an intersection circle with a diameter $> D_o$ ($D_o < D_{*}$), is equal to the ratio of the volume of the sphere section A (Fig. 3.13) to the volume of the hemisphere.

The volume of the sphere section B is equal to:

$$V_B = \frac{1}{6}\pi h(3a^2 + h^2) \quad \text{with } h = \tfrac{1}{2}\, D_{*} - \sqrt{\tfrac{1}{4}\, D_{*}^2 - a^2} \tag{3.8}$$

whilst the volume of the hemisphere:

$$V = \frac{1}{12}\pi D_{*}^3 \tag{3.9}$$

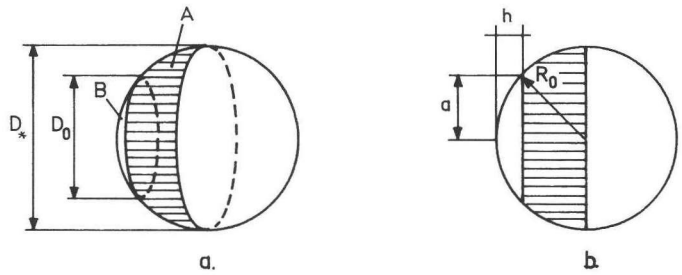

Fig. 3.13.

The probability that a point inside this sphere lies in an intersection circle with $D > D_o$ is equal to

$$p_{D_*}(D > D_o) = \frac{V - V_B}{V} \tag{3.10}$$

Substitution of (3.8) and (3.9) into (3.10) and rearranging results in:

$$p_{D_*}(D > D_o) = 1 - \frac{D_o^2}{D_*^2} - \tfrac{1}{2}\frac{D_o^2}{D_*^2}\sqrt{1 - (\frac{D_o}{D_*})^2} \tag{3.11}$$

So the probability that an arbitrary point in a Z-plane (Fig. 3.4.b) lies in an intersection circle with a diameter $D > D_o$ is obtained by integrating the product of (3.7) and (3.11) over the interval D_o to D_{max}:

$$p_c(D > D_o) = \int_{D_o}^{D_{max}} p'(D_*).p_{D_*}(D > D_o)\, d D_* \tag{3.12}$$

Substitution of (3.7) and (3.11) into (3.12) results in:

$$p_c(D>D_o) = \underbrace{\int_{D_o}^{D_{max}} C.D_*^{-\frac{1}{2}}\, d D_*}_{I} - \underbrace{\int_{D_o}^{D_{max}} C.D_o^2 D_*^{-2.5}\, d D_*}_{II} - \underbrace{\int_{D_o}^{D_{max}} \tfrac{1}{2}C.D_o^2 D_*^{-2.5}\sqrt{1-(\frac{D_o}{D_*})^2}\, dD_*}_{III}$$

Integral I

$$C \int_{D_o}^{D_{max}} D_*^{-\frac{1}{2}} \, d\, D_* = 2\, C.D_*^{\frac{1}{2}} \Big|_{D_o}^{D_{max}} = p_k(1 - D_o^{\frac{1}{2}} D_{max}^{-\frac{1}{2}})$$

Integral II

$$C \int_{D_o}^{D_{max}} D_o^2 D_*^{-2.5} d\, D_* = C.D_o^2 \left[-\frac{2}{3} D_*^{-1.5}\right]_{D_o}^{D_{max}} = p_k(\tfrac{1}{3} D_o^{\frac{1}{2}} D_{max}^{-\frac{1}{2}} - \tfrac{1}{3} D_o^2 D_{max}^{-2})$$

Integral III

$$\int_{D_o}^{D_{max}} \tfrac{1}{2}\, C.D_o^2\, D_*^{-2.5} \sqrt{1 - (\frac{D_o}{D_*})^2}\, d\, D_*$$

This integral is solved by expanding the term $\sqrt{1 - (\frac{D_o}{D_*})^2}$ into a Taylor series:

$$\sqrt{1 + (-\frac{D_o^2}{D_*^2})} = 1 + \tfrac{1}{2}(-\frac{D_o^2}{D_*^2}) - \frac{1}{2.4}(-\frac{D_o^2}{D_*^2})^2 + \frac{1.3}{2.4.6}(-\frac{D_o^2}{D_*^2})^3 - \frac{1.3.5}{2.4.6.8}(-\frac{D_o^2}{D_*^2})^4 .....$$

$$= 1 - 0.5\, D_o^2 D_*^{-2} - 0.125\, D_o^4 D_*^{-4} - 0.063\, D_o^6 D_*^{-6} - 0.039\, D_o^8 D_*^{-8} .....$$

The integral can then be written as:

$$I_{III} = \tfrac{1}{2}\, C.D_o^2 \int_{D_o}^{D_{max}} (D_*^{-2.5} - 0.5\, D_o^2 D_*^{-4.5} - 0.125\, D_o^4 D_*^{-6.5} - 0.063\, D_o^6 D_*^{-8.5}$$

$$- 0.039\, D_o^8 D_*^{-10.5} .....) d\, D_*$$

Integration results in:

$$I_{III} = \tfrac{1}{4}\, p_k . D_{max}^{-0.5}\, D_o^2 \left[- 0.667\, D_*^{-1.5} + 0.143\, D_o^2\, D_*^{-3.5} \right.$$

$$\left. + 0.023\, D_o^4\, D_*^{-5.5} + 0.008\, D_o^6\, D_*^{-7.5} + 0.004\, D_o^8\, D_*^{-9.5} \ldots \right]_{D_o}^{D_{max}}$$

$$= p_k (- 0.167\, D_o^2\, D_{max}^{-2} + 0.036\, D_o^4\, D_{max}^{-4} + 0.006\, D_o^6\, D_{max}^{-6}$$

$$+ 0.002\, D_o^8\, D_{max}^{-8} + 0.001\, D_o^{10} D_{max}^{-10} + 0.122\, D_o^{0.5}\, D_{max}^{-0.5}) \ldots\ldots\ldots)$$

Combination of I, II and III gives:

$$p_c(D > D_o) = p_k (1 - 1.455\, D_o^{0.5}\, D_{max}^{-0.5} + 0.50\, D_o^2\, D_{max}^{-2} - 0.036\, D_o^4\, D_{max}^{-4}$$

$$- 0.006\, D_o^6\, D_{max}^{-6} - 0.002\, D_o^8\, D_{max}^{-8} - 0.001\, D_o^{10} D_{max}^{-10}) \ldots\ldots\ldots) \qquad (3.13)$$

The cumulative distribution function, representing the probability that an arbitrary point in the concrete body, lying in a Z-intersection plane, is located in an intersection circle with a diameter $D < D_o$ can now be calculated, using equation (3.13):

$$p_c(D < D_o) = 1 - p_c(D > D_o) \qquad (3.14)$$

Substitution of (3.13) into (3.14) results in:

$$p_c(D < D_o) = p_k (1.455\, D_o^{0.5}\, D_{max}^{-0.5} - 0.50\, D_o^2\, D_{max}^{-2} + 0.036\, D_o^4\, D_{max}^{-4}$$

$$+ 0.006\, D_o^6\, D_{max}^{-6} + 0.002\, D_o^8\, D_{max}^{-8} + 0.001\, D_o^{10} D_{max}^{-10}) \qquad (3.15)$$

This function is represented in Fig. 3.14.

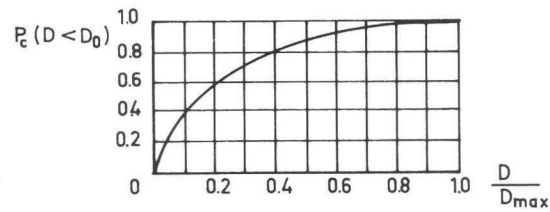

Fig. 3.14 Cumulative distribution function for the diameter of intersection circles

The density function for the probability that an arbitrary point in the concrete body, lying in a Z-plane of intersection, is situated in an intersection circle with a diameter $D = D_o$ is obtained by differentiation of (3.15) to D_o:

$$p'_c(D_o) = p_k(0.727\ D_o^{-0.5}\ D_{max}^{-0.5} - D_o\ D_{max}^{-2} + 0.144\ D_o^3\ D_{max}^{-4} + 0.036\ D_o^5\ D_{max}^{-6} + 0.016\ D_o^7\ D_{max}^{-8} + 0.010\ D_o^9\ D_{max}^{-10}) \quad (3.16)$$

Since the distribution of circles of intersection in the Z-plane is now known, it is possible to establish the frequency of circles D_o which both lie in the Z-plane and are crossed by the crack (Fig. 3.4.b and Fig. 3.15).

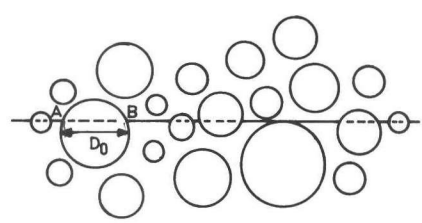

Fig. 3.15 Circles of intersection crossed by the crack

The average length of the intersection line AB for a circle with diameter D_o crossed by the crack is established using Fig. 3.16.

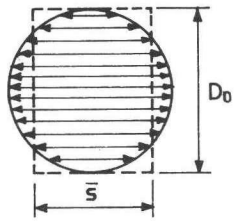

Fig. 3.16 Determination of the average length of intersection for a circle with diameter D_o

The surface area of the circle is $\frac{1}{4}\pi D_o^2$ and the surface area of the equivalent rectangle is $D_o\bar{s}$. The average intersection length is then

$$\bar{s} = \frac{\frac{1}{4}\pi D_o^2}{D_o} = \frac{\pi D_o}{4} \qquad (3.17)$$

If the length of the crack line (intersection of the crack plane and the Z-plane, Fig. 3.4.c) is denoted by 1, the probability density function for the expected length of that part of the line whose points also form part of an intersection circle with a diameter D_o, is obtained by multiplying 1 with $p'_c(D_o)$ (equation 3.16); hence:

$$1(D_o) = p'_c(D_o).1 \qquad (3.18)$$

Then the probability density function for the expected number of intersection circles with a diameter D_o in the Z-plane which also intersect the crack line 1 is obtained from (3.17) and (3.18)

$$n(D_o) = \frac{1(D_o)}{\bar{s}} = \frac{p'_c(D_o).1}{\frac{1}{4}\pi D_o}$$

Per unit length of the crack line 1 this expression is simplified to:

$$n(D_o) = \frac{p'_c(D_o)}{\frac{1}{4}\pi D_o} \qquad (3.19)$$

3.3.b Determination of the expected average contribution of an intersection circle with radius R to the contact lengths a_x and a_y for an arbitrary displacement combination (w, Δ), taking into account a variable embedment depth u

In the preceding section the probability density function for the expected number of intersection circles with an arbitrary diameter D_o, intersected by a unit crack length, has been derived (equation 3.19). However, the position of these circles with regard to the plane of cracking has not yet been taken into account. The distance from the central crack line to the centre of the circle is denoted by u (Fig. 3.17). This value is assumed to be a random variable in the interval $0 \leq u \leq R$. (For $-R \leq u \leq 0$ the circle is in the opposite crack face, for which the same considerations are valid).

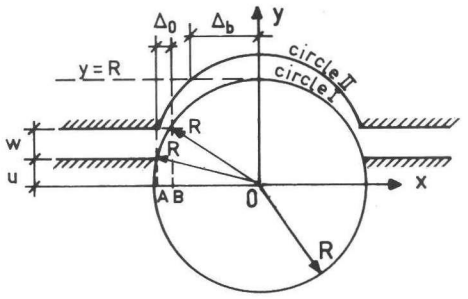

Fig. 3.17 Position of intersection circle characterized by u, randomly varying between 0 and R

If w + u > R, then for no value of the shear displacement Δ can any contact area occur. If w + u < R, then two characteristic values for

Δ can be found. For $\Delta < \Delta_o$ no contact is found (see also Fig. 3.18.a). If $\Delta_o < \Delta < \Delta_b$, a contact area is obtained which increases for increasing value of Δ. This phase is called the "growing contact phase" (Fig. 3.18.b). If $\Delta > \Delta_b$ no increase of contact area by further shear displacement can be obtained. This phase is called the "maximum contact phase" (Fig. 3.18.c).

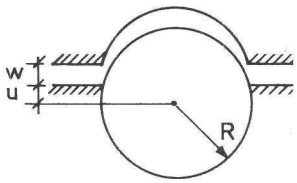

a. Phase of no contact

$0 < \Delta < \Delta_o$

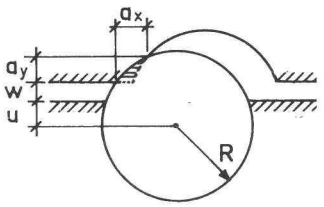

b. Phase of growing contact

$\Delta_o < \Delta < \Delta_b$

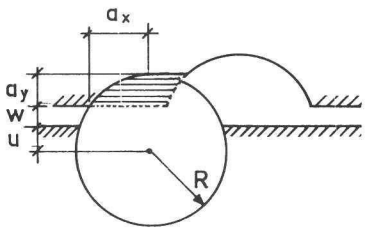

c. Phase of maximum contact

$\Delta_b < \Delta$

Fig. 3.18 Different phases for w + u < R

The values Δ_o and Δ_b are obtained with the help of Fig. 3.17.

$$\Delta_o = OA - OB = \sqrt{R^2 - u^2} - \sqrt{R^2 - (u+w)^2} \qquad (3.20)$$

Δ_b is obtained by calculating the intersection point of circle II with the line y = R

$$x^2 + (R - w)^2 = R^2$$

so that $x = -\sqrt{2\,Rw - w^2}$

or $$\Delta_b = \sqrt{2\,Rw - w^2} \tag{3.21}$$

For the interval $\Delta_o < \Delta < \Delta_b$ the values a_x and a_y, characterizing the contact area, can be expressed as a function of u, w, Δ and R. This derivation is given in Appendix I;

$$a_y = \sqrt{R^2 - \tfrac{1}{4}(w^2 + \Delta^2)}\,\frac{\Delta}{\sqrt{w^2 + \Delta^2}} - \tfrac{1}{2}w - u \tag{3.22}$$

$$a_x = \tfrac{1}{2}\Delta - \sqrt{R^2 - \tfrac{1}{4}(w^2 + \Delta^2)}\,\frac{w}{\sqrt{w^2 + \Delta^2}} + \sqrt{R^2 - (u + w)^2} \tag{3.23}$$

For $\Delta > \Delta_b$ it is easily deduced that

$$a_y = R - (u + w) \tag{3.24}$$

$$a_x = \sqrt{R^2 - (u + w)^2} \tag{3.25}$$

In the previous part of section 3.3.b the contact lengths a_x and a_y have been calculated for an individual intersection circle with a radius R, which resulted in expressions containing the variables w, Δ and u. The following question will now be analysed: What is the average contribution of an intersection circle with a radius R to the contact lengths a_x and a_y if Δ and w have an arbitrary, constant value? If the answer to this question is known, it is possible to find the total projections of the contact lengths Σa_x and Σa_y by integrating the contributions of all single circles over the full range of variation of R.

An intersection circle must be taken into account if it gives a

contact area in its most favourable position. It is evident that the most favourable position is obtained if the embedment depth u is zero. If a circle even in this extreme position is not in contact with the opposite crack face it may be excluded from the calculation. The first demand, if contact is required, is that $R > w$; if $R < w$ there is no contact for any value of Δ, even in the extreme case where $u = 0$ (Fig. 3.19).

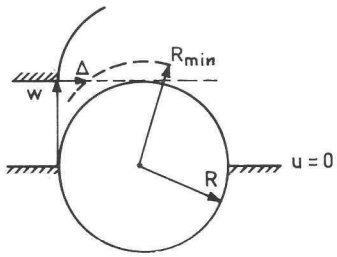

Fig. 3.19 Intersection circle in its most favourable position ($u = 0$)

If contact is not impossible in advance, so if $R_{max} > w$, it will be necessary to analyse the question how the circles contribute to the total contact area, taking into account the different modes of contact, represented in Fig. 3.18.
The value R_1 to which the radius of the intersection circle has to "grow" (Fig. 3.19) in order to provide at least one point of contact can be calculated from equation (3.20). For $u = 0$ it is deduced that just one point of contact is obtained for

$$R_1 = \frac{w^2 + \Delta^2}{2\Delta} \tag{3.26}$$

The value R_2, providing an upper limit for the range in which "maximum contact" (Fig. 3.18) is obtained, is found from equation (3.21):

$$R_2 < \frac{w^2 + \Delta^2}{2w} \tag{3.27}$$

Comparing the expressions (3.26) and 3.27), it is seen that for $\Delta < w$ (designated as the case A), the value R_2 is smaller then the value R_1, so that the "maximum contact phase" has no significance. So for $\Delta < w$ all circles with a radius $R_1 \leq R \leq R_{max}$ can contribute (whether this really happens will depend on the value of the embedment depth u). However, if $\Delta > w$ (case B), then R_2 is greater than R_1, so that both the "growing contact phase" and the "maximum contact phase" are of practical importance. It must furthermore be noted that now the limit value R_1 does not apply, since contact is always guaranteed for $R > w$ (see also Fig. 3.19 for $\Delta > w$). So for $\Delta > w$ all circles with a radius $w \leq R \leq R_2$ can contribute (again dependent on u), and if they do, "maximum contact" is obtained; furthermore all circles with a radius $R_2 \leq R \leq R_{max}$ can contribute, and if they do, "growing contact" is obtained.
The two case A and B are schematically represented in Fig. 3.20.

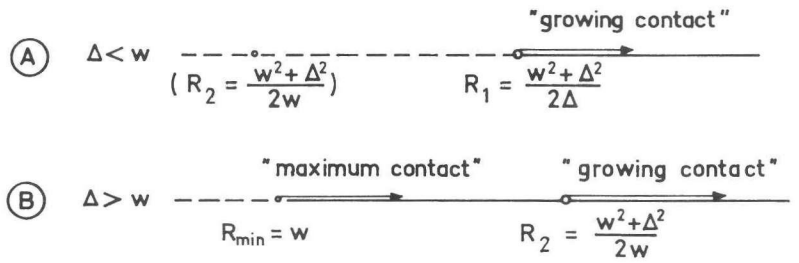

Fig. 3.20 Schematical representation of the fundamental contact modes for varying values of the radius R of the intersection circles

The fundamental cases A and B have to be distinguished, establishing the average expected contributions of the intersection circles to the contact area. This is done in the following derivation.

Case A: $\Delta < w$

If there is any contact area, this is at least the case for the minimum embedment depth u = 0. Solutions are found up to an upper bound u_{max}. This value u_{max} is deduced using Fig. 3.21.

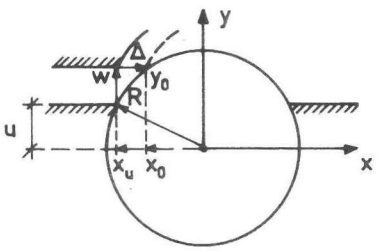

Fig. 3.21 Calculation of maximum embedment depth u_{max} for which contact still exists

For constant values of Δ, w and R, the variable u is increased to such an extent that only a single point of contact remains: at that stage u_{max} is reached.
In Fig. 3.21 it is seen that

$$x_u = - \sqrt{R^2 - u^2}$$

To fulfil the condition that only one point of contact remains, it is sufficient to demand that the point $(x_o, y_o) = (\Delta - \sqrt{R^2 - u^2}, u + w)$ lies on the circle; hence:

$$(u + w)^2 + (\Delta - \sqrt{R^2 - u^2})^2 = R^2$$

or $$2uw + (w^2 + \Delta^2) = 2\Delta \sqrt{R^2 - u^2}$$

Squaring both members of this expression results in:

$$u^2(4w^2 + 4\Delta^2) + 4uw(w^2 + \Delta^2) + (w^2 + \Delta^2)^2 - 4\Delta^2 R^2 = 0$$

which leads to:

$$u_{max} = \frac{-\frac{1}{2}w(w^2 + \Delta^2) + \frac{1}{2}\sqrt{w^2(w^2 + \Delta^2)^2 - (w^2 + \Delta^2)\{(w^2 + \Delta^2)^2 - 4\Delta^2 R^2\}}}{(w^2 + \Delta^2)} \quad (3.28)$$

So values for a_x and a_y are found for the range

$$0 < u < u_{max}$$

The probability density function for the occurrence of a value u is equal to

$$p(u) = \frac{1}{R} \quad (3.29)$$

The expected value for the average contribution of a circle with radius R to the contact lengths a_x and a_y can be formulated, using equation (3.29), as (Fig. 3.22)

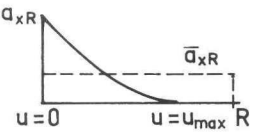

Fig. 3.22 Calculation of the average contribution of a circle with radius R to the contact length a_{xR}

$$\bar{a}_{yR} = \frac{1}{R}\int_{u=0}^{u=u_{max}} a_{yR}\, du \quad (3.30)$$

and

$$\bar{a}_{xR} = \frac{1}{R} \int_{u=0}^{u=u_{max}} a_{xR}\, du \qquad (3.31)$$

in which a_{yR} and a_{xR} are the contact lengths a_y and a_x for a circle with radius R, according to (3.22 and 3.23).

Substitution of (3.22) into (3.30) results in:

$$\bar{a}_{yR} = \frac{1}{R} \int_{0}^{u_{max}} \{ \sqrt{R^2 - \tfrac{1}{4}(w^2 + \Delta^2)}\, \frac{\Delta}{\sqrt{w^2 + \Delta^2}} - \tfrac{1}{2}w - u \}\, du$$

$$\bar{a}_{yR} = \frac{1}{R} \sqrt{R^2 - \tfrac{1}{4}(w^2 + \Delta^2)}\, \frac{\Delta}{\sqrt{w^2 + \Delta^2}} . u_{max} - \tfrac{1}{2}\frac{w}{R} u_{max} - \tfrac{1}{2}\frac{u_{max}^2}{R} \qquad (3.32)$$

Substitution of (3.23) into (3.31) results in:

$$\bar{a}_{xR} = \frac{1}{R} \int_{0}^{u_{max}} \underbrace{\{ \tfrac{1}{2}\Delta - \sqrt{R^2 - \tfrac{1}{4}(w^2 + \Delta^2)}\, \frac{w}{\sqrt{w^2 + \Delta^2}}}_{I} + \underbrace{\sqrt{R^2 - (u + w)^2}\}}_{II}\, du$$

Integration of I results in:

$$I_I = \{ \tfrac{1}{2}\Delta - \sqrt{R^2 - \tfrac{1}{4}(w^2 + \Delta^2)}\, \frac{w}{\sqrt{w^2 + \Delta^2}} \} . u_{max} \qquad (3.33)$$

Integration of II:

$$I_{II} = \int_{0}^{u_{max}} (R^2 - (u + w)^2)^{\frac{1}{2}}\, du \qquad (3.34)$$

Since du = d(u + w), (3.34) can be formulated as:

$$I_{II} = \int_{w}^{w+u_{max}} \sqrt{R^2 - (u + w)^2}\, d(u + w) = \int_{w}^{w+u_{max}} \sqrt{R^2 - t^2}\, dt$$

$$= \left[\frac{t}{2} \sqrt{R^2 - t^2} + \frac{R^2}{2} \arcsin \frac{t}{R} \right]_{w}^{w+u_{max}}$$

$$= \frac{u_{max} + w}{2} \sqrt{R^2 - (w + u_{max})^2} - \frac{w}{2} \sqrt{R^2 - w^2} +$$

$$+ \frac{R^2}{2} \arcsin \frac{w + u_{max}}{R} - \frac{R^2}{2} \arcsin \frac{w}{R}$$

The final expression for $\bar{a}_{xR}$ is then written as:

$$\bar{a}_{xR} = \{ \tfrac{1}{2} \Delta - \sqrt{R^2 - \tfrac{1}{4}(w^2 + \Delta^2)}\, \frac{w}{\sqrt{w^2 + \Delta^2}} \} \frac{u_{max}}{R} + \frac{u_{max} + w}{2R} \sqrt{R^2 - (w + u_{max})^2}$$

$$- \frac{w}{2R} \sqrt{R^2 - w^2} + \frac{R}{2} \arcsin \frac{w + u_{max}}{R} - \frac{R}{2} \arcsin \frac{w}{R} \qquad (3.35)$$

Case B: $\Delta > w$

In Fig. 3.20 it is seen that for $R > \frac{(w^2 + \Delta^2)}{2w}$ the calculation can be carried out in the same way as in case A. For the range

$$w < R < \frac{w^2 + \Delta^2}{2w} \qquad (3.36)$$

the "maximum contact" phase is valid. In the same way as in the "growing contact" phase a circle is in contact with the opposite crack face if the embedment depth u is greater than zero and smaller than a certain upper bound. In Fig. 3.18.c it can easily be seen that this upper bound is obtained for $u = u_{max} = R - w$. For values of R in the range indicated in (3.36) $\bar{a}_{yR}$ is obtained by substituting (3.24) into (3.30):

$$\bar{a}_{yR} = \frac{1}{R} \int_0^{(R-w)} (R - u - w)du = \frac{1}{2R} (R - w)^2 \qquad (3.37)$$

$\bar{a}_{xR}$ is obtained by substituting (3.25) into (3.31):

$$\bar{a}_{xR} = \frac{1}{R} \int_0^{R-w} \sqrt{R^2 - (u + w)^2}\, du \qquad (3.38)$$

Substituting t for (u + w), equation (3.38) can be written as:

$$\bar{a}_{xR} = \frac{1}{R} \int_w^R \sqrt{R^2 - t^2}.dt$$

so that

$$\bar{a}_{xR} = \frac{1}{R} \left[\frac{t}{2} \sqrt{R^2 - t^2} + \frac{R^2}{2} \arcsin \frac{t}{R} \right]_w^R$$

$$= \frac{\pi}{4} . R - \frac{w}{2R} \sqrt{R^2 - w^2} - \frac{R}{2} \arcsin \frac{w}{R} \qquad (3.39)$$

For the range

$$R > \frac{w^2 + \Delta^2}{2w}$$

the formulas (3.32) and (3.35) are valid.

3.3.c Determination of the expected value of the sum of all projections of the contact areas in the X- and Y-directions for a unit surface area of the crack plane

For a unit length of the crack line (line of intersection of the crack plane and a Z-plane (Fig. 3.4.c) it was shown that the probability density function for the expected number of circles with a diameter D_o, intersected on this length, can be expressed by

equation (3.19). The total contact lengths in the X- and Y-directions, provided by all circles with a radius R intersecting the unit crack length, can be expressed as:

$$\Sigma \bar{a}_{yR} = \int_{R_{min}}^{R_{max}} n(R).\bar{a}_{yR}.dR \qquad (3.40)$$

$$\Sigma \bar{a}_{xR} = \int_{R_{min}}^{R_{max}} n(R).\bar{a}_{xR}.dR \qquad (3.41)$$

in which n(R) can be calculated with equation (3.19) and $\bar{a}_{yR}$ and $\bar{a}_{xR}$ can be taken from (3.32) and (3.35) in the case where $\Delta < w$, or from (3.37) and (3.39) in the case where $\Delta > w$.
The expected values for the sum of all projected contact lengths Σa_x and Σa_y for a unit length of the crack line, are obtained by the summation of the contributions of all circles which have such a radius that contact may occur; formulated otherwise: by integrating the expressions (3.40) and (3.41) over the full interval of circles which may provide contact with the opposite crack face.

Case A: $\Delta < w$

Contact is obtained if $R > \frac{(w^2 + \Delta^2)}{2\Delta}$ or $D > \frac{(w^2 + \Delta^2)}{\Delta}$, therefore:

$$\Sigma a_y = \int_{\frac{w^2+\Delta^2}{\Delta}}^{D_{max}} n(D).\bar{a}_{yD}.dD \qquad (3.42)$$

$$\Sigma a_x = \int_{\frac{w^2+\Delta^2}{\Delta}}^{D_{max}} n(D).\bar{a}_{xD}.dD \qquad (3.43)$$

in which n(D) is taken from (3.19), $\bar{a}_{yD}$ from (3.32) and $\bar{a}_{xD}$ from

(3.35). D_{max} is the diameter of the largest aggregate particle. No contact is possible if $D_{max} < \frac{(w^2 + \Delta^2)}{\Delta}$ or, formulated otherwise, if

$$\Delta < \tfrac{1}{2}(D_{max} - \sqrt{D_{max}^2 - 4w^2}).$$

Nor is contact possible if $w > \frac{1}{2} D_{max}$. The physical background of these conditions is shown in Fig. 3.23.

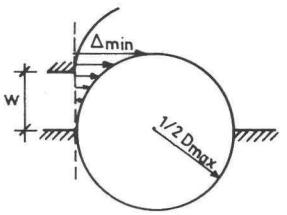

Fig. 3.23 Minimum value of Δ providing contact for the most favourable intersection circle ($D = D_{max}$) and the most favourable embedment depth ($u = 0$)

Case B: $\Delta > w$

Contact is obtained if $D > 2w$. Two modes of contact are distinguished: "maximum contact" is found for $D < \frac{(w^2 + \Delta^2)}{w}$; "growing" contact" is found for $D > \frac{(w^2 + \Delta^2)}{w}$.
This results in:

$$\Sigma a_y = \int_{2w}^{\frac{w^2+\Delta^2}{w}} n(D).\bar{a}_{yD_1}.dD + \int_{\frac{w^2+\Delta^2}{w}}^{D_{max}} n(D).\bar{a}_{yD_2}.dD \qquad (3.44)$$

$$\Sigma a_x = \int_{2w}^{\frac{w^2+\Delta^2}{w}} n(D).\bar{a}_{xD_1}.dD + \int_{\frac{w^2+\Delta^2}{w}}^{D_{max}} n(D).\bar{a}_{xD_2}.dD \qquad (3.45)$$

With the formulas (3.42 - 3.45) the expressions are given for the most probable projected contact lengths in the X- and Y-directions, for a crack surface with a unit length. Since the Z-plane of intersection has been arbitrarily chosen (Fig. 3.4.c), the projected contact areas A_x and A_y for a crack with a unit length and a unit width are obtained by multiplying the values Σa_x and Σa_y by that unit width.
Substitution of (3.19, 3.32, 3.35, 3.37 and 3.39) into (3.42 - 3.45) results in the final set of equations, representing the contact areas in the X- and Y-directions for a unit crack surface area.

Case A: $\Delta < w$

$$A_y = \int_{\frac{w^2+\Delta^2}{\Delta}}^{D_{max}} p_k \cdot \frac{4}{\pi} \cdot F\left(\frac{D}{D_{max}}\right) \cdot G_1(\Delta, w, D) \cdot dD \qquad (3.46)$$

$$A_x = \int_{\frac{w^2+\Delta^2}{\Delta}}^{D_{max}} p_k \cdot \frac{4}{\pi} \cdot F\left(\frac{D}{D_{max}}\right) \cdot G_2(\Delta, w, D) \cdot dD \qquad (3.47)$$

Case B: $\Delta > w$

$$A_y = \int_{2w}^{\frac{w^2+\Delta^2}{w}} p_k \cdot \frac{4}{\pi} \cdot F\left(\frac{D}{D_{max}}\right) \cdot G_3(\Delta, w, D) \cdot dD$$

$$+ \int_{\frac{w^2+\Delta^2}{w}}^{D_{max}} p_k \cdot \frac{4}{\pi} \cdot F\left(\frac{D}{D_{max}}\right) \cdot G_1(\Delta, w, D) \cdot dD \qquad (3.48)$$

$$A_x = \int_{2w}^{\frac{w^2+\Delta^2}{w}} p_k \cdot \frac{4}{\pi} \cdot F\left(\frac{D}{D_{max}}\right) \cdot G_4(\Delta,\ w,\ D) \cdot dD$$

$$+ \int_{\frac{w^2+\Delta^2}{w}}^{D_{max}} p_k \cdot \frac{4}{\pi} \cdot F\left(\frac{D}{D_{max}}\right) \cdot G_1(\Delta,\ w,\ D) \cdot dD \qquad (3.49)$$

with

$$G_1(\Delta,w,D) = D^{-3}\left(\sqrt{D^2 - (w^2+\Delta^2)}\ \frac{\Delta}{\sqrt{w^2+\Delta^2}} \cdot u_{max} - w \cdot u_{max} - u_{max}^2\right)$$

$$G_2(\Delta,w,D) = D^{-3}\{(\Delta - \sqrt{D^2 - (w^2+\Delta^2)}\ \frac{w}{\sqrt{w^2+\Delta^2}} \cdot u_{max} + (u_{max} + w) \cdot$$

$$\sqrt{\tfrac{1}{4} D^2 - (w + u_{max})^2} - w\ \sqrt{\tfrac{1}{4} D^2 - w^2} + \tfrac{1}{4} D^2 \arcsin \frac{w + u_{max}}{\frac{1}{2} D}$$

$$- \frac{D^2}{4} \arcsin \frac{2w}{D}\} dD$$

$$G_3(\Delta,w,D) = D^{-3}\ (\tfrac{1}{2} D - w)^2$$

$$G_4(\Delta,w,D) = D^{-3}\ (\frac{\pi}{8} D^2 - w\ \sqrt{\tfrac{1}{4} D^2 - w^2}\ - \frac{D^2}{4} \arcsin \frac{2w}{D})$$

$$F\left(\frac{D}{D_{max}}\right) = 0.727\ \left(\frac{D}{D_{max}}\right)^{0.5} - \left(\frac{D}{D_{max}}\right)^2 + 0.144\ \left(\frac{D}{D_{max}}\right)^4 + 0.036\ \left(\frac{D}{D_{max}}\right)^6 +$$

$$+ 0.016\ \left(\frac{D}{D_{max}}\right)^8 + 0.010\ \left(\frac{D}{D_{max}}\right)^{10}$$

$$u_{max} = \frac{-\frac{1}{2} w (w^2 + \Delta^2) + \frac{1}{2} \sqrt{w^2 (w^2 + \Delta^2)^2 - (w^2 + \Delta^2)\{(w^2 + \Delta^2)^2 - \Delta^2 D^2\}}}{(w^2 + \Delta^2)}$$

p_k = volume of aggregate/volume of concrete.

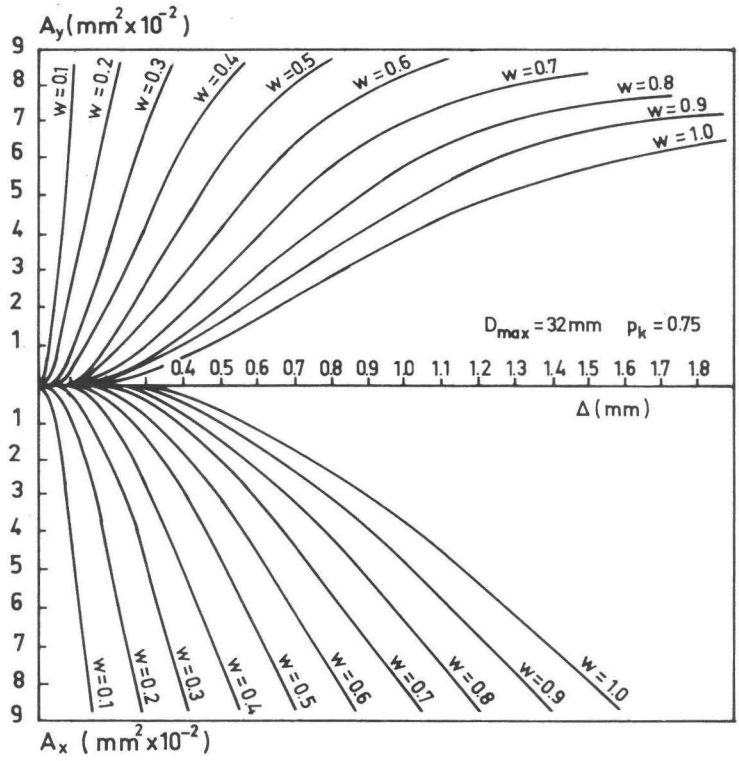

Fig. 3.24 Total projected contact areas A_y and A_x for 1 mm^2 crack plane, as a function of crack width w and shear displacement Δ, calculated with the equations (3.46 - 3.49)

Integration of (3.46 - 3.49) was performed numerically. For this purpose an Algol program was developed. For the text of this program see [85]. A stepwise integration in 10 steps appeared to be

accurate enough: an extension to 100 steps resulted in differences smaller than 2%. In this way the contact areas in the X- and Y-directions for a unit crack area of 1 mm^2 are obtained for varying (w, Δ) combinations.

Fig. 3.24 shows the result of a calculation for a concrete mix with a maximum aggregate particle diameter of 32 mm and a p_k value equal to 0.75.

The relations between the stress conditions in the crack on the one hand and the displacement components on the other hand were expressed earlier by the equations (3.4):

$$\sigma = \sigma_{pu} (A_x - \mu.A_y)$$
$$\tau = \sigma_{pu} (A_y + \mu.A_x) \qquad (3.50)$$

in which A_x and A_y depend on w and Δ (equations 3.46 - 3.49). The validity of these relations will be investigated in an experimental program. If it can be shown that good agreement exists between theory and experiments, the unknown parameters σ_{pu}, the yielding strength of the matrix, and μ, the coefficient of friction, will be established. The experimental part of the analysis is described in Chapter 4. The comparisons between experimental and theoretical values are made in Chapter 5.

4 EXPERIMENTS

4.1 General

In Chapter 2 it was concluded that lack of knowledge about the transmission of forces across cracks concerns predominantly aggregate interlock as an individual mechanism and its role in the interaction with other components in reinforced cracks. Accordingly, the experimental part of this research program was split into two parts. In one part, tests on pure aggregate interlock were carried out, the results of which were planned to be used for a direct comparison with the theory. In another part, tests on reinforced cracks were carried out in which the role of all parameters possibly influencing the behaviour was studied; for the interpretation of this part of the experiments the results of the first part have to be known.

In all, 83 tests have been carried out. Only the main aspects of this experimental program will be dealt with in this chapter. A full survey of all results, containing all measurements and technical details, has been given in [84].

4.2 Pure aggregate interlock tests

4.2.1 Test specimens, instrumentation and testing procedures

The tests were carried out on push-off specimens with external restraint bars of various stiffness (Fig. 4.1.a).
The shear area of all specimens was 36000 mm^2 (300 x 120 mm). The specimens were supported on roller bearings and were loaded by a vertical load, applied on top via a knife hinge. With this method of loading, shear without bending moment is produced in the shear plane. The head and the sides of the specimens were reinforced in order to avoid premature failure due to secondary cracks. Measurements of the crack width and the shear displacement were performed at two points on the front and at two on the back of the specimens,

by means of so-called plate spring gauges, which were directly mounted on the specimens and had an accuracy of 0.01 mm. The vertical external load was measured by a load cell. The passive restraint force normal to the crack plane was determined using strain gauges attached to the external bars, the force-strain relation of which was established before testing. The external bars were mounted in such a way that only axial forces could develop.

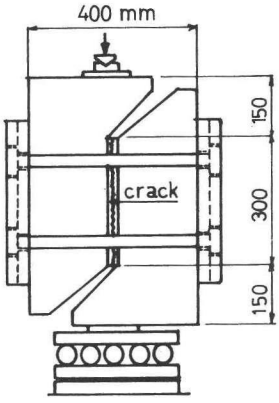

Fig. 4.1.a Test specimen with external restraint bars

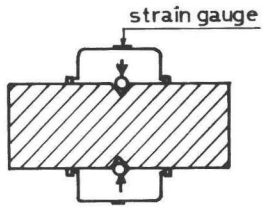

Fig. 4.1.b Precracking of a specimen

Prior to testing, the specimens were cracked along the shear plane by pulling steel rods in V-shaped grooves at the front and rear faces of the specimen (Fig. 4.1.b). The displacements of the specimen across the crack plane during this precracking operation were controlled by strain gauges.

During the actual shear test the specimens were subjected to a monotonically increasing load. During the first three minutes the shear displacement rate was 0.004 mm/min., which was subsequently increased to 0.02 mm/min. The tests were stopped when the shear displacement had reached a value of 2 mm.

4.2.2 Variables

The variables in the tests were the concrete strength and composition, the external restraint stiffness and the initial crack width. Four different concrete mixes were tested. Three of these had the same maximum particle size (16 mm) but different cube crushing strengths $f'_{cc} \approx$ (13, 37 and 59 N/mm^2), one had a maximum particle size of 32 mm and a cube strength of 33 N/mm^2.
The aggregate in all the mixes was distributed according to a Fuller grading curve, permitting a direct comparison with the theoretical values according to Chapter 3. Detailed data on the mixture compositions are listed in Table 4.I.

Table 4.I Mixture compositions in kg/m^3

		mix 1 *)	mix 3	mix 4	mix 5
Cement B		250	400	195	209
Water		156	160	165	104
Quartz powder		50	-	143	34
gravel/ sand	16 - 32 mm	-	-	-	598
	8 - 16 mm	613	702	682	507
	4 - 8 mm	433	378	378	227
	2 - 4 mm	307	306	296	80
	1 - 2 mm	217	224	215	106
	0.5 - 1 mm	153	114	113	219
	0.25- 0.5 mm	108	136	135	262
	0.1 - 0.25 mm	119	18	11	34
		1950	1878	1830	2033
Mixture weight in kg/m^3		2406	2438	2333	2380
f'_{cc}		29-37	56-60	13-20	33-38

*) Mix 2 is a variant of mix 1, only tested in reinforced specimens.

In order to obtain a wide range of displacement combinations (w, Δ), combined with stress measurements, three different initial crack widths have been chosen (0.0, 0.2 and 0.4 mm), in combination with varying external restraint stiffnesses against crack opening. It was not attempted to vary this restraint stiffness systematically, since it was not only a function of the diameter of the external bars, but depended also on the properties of the transverse plate on the short sides of the specimens and the thin layer of rapidly hardening sand-cement paste, which was necessary to ensure good bearing contact between these plates and the specimen.

4.2.3 Results

In all, 32 tests were carried out. Fig. 4.2 shows a characteristic set of results for mix 1 (see Table 4.I). The individual specimens have been assigned identifying numbers, consisting of three characteristics separated by oblique strokes. The first number denotes the mix number, the second the initial crack width in mm, and the third the restraint force per unit crack area (equivalent normal restraint stress) at a crack width of 0.6 mm (arbitrarily chosen).

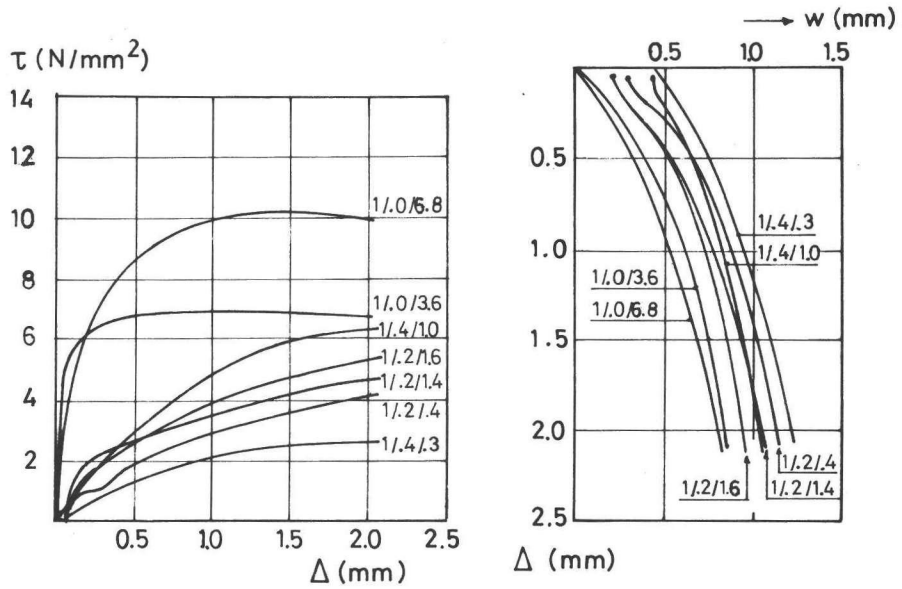

a b

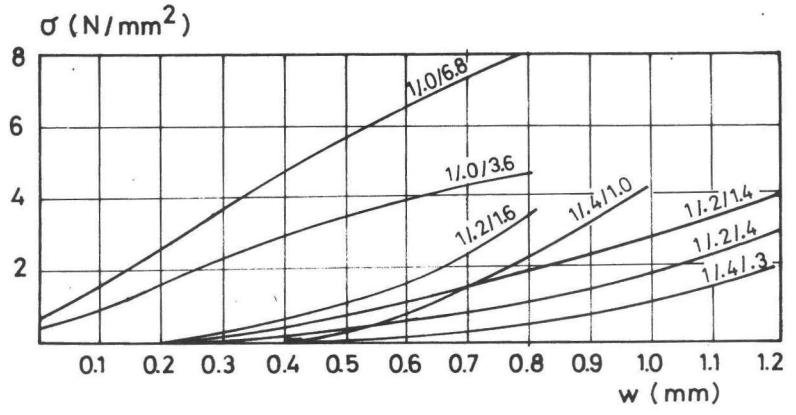

c

Fig. 4.2.a,b,c Set of results of tests, carried out on specimens made of concrete mixture type 1 (f'_{cc} = 37.6 N/mm^2)

Fig. 4.2.a shows the development of the average shear stress on the crack plane as a function of the shear displacement, Fig. 4.2.b shows the relation between the crack width and the shear displacement (crack opening path), and Fig. 4.2.c the average equivalent restraint stress normal to the crack plane as a function of the crack width. A characteristic feature was that in all experiments the crack opening path was influenced by the external restraint stiffness. This is shown in Fig. 4.3.a and b, in which the crack opening path has been represented for displacements of less than 0.5 mm for the tests on the specimens made of the mixes 1 (f'_{cc} = 37.6 - 38.5 N/mm^2) and 3 (f'_{cc} = 57.4 - 60.8 N/mm^2). It is seen that the crack opening path is steeper for greater restraint stiffness (note the last numbers of the specimen codes).

In none of the specimens tested in this part of the program were there any discernible secondary cracks influencing the behaviour of the specimens.

A substantial proportion of the results will be used in Chapter 5 for evaluating the theory. Therefore they will not be further dis-

cussed here; a complete survey of the results of all the tests can be found in [84].

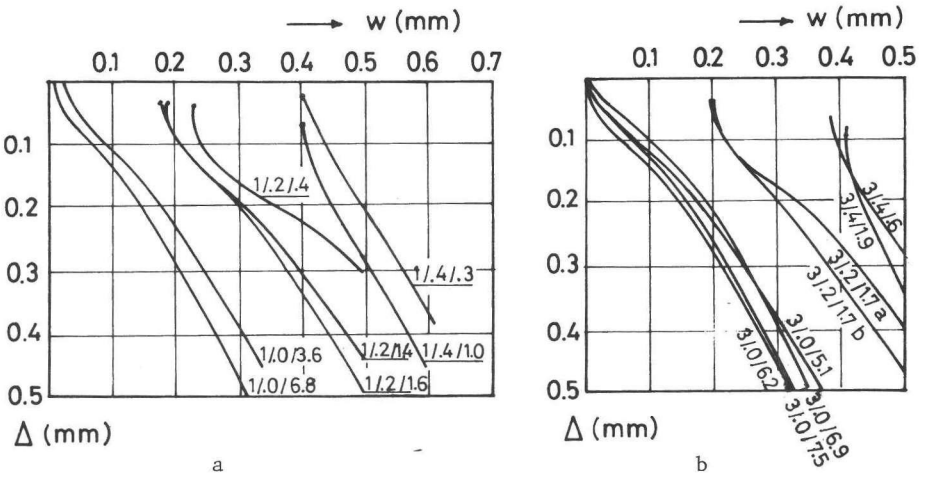

Fig. 4.3.a,b Crack opening paths for the mixes 1 and 3

It must be noted that all crack displacements represented here are the direct results of the measurements. As such these values include also some elastic deformations of the concrete adjacent to the crack, between the measuring points (see also the measuring devices in Fig. 4.5.b). It can be shown that these deformations are so small with regard to the crack displacement that they can be neglected. Furthermore the elastic deformations are not uniform over the length of the crack, so that a correction would be even rather speculative.

4.3 Tests on reinforced cracks

4.3.1 Specimens, instrumentation and testing procedures

The tests on reinforced cracks were also carried out on push-off specimens. Two variants were used, as shown in Fig. 4.4.a and b.

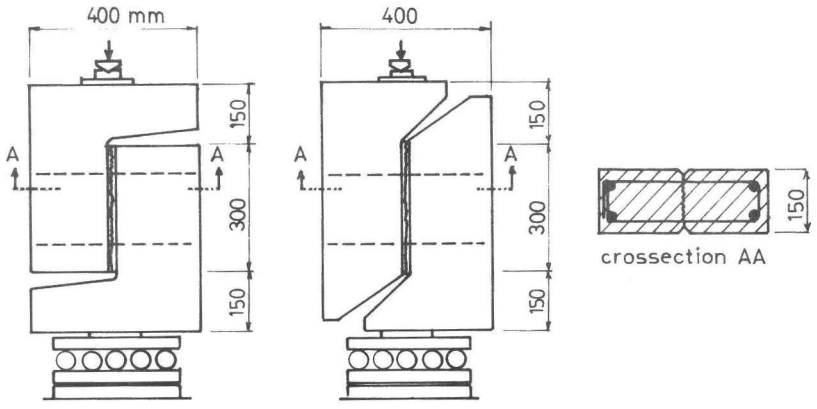

Fig. 4.4 Specimen geometries for tests on reinforced cracks

The geometry, represented in the left part of Fig. 4.4 (a) was used only in a limited number of tests. These tests were carried out as pilot tests in the early stage of the program. It appeared that the specimen shape shown in Fig. 4.4 (b) was somewhat more practical, not only because it enables inclined reinforcement to be used, but also because better introduction of stresses around the re-entrant angle is obtained. In both cases (a) and (b) the shear area was 36000 mm^2 (300 x 120 mm). Apart from the auxiliary reinforcement in the head and along the sides of the specimen, reinforcement was applied crossing the crack plane. This reinforcement consisted of closed stirrups, overlapped on one of the short sides to ensure effective anchorage.

Measurements of the crack width and the shear displacement were carried out across the crack on both sides of the specimens on three places (Fig. 4.5.a and b). With this configuration, which was not possible in the pure aggregate interlock tests, due to the position of the external restraint bars, control of the uniformity of the displacements was possible.

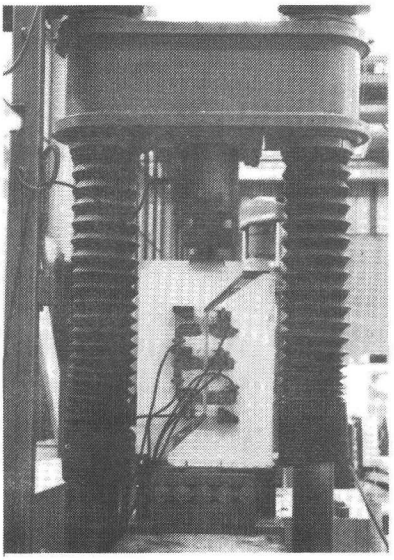

Fig. 4.5.a Test specimen during loading

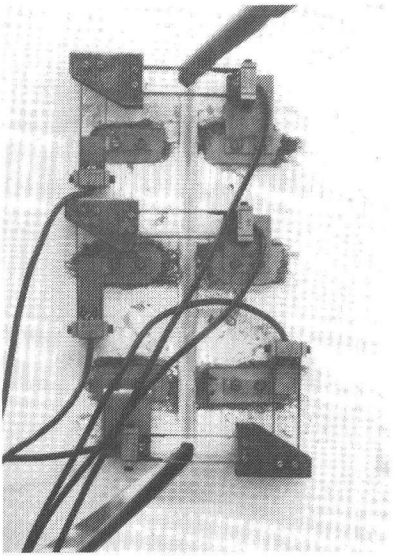

Fig. 4.5.b Measuring devices on the crack

The other test conditions were the same as in the case of external restraint bars; the specimens were supported on roller bearings and were loaded through a knife hinge at the top, during which the load was measured by means of a load cell. Also the precracking procedure and the actual shear tests were carried out in a comparable way.

4.3.2 Variables

Five different types of concrete were used. Apart from the mix types as applied in the tests on specimens with external restraint bars, represented in Table 4.I, a special gap-graded mix was designed, approximately similar to mix 1, except for the fact that all particles between 0.25 and 1 mm (the order of the crack displacements) were replaced by quartz powder: the weight of the remaining fractions was proportionally increased, in order to get the same total aggregate weight as in mix 1. This mix (further denoted as mix 2) was specially designed for investigating the statement found in [51] (see also section 2.4) that the behaviour of reinforced

cracks is probably a function of overriding of sand particles. If that were true, the omission of an important sand fraction would have to affect the results.

With all five concretes a basic series of four specimens was made, reinforced with 2, 4, 6 and 8 closed stirrups ϕ 8 mm, corresponding to reinforcement ratios of 0.56 - 2.24%. In the case of mix 1 this range was extended to 0.14% (2 stirrups ϕ 4 mm) and 3.36% (3 stirrups ϕ 16 mm). In order to investigate the influence of the bar diameter, additional specimens were made with the same reinforcement ratio as others, but different bar diameter: 7 stirrups ϕ 6 mm, comparable with 4 stirrups ϕ 8 mm, and 2 stirrups ϕ 16 mm, comparable with 8 stirrups ϕ 8 mm. Furthermore some tests were repeated with completely similar specimens, in order to obtain an impression of the scatter of the results. A schematical representation of the program is represented in Table 4.II.

Table 4.II Basic program of test on reinforced cracks

	Reinforcement ratio ρ_o Number of stirrups and diameters in mm					
Mix number and properties	0.14%	0.56%	1.12%	1.68%	2.24%	3.36%
Mix 1 D_{max} = 16 mm f'_{cc} = 29.4-36.6 N/mm^2	2 ϕ 4	2 ϕ 8	4 ϕ 8 7 ϕ 6	6 ϕ 8	8 ϕ 8 2 ϕ 16	3 ϕ 16
Mix 2 D_{max} = 16 mm f'_{cc} = 29.2-29.5 N/mm^2		2 ϕ 8	4 ϕ 8 7 ϕ 6	6 ϕ 8	8 ϕ 8 2 ϕ 16	
Mix 3 D_{max} = 16 mm f'_{cc} = 56.1 N/mm^2		2 ϕ 8	4 ϕ 8	6 ϕ 8	8 ϕ 8	
Mix 4 D_{max} = 16 mm f'_{cc} = 19.9 N/mm^2		2 ϕ 8	4 ϕ 8	6 ϕ 8	8 ϕ 8	
Mix 5 D_{max} = 32 mm f'_{cc} = 38.2 N/mm^2		2 ϕ 8	4 ϕ 8	6 ϕ 8	8 ϕ 8	

The stress-strain relations of the steel, used for the stirrups, are represented in Fig. 4.6.

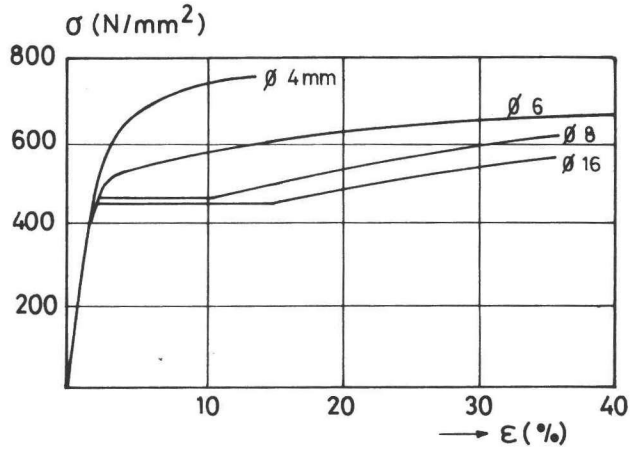

Fig. 4.6 Stress-strain relations for the steel, used for the stirrups

The initial crack widths in the tests were generally smaller than 0.04 mm. A number of specimens were unloaded after reaching the top of the load-shear displacement curve and subsequently reloaded in order to obtain an impression of the behaviour under repeated loading.
Additionally to the specimens represented in Table 4.II, some specimens were made with a somewhat greater initial crack width (0.07 - 0.09 mm), to see how this would affect the results.
Next, the influence of inclination of the reinforcement was investigated in a separate series of specimens, made of concrete mix 1 with f'_{cc} = 34.2 N/mm^2, which were all reinforced with 2 stirrups ø 8 mm, inclined at various angles with the crack plane (45°, 68°, 90°, 112° and 135°, in which for 90° the average results of earlier tests (Table 4.II) were used).

4.3.3 Results

In none of the specimens were secondary cracks inclined to the pre-

formed crack observed, as reported in [51] for comparable specimens. In some of the more heavily reinforced specimens, spalling of the concrete at the ends of the crack occurred (Fig. 4.7).

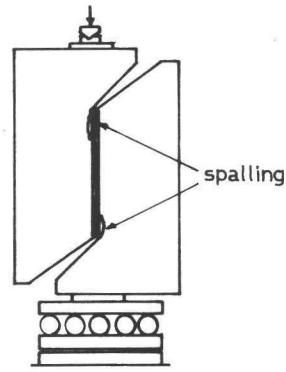

Fig. 4.7 Local spalling in some of the heavily reinforced specimens

This phenomenon was more significant for lower concrete strengths: for mix 4 (f'_{cc} = 19.9 N/mm^2) spalling was observed in the specimens with 6 and 8 stirrups ϕ 8 mm, resulting in a reduction of the fully resisting shear plane of, on a rough estimate, 15 - 25%. However, for mix 3, with f'_{cc} = 56.1 N/mm^2, even for 8 stirrups ϕ 8 mm there was no spalling. Furthermore it was observed that the specimens of the type shown in Fig. 4.4.a (left) were more susceptible to this spalling than the others. Therefore this type was abandoned after a limited number of tests on the specimens made of the concretes type 1 and 2 (Table 4.II). A later attempt to establish the influence of the shape, by reproducing some specimens of these series, but with the improved geometry, was not fully succesful, because the concrete strength was found to be 20% higher than in the first case. Anyhow, this phenomenon of spalling has to be taken into account when interpreting the results of some of the heavily reinforced specimens.

The measurements at the various levels of the crack (Fig. 4.5) did

not exhibit significant differences.
The most important features of the results will now be presented. Detailed information on all the individual tests can be found in [84].

a. Repetition of similar tests and initial crack width:

Two results of repeated similar tests are shown in Fig. 4.8 and 4.9 (solid lines). In both cases (mix 1, 2 stirrups ϕ 8 mm in Fig. 4.8 and mix 1, 8 stirrups ϕ 8 mm in Fig. 4.9) good agreement is obtained. Testing similar specimens with greater initial crack widths (dashed lines) showed that the crack faces did not immediately jump on the original crack opening path, but rather tended to join it very steadily (Fig. 4.8.b and 4.9.b). The development of the shear stress as a function of the shear displacement was also retarded, but tended to reach the same level.

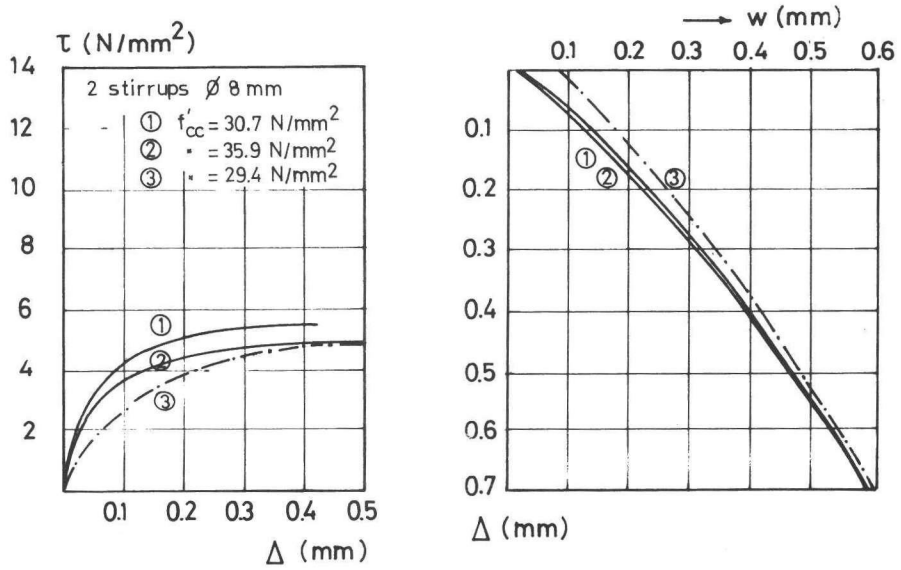

Fig. 4.8 Shear stress-shear displacement relation (a) and crack opening path (b) for three specimens made of mix 1, reinforced with 2 stirrups ϕ 8 mm (ρ_o = 0.56%).

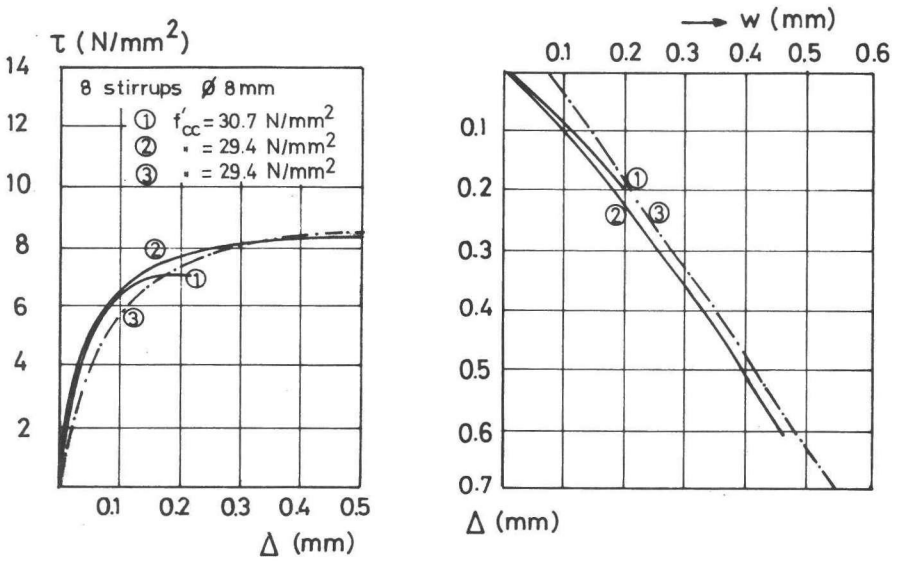

a b

Fig. 4.9 Shear stress-shear displacement relation (a) and crack opening path (b) for three specimens made of mix 1, reinforced with 8 stirrups ϕ 8 mm (ρ_o = 2.24%)

b. Unloading and reloading:

In all cases unloading and reloading resulted in a considerable amount of hysteresis. If the test was continued immediately, no influence of load history was manifest. In some tests, reloading was carried out after 5 months. In that case the shear resistance seemed to have increased as a result of the strength development of the concrete in this period. The crack opening path was apparently not affected. Fig. 4.10 shows a representative result of a test on a specimen made of mix 1 (f'_{cc} = 30.7 N/mm^2) and reinforced with 4 stirrups ϕ 8 mm.

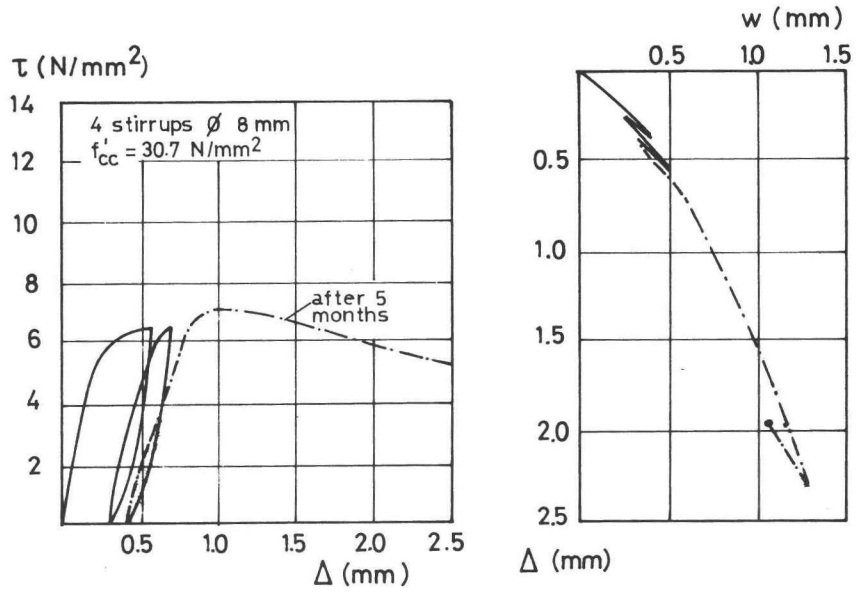

a b

Fig. 4.10 The effect of unloading and reloading after a short time and after a long time (5 months: dashed line) on the shear stress-shear displacement relation (a) and on the crack opening path (b) of a specimen made of concrete mix 1 and reinforced with 4 stirrups ϕ 8 mm (ρ_o = 1.12%)

c. The influence of the bar diameter at constant reinforcement ratio and constant concrete quality:

Only very slight differences between comparable tests occurred. The greatest deviation was found between specimens made of mix 2, one reinforced with 2 stirrups ϕ 16 mm and one with 8 stirrups ϕ 8 mm. It is seen that even in this case the differences were insignificant.

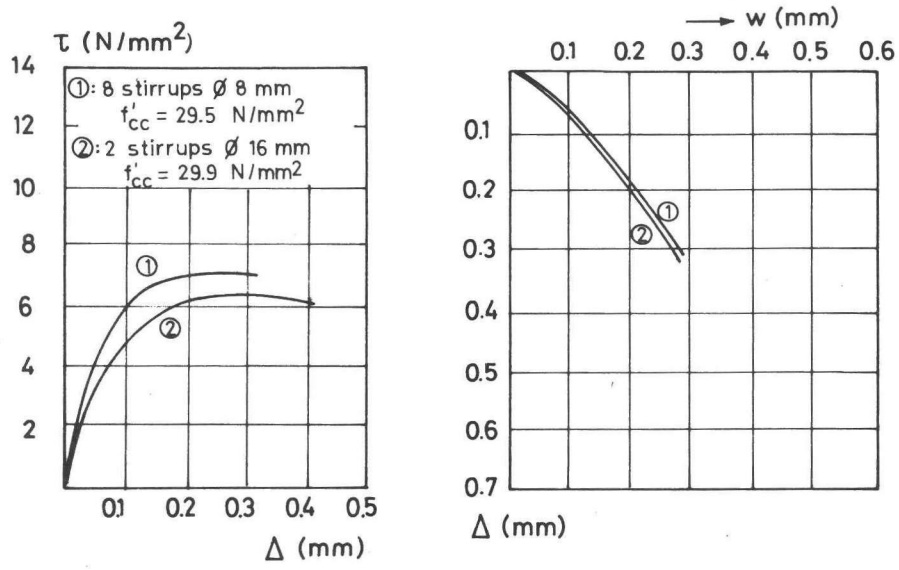

Fig. 4.11 The influence of the variation of bar diameter at constant reinforcement ratio on the shear stress-shear displacement relation (a) and on the crack opening path (b) for two specimens, one reinforced with 8 stirrups ϕ 8 mm and one with 2 stirrups ϕ 16 mm (ρ_o = 2.24%)

d. Concrete type and reinforcement ratio:

The influence of these parameters can be studied by comparing Figs. 4.12 - 4.13 representing the shear stress-shear displacement relations (left) and the crack opening paths (right) for a number of basic series (see also Table 4.II).
It is seen that for all individual concrete qualities an increase of the shear strength is obtained with increased reinforcement ratio. The crack opening path, however, seems not to be significantly influenced by the reinforcement ratio. It is to be noted that this result is contrary to what has been observed in the tests on specimens with external restraint bars, exhibiting

a dependence of the crack opening path on the restraint stiffness (Fig. 4.3). On comparing the diagrams of Fig. 4.12 it is clear that the shear resistance increases with higher concrete strength.

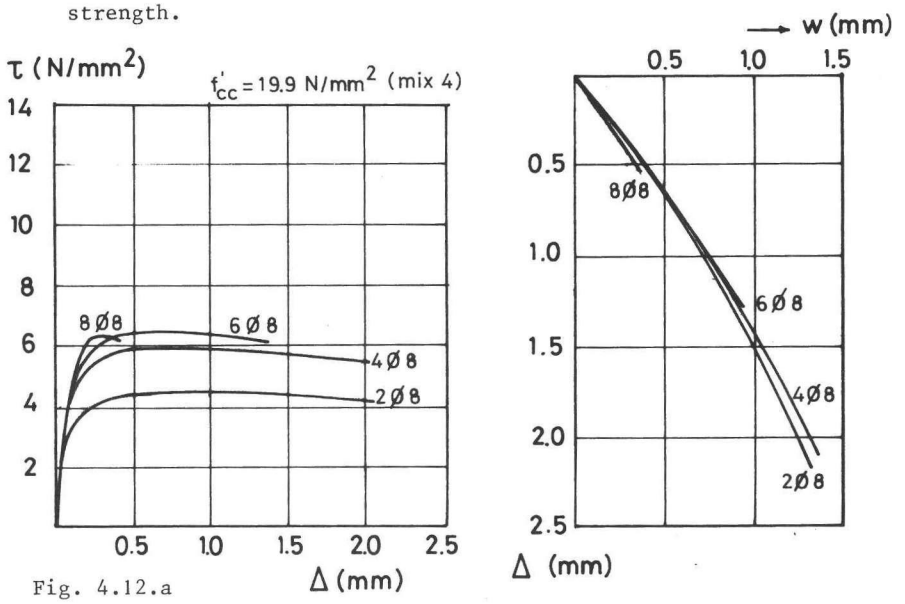

Fig. 4.12.a

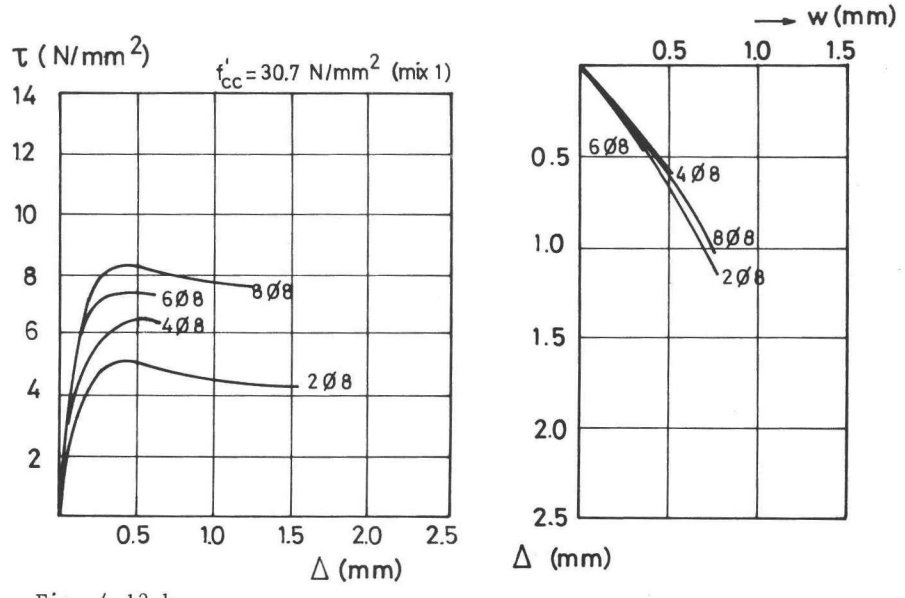

Fig. 4.12.b

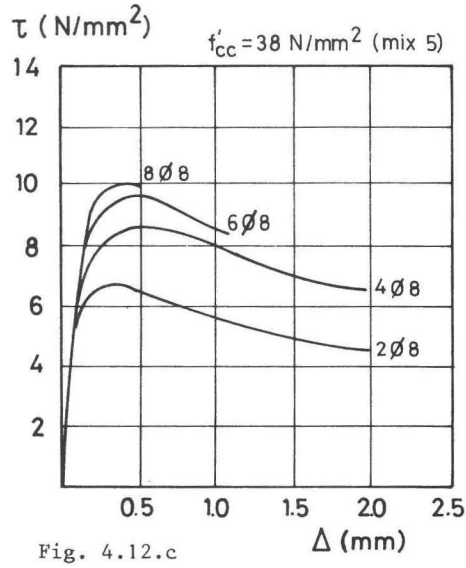

Fig. 4.12.c

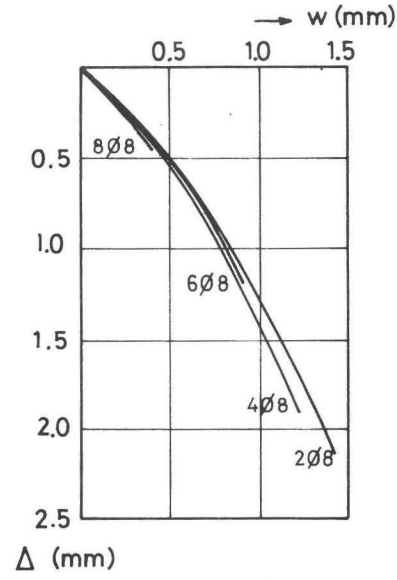

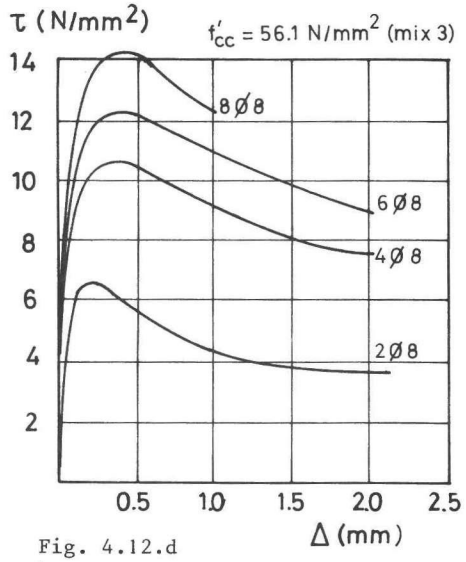

Fig. 4.12.d

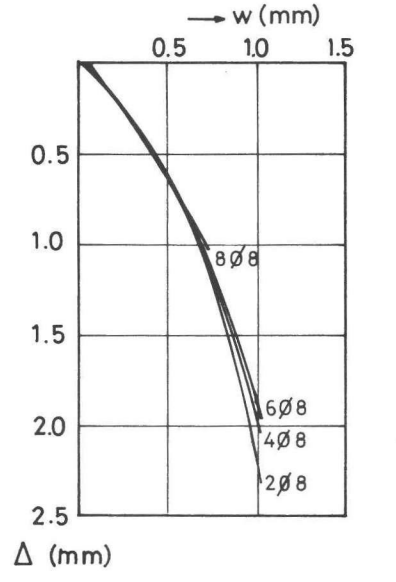

Fig. 4.12 Shear stress-shear displacement relations (left) and crack opening paths (right) for four basic series, all containing four specimens, reinforced with 2, 4, 6 and 8 stirrups ϕ 8 mm (ρ_o = 0.56 - 2.24%)

4.12.a: Mix 4: f'_{cc} = 19.9 N/mm², D_{max} = 16 mm

b: Mix 1: f'_{cc} = 30.7 N/mm², D_{max} = 16 mm

c: Mix 5: f'_{cc} = 38.2 N/mm², D_{max} = 32 mm

d: Mix 3: f'_{cc} = 56.1 N/mm², D_{max} = 16 mm

Also the series with concrete type 5, in which the maximum aggregate diameter was twice that of the other series, seems to fit into this generally observed regularity. Besides, the influence of the concrete strength on the crack opening path is rather small. The crack opening lines for the concretes with strengths between 19.9 and 38.2 N/mm^2 nearly coincide. The lines of mix 3, with f'_{cc} = 56.1 N/mm^2, deviate slightly (greater shear displacements). An explanation for this difference may be that in the high-strength concrete a number of particles are intersected by the crack, so that greater shear displacements are necessary to obtain the same contact area between the crack faces.

Finally, in Fig. 4.13 a diagram is shown in which all the results of the tests carried out on specimens made of concrete type 1 are represented. The solid lines resulted from the tests of the basic series (Table 4.II); the dashed lines are the results obtained in additional tests, carried out with the improved specimen geometry (Fig. 4.4.b).

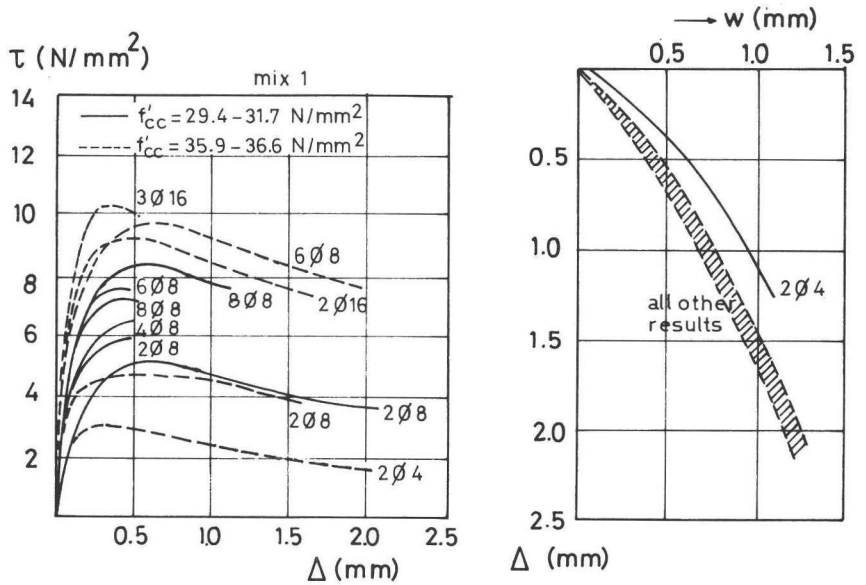

Fig. 4.13 Shear stress-shear displacement relations and crack opening paths for all the tests carried out on specimens made of concrete type 1

It is seen that only the crack opening path of the specimen with 2 stirrups ϕ 4 mm (ρ_o = 0.14%) deviated. All the others, with $0.56 \leq \rho_o \leq 2.24\%$, were located between narrow limits.

e. Gap-graded concrete:

Fig. 4.14 shows the comparison between the results of the basic series, made of concrete type 1 with a continuous grading curve, and those of the basic series, made of concrete mix 2 with a discontinuous grading curve, in which all particles between 0.25 and 1 mm were eliminated. It appears that there is no perceptible influence.

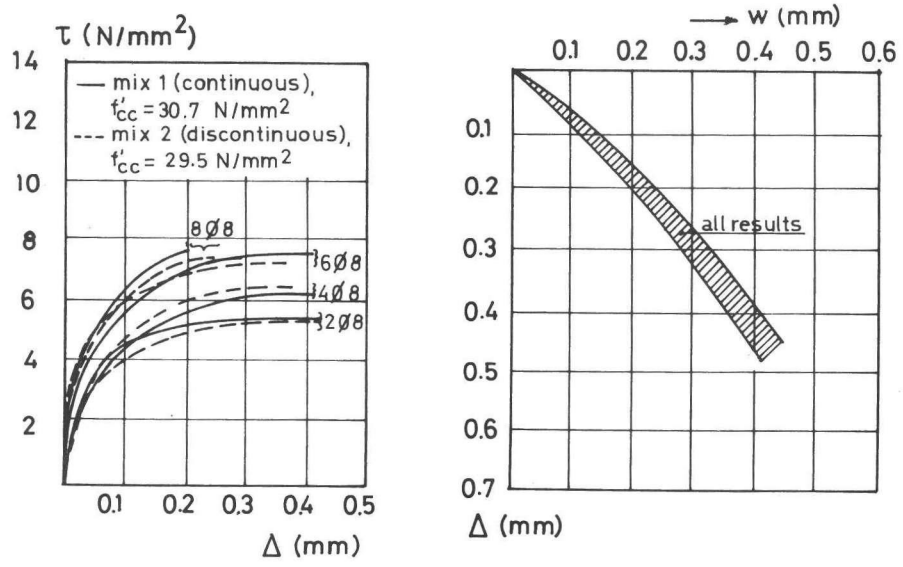

Fig. 4.14 Shear stress-shear displacement relations and crack opening paths for basic series with discontinuous and continuous grading curves

f. The influence of the inclination of the reinforcement to the crack plane:

Fig. 4.15 shows that the effectiveness of the reinforcement is increased with decreasing value of θ. The crack opening paths are similar for all inclinations, except for $\theta = 135^{o}$.

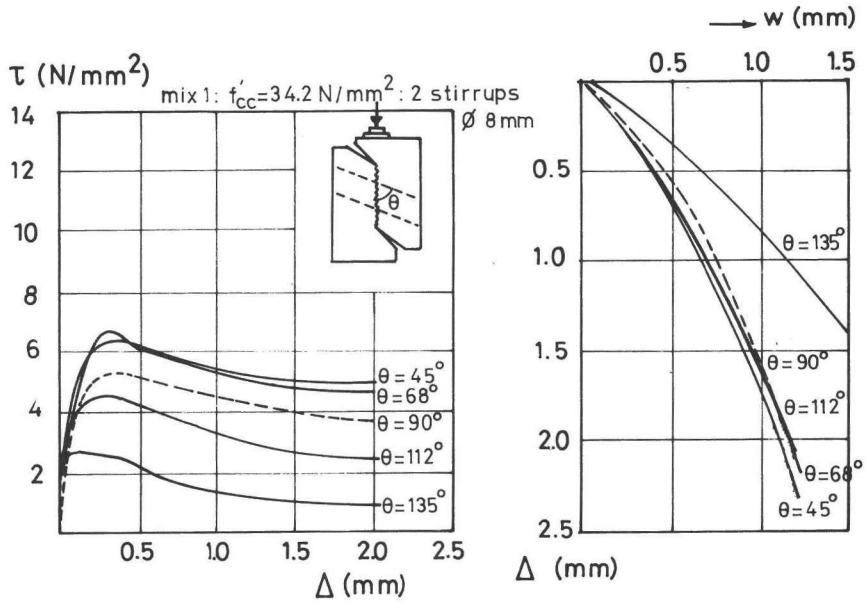

Fig. 4.15 Shear stress-shear displacement relations and crack opening paths for various inclinations of the reinforcement

5 INTERPRETATIONS AND FURTHER ANALYSIS

This chapter, like the previous one, is subdivided into two parts. The first deals with pure aggregate interlock: the experiments are used to evaluate the theory and subsequently the theory is used for further analysis. The second focuses on the transmission of forces in reinforced cracks. For the interpretation of this second part, the results of the first part are used.

5.1 Aggregate interlock

5.1.1 Comparison of theory and results

The relations between the stresses in a crack on the one hand and the displacement components on the other hand have earlier been formulated as:

$$\sigma = \sigma_{pu} (A_x - \mu . A_y)$$
$$\tau = \sigma_{pu} (A_y + \mu . A_x) \qquad (3.50)$$

in which A_x and A_y depend on the crack width w, the shear displacement Δ, the maximum particle diameter D_{max} and the total aggregate volume per unit volume of the concrete p_k, as expressed in the functions (3.46 - 3.49).
The parameters σ_{pu}, the matrix yielding strength and the coefficient of friction μ, are established by fitting the equations (3.50) to be experimental results obtained in the tests on specimens with external restraint bars (Fig. 5.1 - 5.4). It appeared that the best results are obtained for a friction coefficient of $\mu = 0.50$ for all mixes. The matrix yielding strength σ_{pu}, which has to be inserted to get optimal fitting, depends on the uniaxial concrete strength. The best results are obtained for

$$\sigma_{pu} = 5.83 \, f'^{0.63}_{cc} \qquad (5.1)$$

These values for μ and σ_{pu} are in adequate agreement with what was expected (section 3.2): the coefficient of friction μ is of the same order as found by Weiss [88] in his tests; the matrix yielding strength is higher than the uniaxial cube compressive strength, whilst a tendency to lower relative matrix strength for higher concrete strength is reflected by equation (5.1), which can be represented in a modified form as $\sigma_{pu}/f'_{cc} = 5.83\ f'^{-0.37}_{cc}$. It must be realized that this is only a provisional, approximate relation. Actually the relation between σ_{pu} and f'_{cc} is not unique.

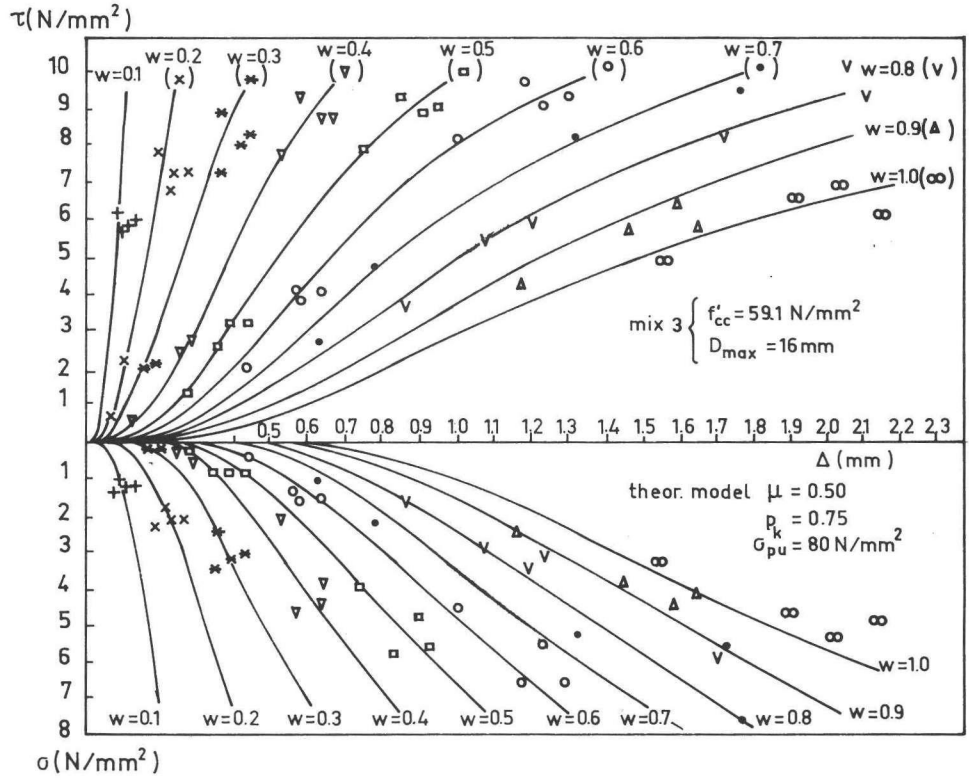

Fig. 5.1 Comparison between experimental values for mix 3 (f'_{cc} = 59.1 N/mm^2, D_{max} = 16 mm) and theoretical model, with p_k = 0.75, μ = 0.50 and σ_{pu} = 80 N/mm^2

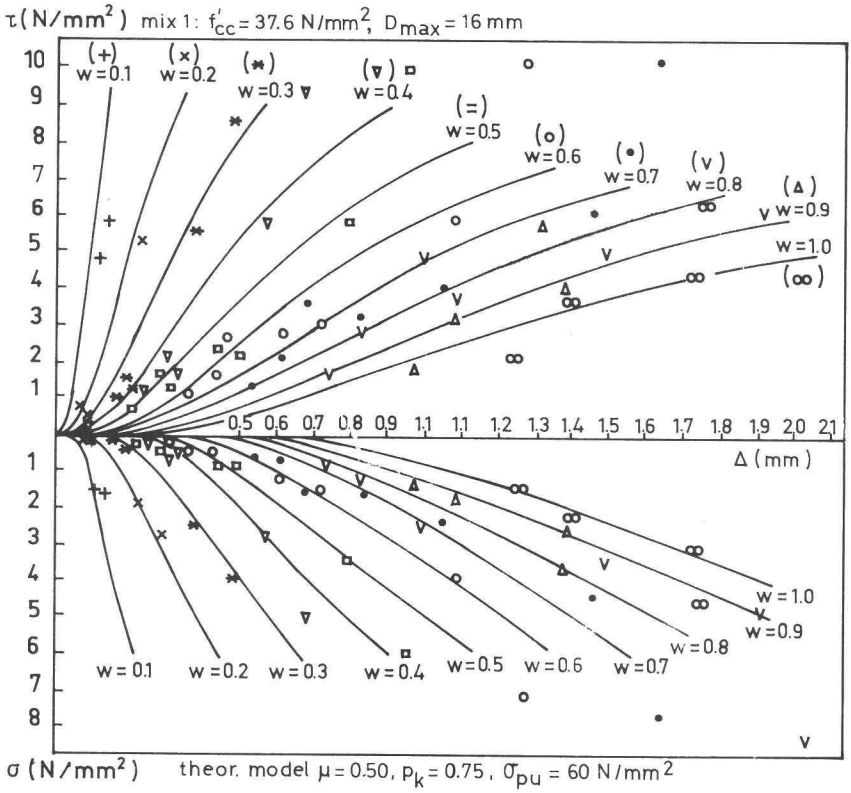

Fig. 5.2 Comparison between experimental values for mix 1 (f'_{cc} = 37.6 N/mm², D_{max} = 16 mm) and theoretical model, with p_k = 0.75, μ = 0.50, σ_{pu} = 60 N/mm²

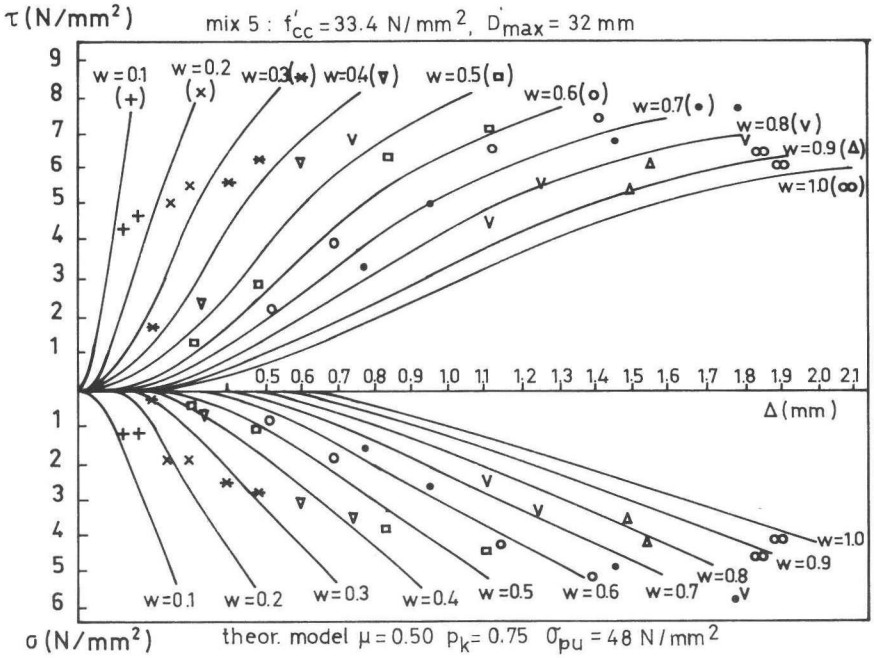

Fig. 5.3 Comparison between experimental values for mix 5 (f'_{cc} = 33.4 N/mm², D_{max} = 32 mm) and theoretical model, with p_k = 0.75, μ = 0.50, σ_{pu} = 48 N/mm²

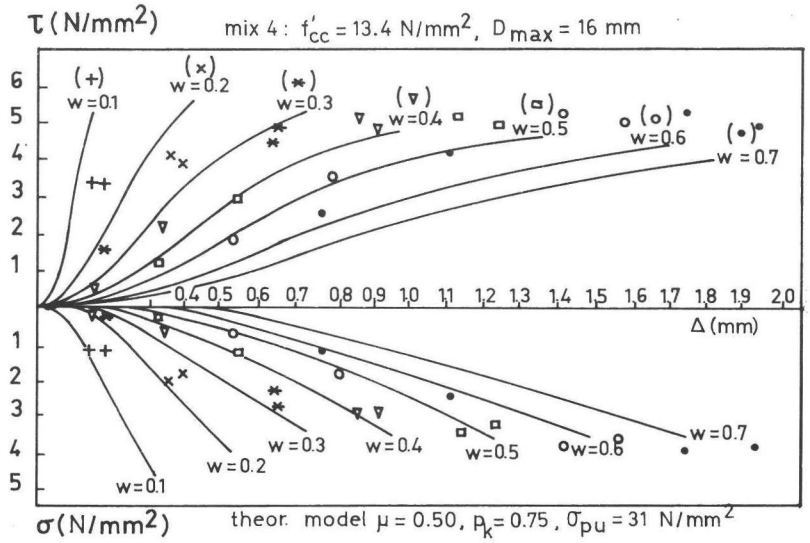

Fig. 5.4 Comparison between experimental values for mix 4 (f'_{cc} = 13.4 N/mm², D_{max} = 16 mm) and theoretical model, with p_k = 0.75, μ = 0.50, σ_{pu} = 31 N/mm²

An example is represented in Fig. 5.5, which shows that for the same matrix the prism compressive strength varies as a function of the scale of the aggregate. In order to avoid too great complexity, such effects are not taken into account.

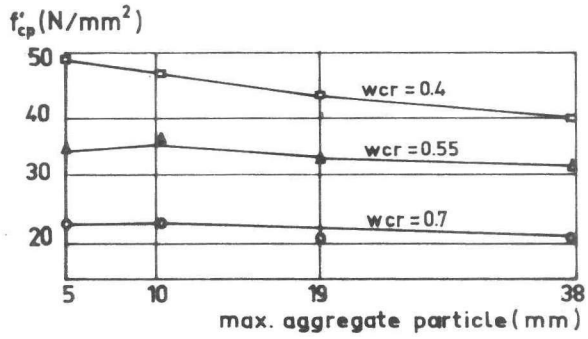

Fig. 5.5 The influence of the maximum particle size on the prism compressive strength for various water-cement ratios, according to Cordon and Gillespie [14]

5.1.2 Analysis of some aspects of aggregate interlock on the basis of the model developed

The model that has been developed allows a further analysis of the phenomenon. Some aspects will be dealt with:

a. The role of friction between the aggregate particles and the matrix material.

It was shown that equilibrium in the contact area was obtained by combinations of normal (yielding) stresses and shear (friction) stresses. It was shown that with a friction coefficient equal to 0.5 the best fitting of the curves to the experimental results was obtained. By doing a calculation with a friction coefficient $\mu = 0$ the influence of friction can be visualized.

A calculation is carried out for a mix with maximum aggregate size D_{max} = 16 mm, σ_{pu} = 48 N/mm^2, p_k = 0.75 and μ = 0.0 resp. 0.5. The results are shown in Fig. 5.6 for some crack widths (w = 0.2, 0.6 and 1.0 mm).

It is seen that the friction increases the shear stress by up to about 50%, whereas the normal restraint stresses to provide equilibrium are reduced.

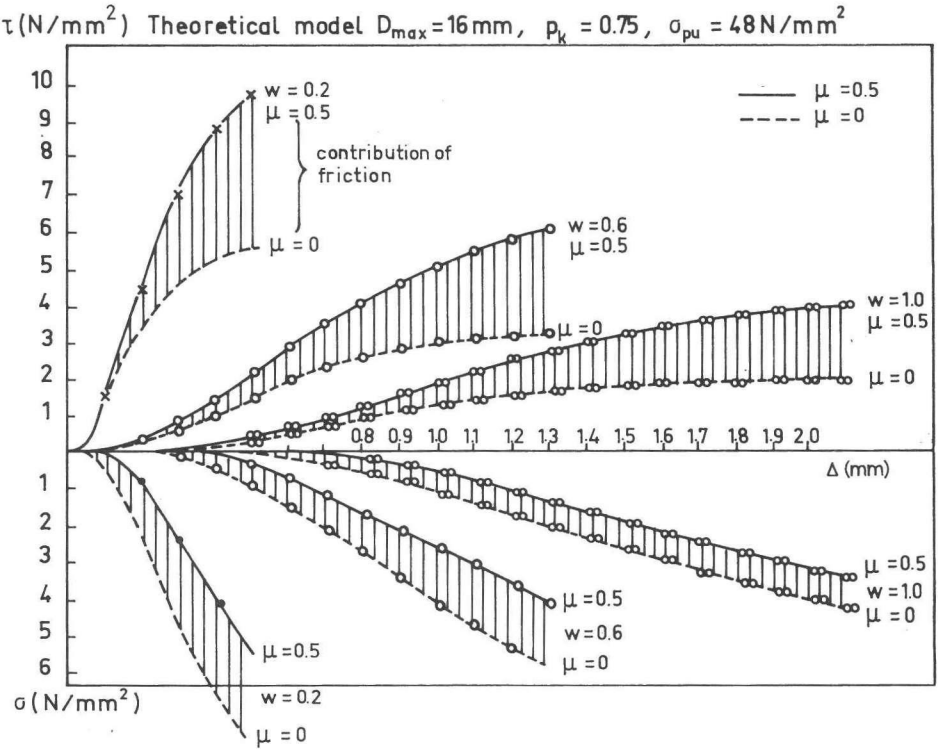

Fig. 5.6 The role of friction between aggregate and matrix in the transfer of stresses in a crack

b. The contribution of the various aggregate fractions to the transfer of stresses in a crack.

By a slight modification in the derivation of the equations re-

presenting the relations between stresses and displacements in the crack it is possible to ascertain the contribution of only a part of the aggregate particles.
The equation (3.15) was found by integrating the product of equation (3.7) and (3.11) over the range $D_o \rightarrow D_{max}$. By integrating only over the range $D_o \rightarrow n.D_{max}$ ($n < 1$) the cumulative distribution function is obtained, representing the probability that an arbitrary point in the concrete body, located in a Z-intersection plane, is situated in an intersection circle with a diameter $D < D_o$, with as an additional condition that it must also be situated in a sphere with a diameter $D < n.D_{max}$. An elaboration of this integration results in a modified expression (3.15):

$$p_c(D < D_o) = p_k(1-n^{\frac{1}{2}} + 1.455\ D_o^{0.5}\ D_{max}^{-0.5} - 0.50\ n^{-1.5}\ D_o^{2}\ D_{max}^{-2} +$$

$$+ 0.036\ n^{-3.5}\ D_o^{4}\ D_{max}^{-4} + 0.006\ n^{-5.5}\ D_o^{6}\ D_{max}^{-6} +$$

$$+ 0.002\ n^{-7.5}\ D_o^{8}\ D_{max}^{-8} + 0.001\ n^{-9.5}\ D_o^{10}\ D_{max}^{-10})$$

The probability density function is obtained by differentiation with respect to D_o:

$$p'_c(D_o) = p_k.(0.727\ D_o^{-0.5}\ D_{max}^{-0.5} - n^{-1.5}\ D_o\ D_{max}^{-2} +$$

$$+ 0.144\ n^{-3.5}\ D_o^{3}\ D_{max}^{-4} + 0.036\ n^{-5.5}\ D_o^{5}\ D_{max}^{-6} +$$

$$+ 0.016\ n^{-7.5}\ D_o^{7}\ D_{max}^{-8} + 0.01\ n^{-9.5}\ D_o^{9}\ D_{max}^{-10})$$

On substituting this expression into (3.19), and (3.19) into

(3.42 - 3.45), the same set of final equations (3.46 - 3.49) is obtained, with only a modified expression for $F(\frac{D}{D_{max}})$:

$$F(\frac{D}{D_{max}}) = 0.727(\frac{D}{D_{max}})^{0.5} - n^{-1.5}(\frac{D}{D_{max}})^{2} + 0.144\, n^{-3.5}(\frac{D}{D_{max}})^{4} +$$

$$+ 0.036\, n^{-5.5}(\frac{D}{D_{max}})^{6} + 0.016\, n^{-7.5}(\frac{D}{D_{max}})^{8} +$$

$$+ 0.010\, n^{-9.5}(\frac{D}{D_{max}})^{10} \qquad (5.2)$$

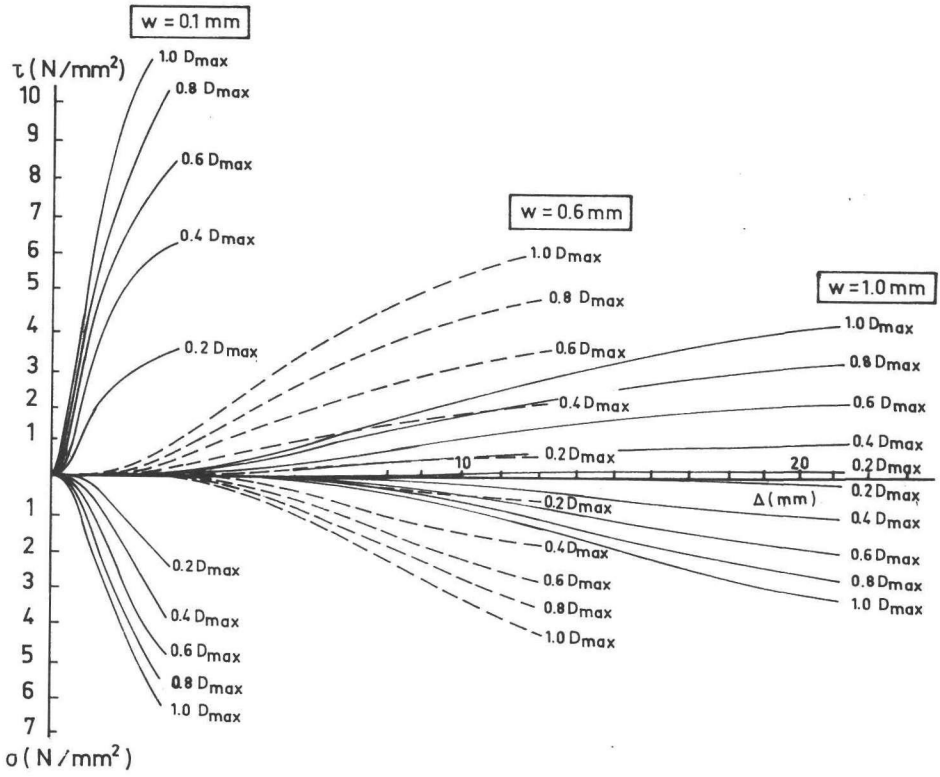

Fig. 5.7 Contributions of the various aggregate fractions to the transfer of stresses in cracks for crack widths w = 0.1, 0.6 and 1.0 mm (Mix: σ_{pu} = 48 N/mm², p_k = 0.75, μ = 0.50, D_{max} = 16 mm)

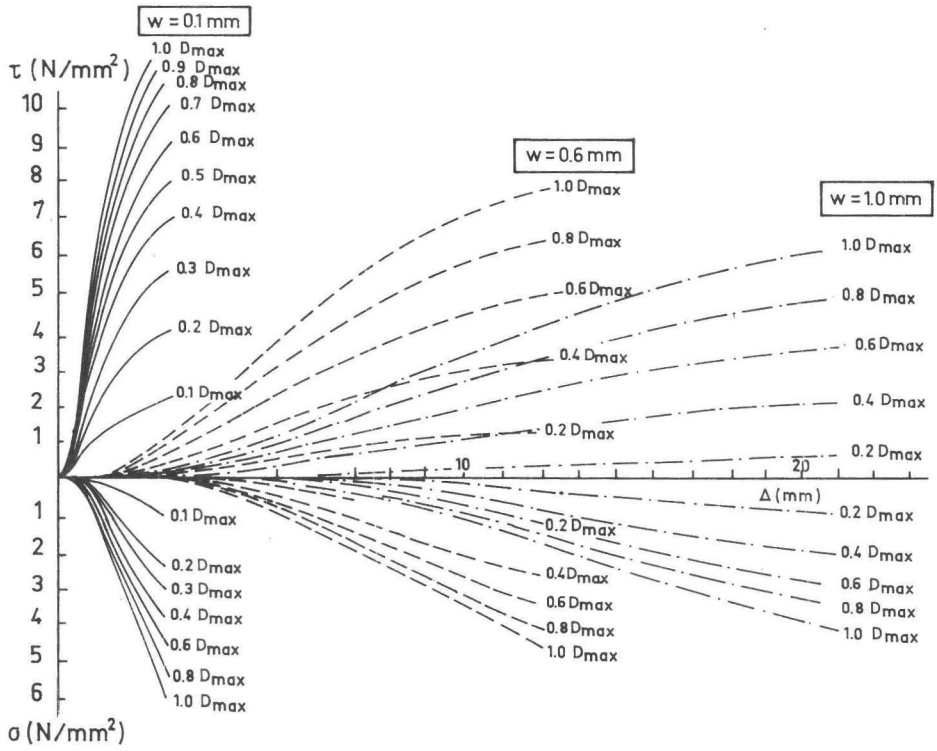

Fig. 5.8 Contributions of the various aggregate fractions to the transfer of stresses in cracks for crack widths w = 0.1, 0.6 and 1.0 mm (Mix: σ_{pu} = 48 N/mm^2, p_k = 0.75, μ = 0.50, D_{max} = 32 mm)

With these equations the contributions of a number of fractions have been established and represented for a small (0.1 mm), an average (0.6 mm) and a large (1.0 mm) crack width. Two mixes were analysed, both with σ_{pu} = 48 N/mm^2, μ = 0.50, p_k = 0.75, but different maximum aggregate size (D_{max} = 16 mm and D_{max} = 32 mm). (Fig. 5.7 and 5.8).

The curves in these diagrams represent the relations between σ, τ, w and Δ, if only the particles with a diameter between 0 and a varying fraction of D_{max} are considered. It is seen that

the small aggregate fractions lose importance as the crack width increases.

c. Scale effect of the aggregate.

To obtain some idea of the effect of the scale of the aggregate, two mixes were compared. Both had the same properties, except for the maximum particle diameter, which was 16 mm and 32 mm respectively. The results of this comparison are shown in Fig. 5.9.

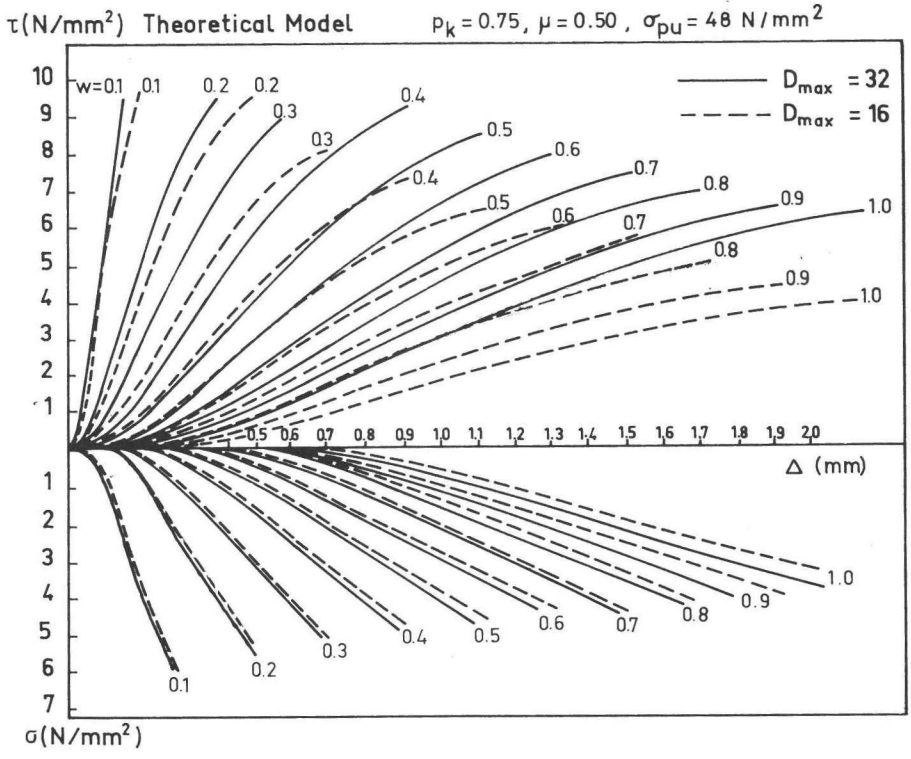

Fig. 5.9 The effect of the maximum aggregate particle size on the transfer of stresses in a crack. Maximum diameter D_{max} = 16 and 32 mm. Mix properties: p_k = 0.75, μ = 0.50, σ_{pu} = 48 N/mm², Fuller aggregate distribution

It is seen that the normal stress σ is not very susceptible to this variation, but that the shear stress τ is more affected according as the crack width is greater. This tendency is confirmed by the results of the experimental part of this investigation (Fig. 5.2 and 5.3).

d. Effect of grading curve.

In the previous analyses and in the experiments a Fuller-curve was always adopted. However, in practice most Codes allow a permissible grading curve region. The ideal Fuller-curve is near the lower boundary of this area. To study the influence of the grading curve a curve is chosen which approximates to the upper limit given in the Netherlands Code of Practice, the VB'74, for D_{max} = 16 mm and D_{max} = 32 mm (Fig. 5.10 and 5.12).
The relations between stresses and displacements for the concrete confirming to the grading curves B in Fig. 5.10 and 5.12 were calculated. Other values adopted for D_{max} = 16 mm and D_{max} = 32 mm were p_k = 0.75, μ = 0.50 and σ_{pu} = 48 N/mm^2.
Although these concretes have the same maximum particle diameter D_{max} as the comparable Fuller mixes, they contain a much higher proportion of sand particles. The results previously obtained under b, where the contribution of the individual aggregate fractions to the transfer of stresses in a crack was established, were used for the calculations. The results for the concretes, designed with the grading curves B are represented in the Figs. 5.11 and 5.13 by the dashed lines, and are compared with the results for the Fuller concretes calculated earlier (Fig. 5.9).
It is seen that in both cases the influence of the grading curve on the normal stresses σ is not great, but is significant for the shear stresses. The most pronounced differences are obtained for larger crack widths. This is to be expected, since the sandy mixes according to curve B provide a smaller potential contact area for larger crack width.

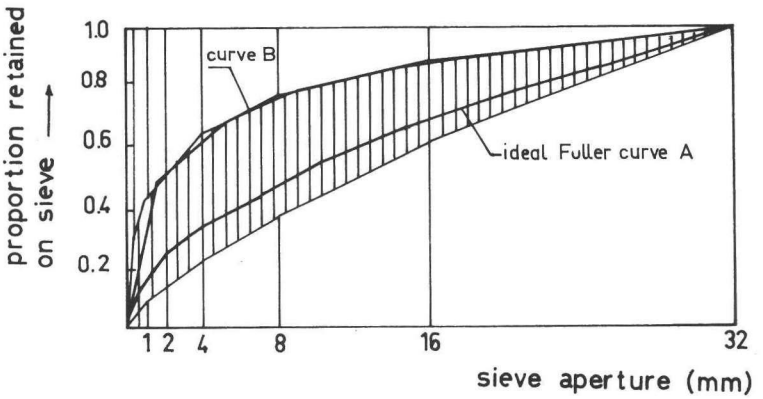

Fig. 5.10 Permissible grading curve region in the VB'74 for D_{max} = 32 mm

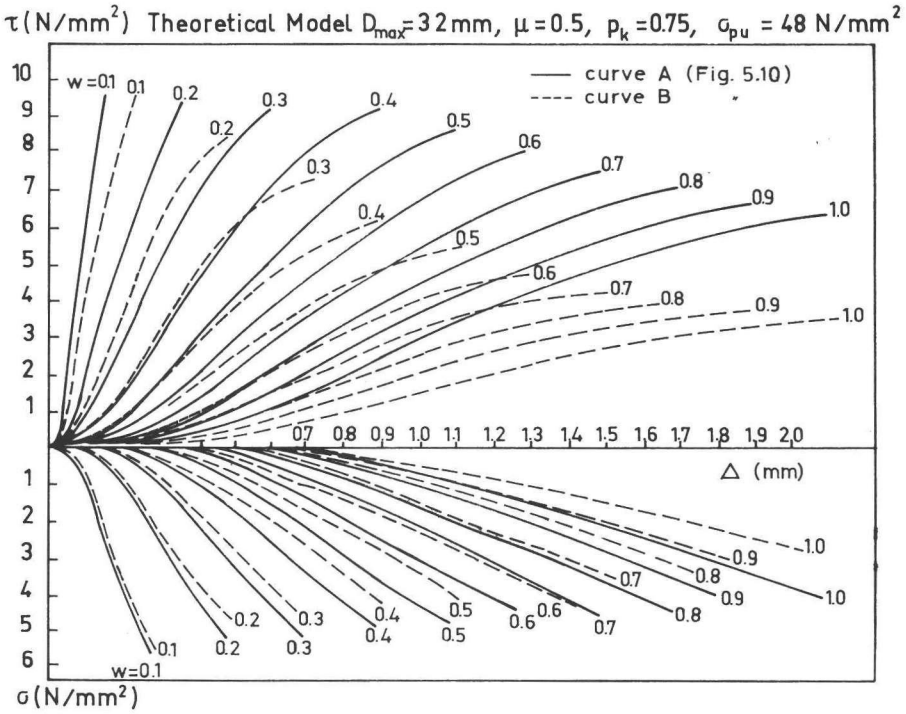

Fig. 5.11 The effect of the grading curve on the transfer of stresses in a crack for two comparable mixes confirming to different grading curves (D_{max} = 32 mm, p_k = 0.75, σ_{pu} = 48 N/mm², μ = 0.50)

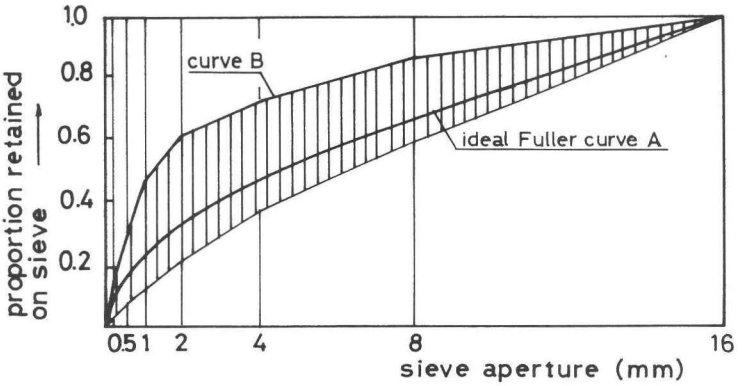

Fig. 5.12 Permissible grading curve region in the VB'74 for D_{max} = 16 mm

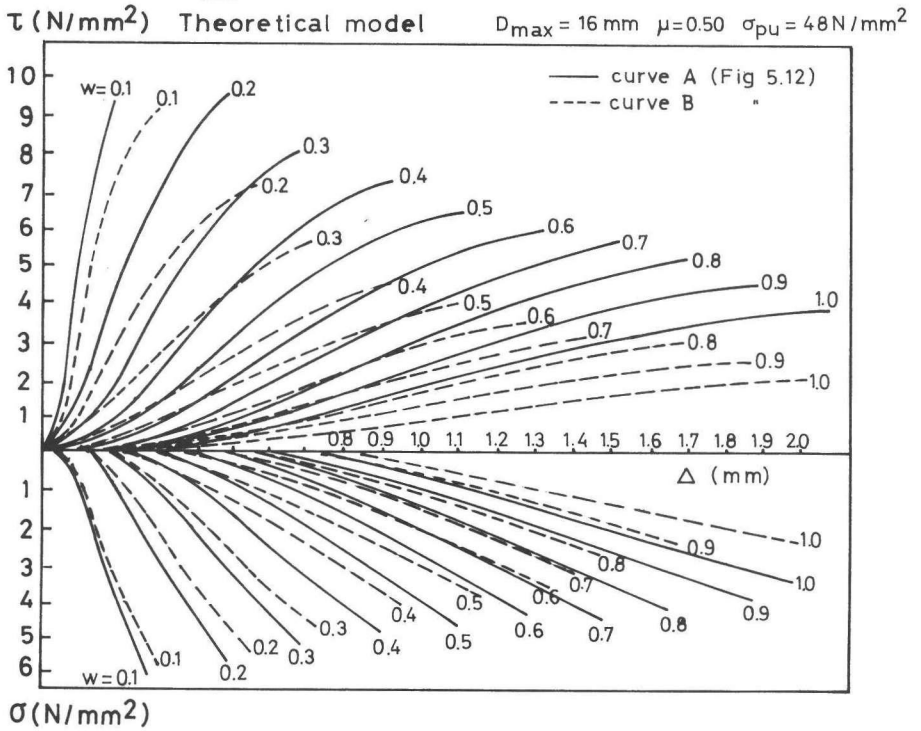

Fig. 5.13 The effect of the grading curve on the transfer of stresses in a crack for two comparable mixes confirming to different grading curves (D_{max} = 16 mm, p_k = 0.75, σ_{pu} = 48 N/mm², μ = 0.50)

e. Cyclic loading.

From tests [40, 89] it is known that in the case of cyclic loading a considerable difference exists between the behaviour of the crack plane during the first loading cycle and the subsequent cycles. The shear stress-shear displacement relationship of the initial cycle is nearly linear, and after unloading a considerable amount of hysteresis can be observed. The shear stress-shear displacement relationship for the later loading cycles is highly non-linear, and a hardening type of behaviour is observed. This overall behaviour can be explained with the theory developed. As an example a fictitious specimen according to Fig. 5.14 is considered.

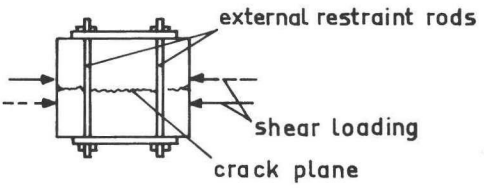

Fig. 5.14 Fictitious specimen considered

The specimen consists of two parts, separated by a crack, the initial width of which is assumed to be w_o = 0.50 mm. The two halves are loaded by shear forces, while enlargement of the crack width is counteracted by external restraint rods. The stiffness of these rods is assumed to be such that an increase of the crack width of Δw = 0.1 mm results in an increase of the normal stress on the crack plane of $\Delta\sigma$ = 0.5 N/mm^2. The maximum shear stress applied is assumed to be τ = 3 N/mm^2.
The assumed concrete quality is f'_{cc} = 33.4 N/mm^2 with D_{max} = 32 mm, so that the relations represented in Fig. 5.3 can be used to construct the ascending branch OA of the τ-Δ relation (Fig. 5.15).

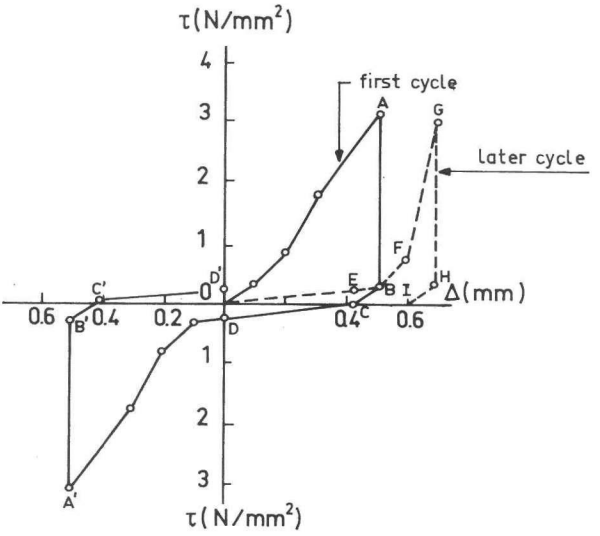

Fig. 5.15 Response to cyclic loading of fictitious specimen, calculated with theoretical model

A description of this procedure is given in Appendix II. The unloading branch is calculated by a different method: just before unloading, the relations (3.50) are valid:

$$\sigma_1 = \sigma_{pu} \, (A_x - \mu . A_y) \tag{5.3}$$

$$\tau_1 = \sigma_{pu} \, (A_y + \mu . A_x) \tag{5.4}$$

At that moment the friction still has its maximum value ($\mu = 0.50$). This situation can be compared with that of a body on an inclined plane, with frictional forces acting between the body and supporting surface, and the resultant of the horizontal force V and vertical force N acting in the direction of the line b-b'. Unloading is done by diminishing the horizontal (shear) force V. Movement of the two halves of the specimens relatively to each other can only occur if V is so small that the maximum frictional resistance in the other direction is

reached (comparable with the situation in Fig. 5.16, where the resultant is in the direction of a-a').

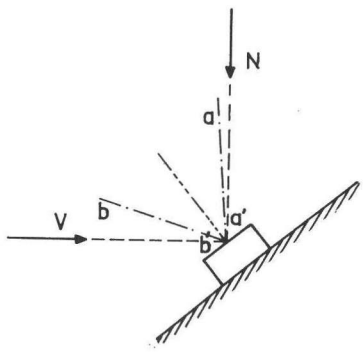

Fig. 5.16 Body on a rough inclined plane as an analogy for the behaviour of a crack under cyclic loading

Movement of the crack faces occurs if μ has become $-\mu$. At that moment the normal stress on the surface of the aggregate particles, originally equal to σ_{pu}, is reduced to a value σ_{p_1}, as a result of the reduction of V.
Substituting these values into (5.3), the normal stress acting between the crack faces is expressed as:

$$\sigma_2 = \sigma_{p_1} (A_x + \mu . A_y) \qquad (5.5)$$

However, just before sliding back, the external normal stress is still the same as at the start of unloading, since the external restraint rods have not been subjected to any change in length during the period during which V was reduced.
So, because $\sigma_1 = \sigma_2$, combination of (5.3) and (5.5) results in:

$$\sigma_{p_1} = \frac{\sigma_{pu} (A_x - \mu . A_y)}{(A_x + \mu . A_y)} \qquad (5.6)$$

If the crack planes are about to move, the shear stress τ_2 can be formulated by replacing μ in (5.4) by $-\mu$, and σ_{pu} by σ_{p_1}.

$$\tau_2 = \sigma_{p_1} (A_y - \mu.A_x) \tag{5.7}$$

Substitution of (5.6) into (5.7) results in:

$$\tau_2 = \sigma_{pu} \left(\frac{A_x - \mu.A_y}{A_x + \mu.A_y}\right).(A_y - \mu.A_x) \tag{5.8}$$

τ_2 can be expressed as a function of τ_1, comparing (5.8) with (5.4)

$$\tau_2 = \xi.\tau_1 \tag{5.9}$$

with

$$\xi = \frac{A_x - \mu.A_y}{A_x + \mu.A_y} \cdot \frac{A_y - \mu.A_x}{A_y + \mu.A_x}$$

In this way it is possible to determine the position of point B in Fig. 5.15. For the case considered it was calculated that $A_x = 3.13 * 10^{-2}$ mm and $A_y = 4.49 * 10^{-2}$ mm . With $\mu = 0.50$ a value $\xi = 0.080$ is obtained.

If the frictional resistance of the crack faces is exceeded, a displacement will occur. This displacement will continue until no areas of contact and no external forces remain. To reach this stage the crack width has to attain its original value, but the shear displacement need not return to zero. This is explained with the aid of Fig. 5.17.

The position of the crack faces before loading is represented in Fig. 5.17.a. At peak stress level the crack width has been increased by Δw and the shear displacement by Δ. As a result of the rigid-plastic character of the matrix material a cavity has been formed (shaded area in Fig. 5.17.b). Due to this cavity

the "no contact phase" after unloading is reached before the shear displacement has returned to zero (Fig. 5.17.c).

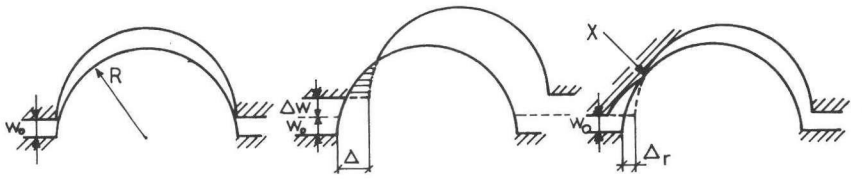

a b c

Fig. 5.17 Three characteristic stages during the first loading cycle: a. Before loading
b. Peak stress
c. After unloading

The "no contact phase" is considered to be reached, if in the most unfavourable case ($R = \frac{1}{2} D_{max}$ and $u = 0$) contact no longer exists. For the case considered ($D_{max} = 32$ mm, $w_o = 0.5$ mm) it can easily be calculated (Appendix II, using the formulas of Appendix I) that the remaining shear displacement Δ_r is equal to 0.41 mm (point C in Fig. 5.15). To restore the two halves of the specimen to their neutral position a small shear force may be necessary, since the rubble between the crack faces due to deterioration of matrix material during loading may cause some frictional resistance (point D in Fig. 5.15). If the shear force is applied in the other direction, the same type of behaviour can be expected, since those parts of the crack surfaces where contact occurs in this reversed cycle are not yet damaged (Fig. 5.17). Hence a similar loading and unloading curve can be expected (Fig. 5.15, points A', B', C', D').
In the subsequent loading cycles the presence of the cavities worn out in the first cycle of loading considerably affect the behaviour of the specimen. At first a shear displacement will

occur at a small shear force, until contact between the opposing areas occurs ($\Delta \geq 0.41$ mm (point E)). Then in a short interval of Δ full contact between the cavities will be obtained. In this short interval a process of gradual wearing-off will occur at places of high contact stresses (point X in Fig. 3.34.c). Hence a steeply ascending branch (EFG) may be expected, slightly shifted from the foregoing loading line. On unloading, behaviour similar to that in the first cycle may be expected (GHI - Fig. 5.15).

A comparison of the τ-Δ relation based on the theoretical model (Fig. 5.15) with experiments carried out by Laible, White and Gergely [40], shows fairly good agreement in behaviour (Fig. 2.9).

f. Comparison with other static tests.

Tests on cracks in plain concrete were performed by, among others, Paulay and Loeber [60], who applied constant crack widths (w = 0.13, 0.25 and 0.51 mm). The concrete had a D_{max} of 19 mm and an average cube compressive strength of f'_{cc} = 37 N/mm^2.

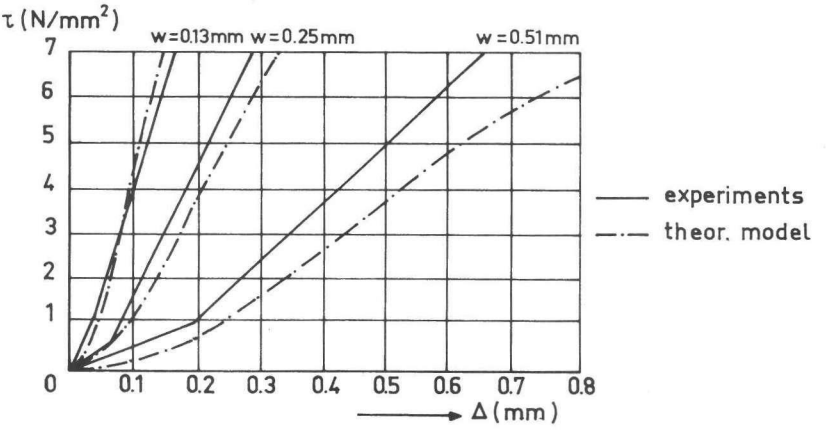

Fig. 5.18 Comparison between the experimental results of Paulay/ Loeber [60] and the predictions of the theoretical model developed

The experimental results have been compared with the results of the theoretical model, on the assumptions that D_{max} = 19 mm, μ = 0.50, p_k = 0.75 and σ_{pu} = 57 N/mm^2 (according to equation 5.1). This comparison is represented in Fig. 5.18. The agreement between experimental and theoretical values, taking into consideration the differences in grading curve and experimental set-up between both investigations, is satisfactory.

g. Simplified equations for the relations between τ, Δ, w and σ, Δ, w.

On the basis of a regression analysis, simplified equations have been derived which fit the experimental results. In these equations only the cube crushing strength has been considered as a variable. The aggregate scale effect has not been taken into account, since it is only of minor influence in the range tested. The formulas derived are suitable in principle for the type of mixes used (Fuller-curves), the interval of D_{max} ($16 \leq D_{max} \leq 32$ mm), and the range of Δ and w-values tested. The curves which most closely fitted the results are:

$$\tau = -\frac{f'_{cc}}{30} + \{1.8\, w^{-0.80} + (0.234\, w^{-0.707} - 0.20).f'_{cc}\}\Delta \quad (\tau \geq 0) \qquad (5.10)$$

and

$$\sigma = -\frac{f'_{cc}}{20} + \{1.35\, w^{-0.63} + (0.191\, w^{-0.552} - 0.15).f'_{cc}\}\Delta \quad (\sigma \geq 0) \qquad (5.11)$$

A comparison of these bilinear approximations with the experimental results of the various series is represented in the Figs. 5.19 - 5.22.

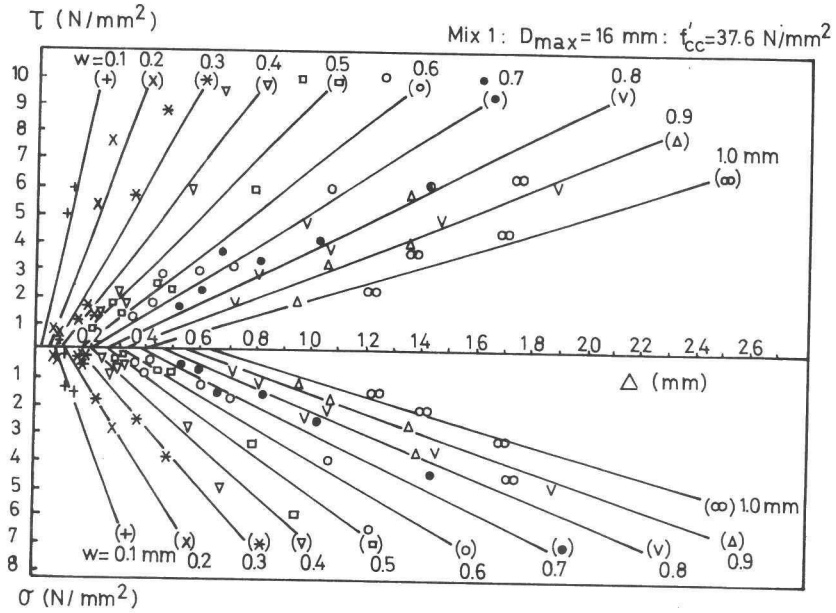

Fig. 5.19 Comparison of equation (5.10) and equation (5.11) with experimental results (Mix 1)

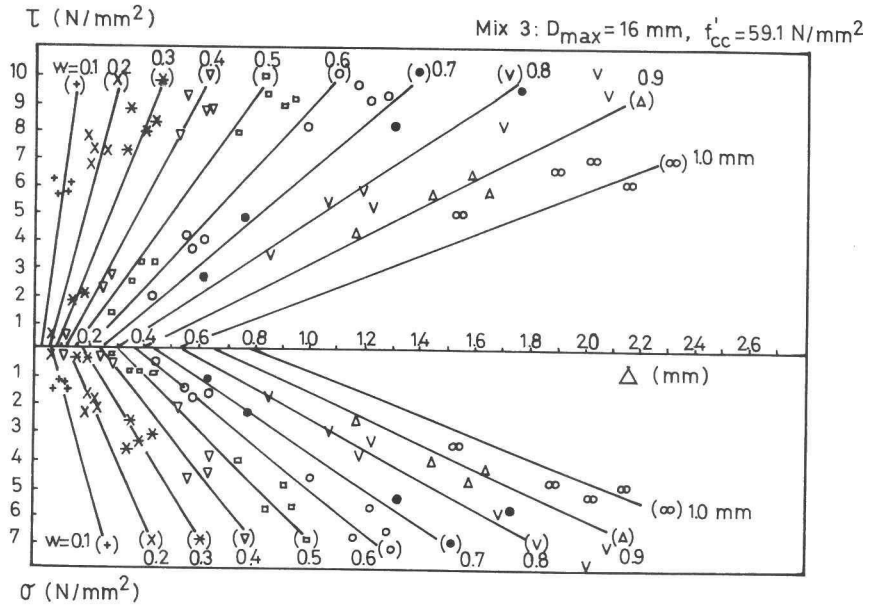

Fig. 5.20 Comparison of equation (5.10) and equation (5.11) with experimental results (Mix 3)

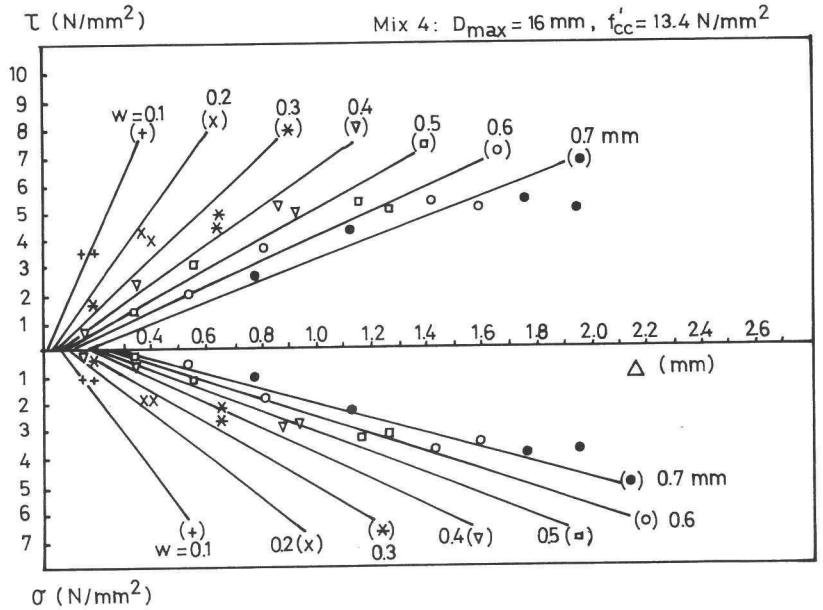

Fig. 5.21 Comparison of equation (5.10) and equation (5.11) with experimental results (Mix 4)

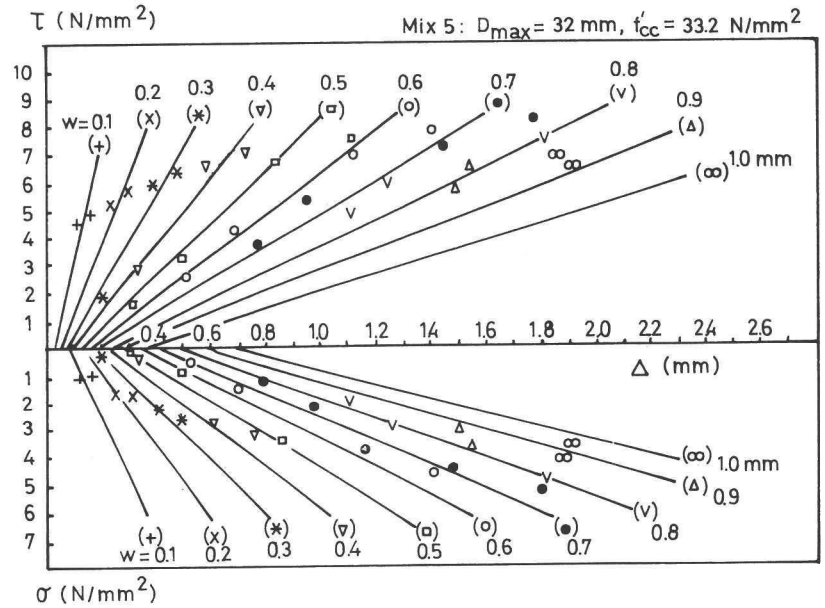

Fig. 5.22 Comparison of equation (5.10) and equation (5.11) with experimental results (Mix 5)

5.2 Transmission of forces across reinforced cracks

5.2.1 Components involved in the transmission of forces

Prior to analysing the overall mechanism, the individual components are considered. As far as necessary, expressions are derived, enabling an estimation of the forces acting across the crack, as a function of the displacements between the crack faces. As already stated, the overall behaviour must be a function of the interaction between aggregate interlock, dowel action and axial forces in the reinforcement.

a. Aggregate interlock.

Adequate information can be obtained by consulting the first part of this chapter.

b. Axial forces in the reinforcement.

The relations between the axial forces in the reinforcing bars and the slip can be obtained by using a finite difference method, as proposed by Rehm et al. [63] (see section 2.3).

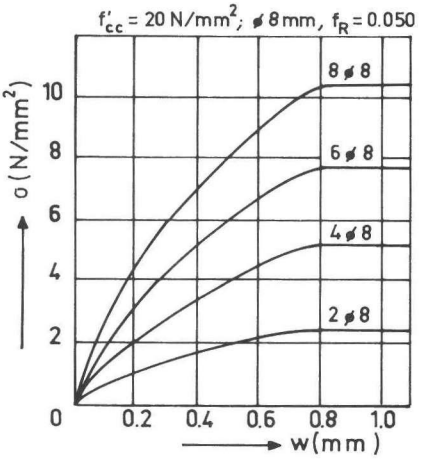

a

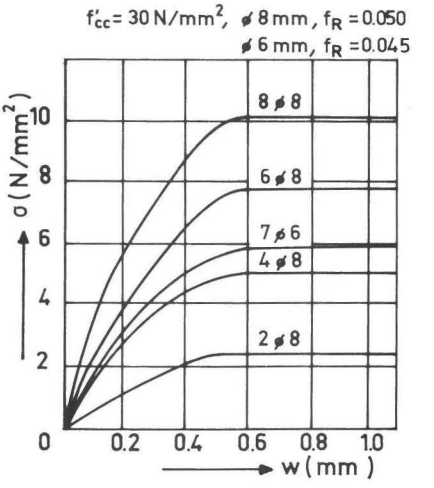

b

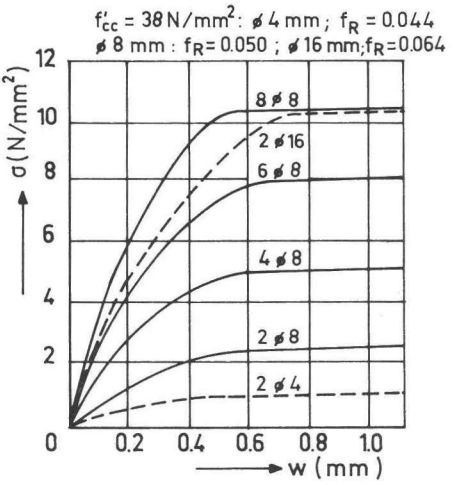

c

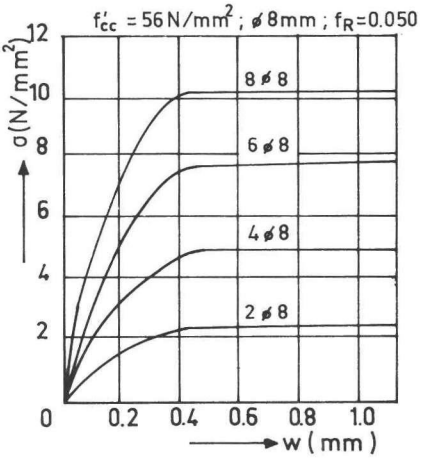

d

Fig. 5.23.a-d Equivalent stress normal to the crack plane as a function of the crack width for various amounts of stirrups with various diameters and four concrete qualities

This has been carried out for all bars crossing the crack plane, taking into account the bar diameters, the related rib areas and the concrete qualities. Detailed information on this calculation can be found in [85]. These relations have been used to construct diagrams in which the equivalent stress normal to the crack plane is represented as a function of the crack width (Fig. 5.23.a-d).

c. Dowel action.

The available knowledge about dowel action and its physical background has been reviewed and discussed in section 2.2. It was shown that the behaviour can be approximately described by the model of a beam on an elastic foundation. For the case that

no axial force is acting, the dowel force can be expressed by equation (2.13):

$$F_d = 3.56\ \phi^{1.75}\ G_f^{0.75}\ \Delta \qquad (5.12)$$

Tests by several authors [17, 59, 70] demonstrated that G_f does not depend on the bar diameter ϕ. In experiments by Paulay [59], carried out with a constant concrete quality of $f'_{cc} \approx 30$ N/mm^2, the value of G_f was found to be a decreasing function of Δ (Fig. 2.19). A comparison of (5.12) with these experimental relations results in an expression for G_f, equal to

$$G_f = 188\ \Delta^{-0.85} \qquad (5.13)$$

However, G_f must also be a function of the concrete strength. Because the modulus of elasticity E_c is generally related to the concrete strength according to:

$$E_c = C_1 \sqrt{f'_{cc}}$$

a similar relation has been adopted for the foundation modulus:

$$G_f = C_2 \sqrt{f'_{cc}}$$

Using this relation, equation (5.13) is modified to

$$G_f = 34\ \sqrt{f'_{cc}}\ \Delta^{-0.85} \qquad (5.14)$$

This relation, however, is only based on experiments without axial tensile forces in the bars, i.e., for w = 0. Tests, carried out by Eleiott [17, 90] showed that an axial tensile force in a bar reduces its dowel stiffness considerably (see also Fig. 2.24): a tensile stress of 175 N/mm^2 in a bar with ϕ 12.8 mm reduced the dowel stiffness by about 50%, whilst an increase to 350 N/mm^2 resulted again in a reduction of 40%. For the experiments in the author's own program, a stress level of 175 N/mm^2

is approximately obtained for a crack width of w = 0.2 mm and a stress of 350 N/mm^2 for w = 0.4 mm (Fig. 5.23). Taking these values into account, an approximate reduction factor can be formulated as:

$$\xi = 0.20\ (w + 0.2)^{-1} \tag{5.15}$$

Combining (5.12, 5.14 and 5.15), an approximate estimation of the dowel force is obtained, taking into account the influences of crack width, shear displacement, bar diameter and concrete quality:

$$F_d = 10\ (w + 0.2)^{-1}\ \Delta^{0.36}\ \phi^{1.75}\ f_{cc}'^{0.38} \tag{5.16}$$

Comparing the values, obtained with (5.16) for the measured crack opening path, with the total shear force in the experiments, it is seen that dowel action is of minor importance (Fig. 5.24).

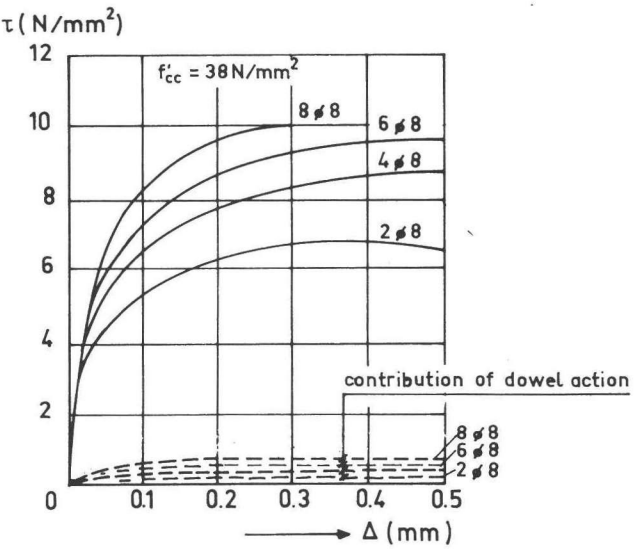

Fig. 5.24 Contribution of dowel action, calculated with equation (5.16), to the total shear stress in a crack, for the basic series made with concrete mix 5, reinforced with 2, 4, 6 and 8 stirrups ϕ 8 mm

5.2.2 Comparison between reinforced and unreinforced cracks

For unreinforced cracks it was shown that there is a unique relationship between the stresses τ and σ and the displacements w and Δ. This implies that if two of these parameters are given, the two remaining ones are also known. If, for instance, a certain combination of w and σ is given (point A in Fig. 5.25), the related values of Δ and τ are known.

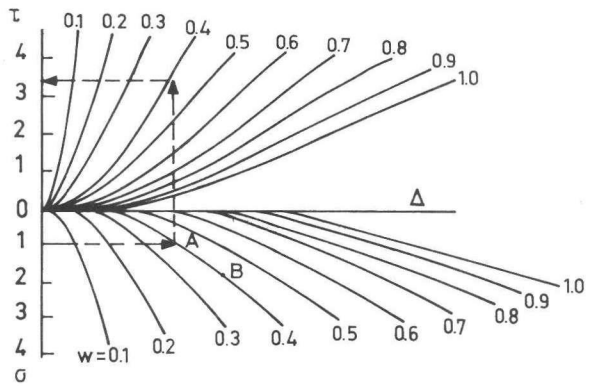

Fig. 5.25 Construction of τ-Δ and w-Δ relations for given restraint stiffness

If, more generally, the external restraint stiffness is given (the collection of points A), both the w-Δ relation and the τ-Δ relation can be constructed. An important property of the mechanism is that an increase in restraint stiffness (greater σ for the same w, point B in Fig. 5.25) results in a greater Δ or in a "steeper" crack opening path.
This sensitivity to the restraint stiffness is the main difference between the response of unreinforced and reinforced cracks to shear forces. Whereas for unreinforced cracks even small differences in restraint stiffness were perceptible (Fig. 4.2), for reinforced

cracks a variation of this stiffness over a wide interval (Fig. 5.23) did not result in any significant difference in the w-Δ relations (Fig. 4.12). Hence, an attempt to construct the τ-Δ and the w-Δ relations for reinforced cracks on the basis of the aggregate interlock diagrams and the restraint stiffness in the way indicated in Fig. 5.25, possibly correcting the value with a small dowel term, is doomed to fail. This is demonstrated in the Figs. 5.26 and 5.27 for the concrete mixes 1 and 4. It is seen that good agreement is achieved only for low reinforcement ratios ($\rho_o \leq 0.56\%$), while increasingly large deviations are observed with increasing values of ρ_o. The same tendencies were observed in other series.

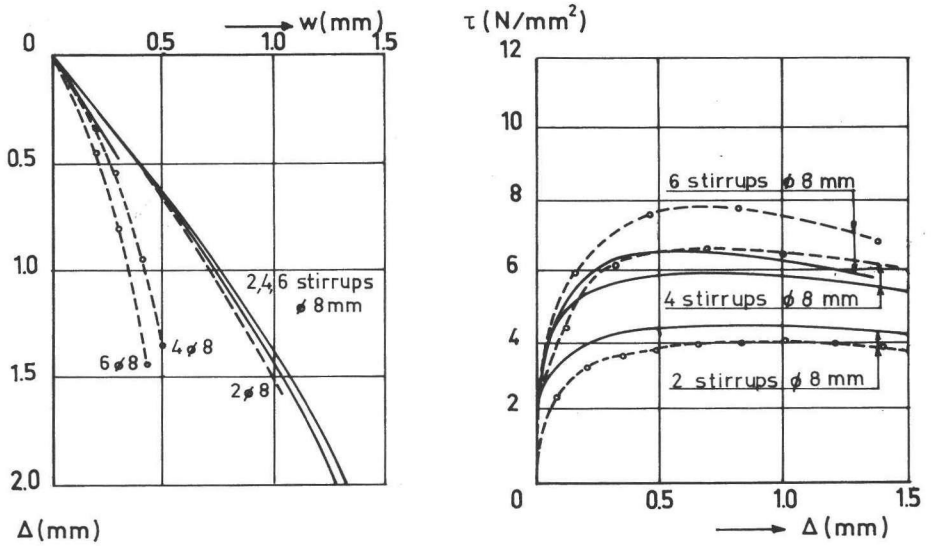

Fig. 5.26 Comparisons between experimental results (solid lines) for basic series 4 (f'_{cc} = 19.9 N/mm², 2, 4 and 6 stirrups ϕ 8 mm), with hypothetical ones, constructed on the basis of Fig. 5.27 (dotted lines)

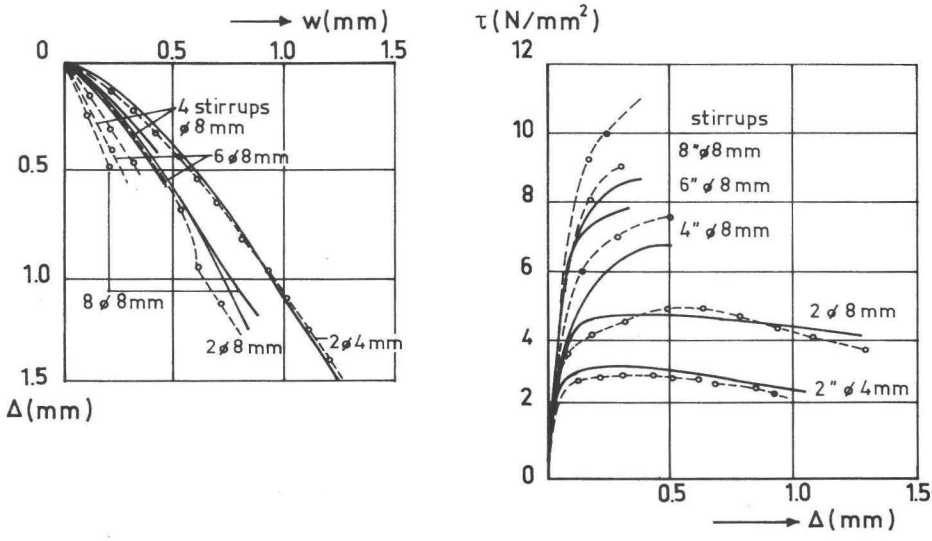

Fig. 5.27 Comparisons between experimental results (solid lines) for basic series 1 (f'_{cc} = 30 N/mm^2, 2, 4, 6, 8 stirrups ø 8 mm and 2 stirrups ø 4 mm) with hypothetical ones, constructed according to Fig. 5.27 (dotted lines)

It was believed that local disturbance of the crack structure around the bars was responsible for this difference in behaviour. This disturbance may be caused by local splitting forces originating from the ribs of the reinforcing bars when these are pulled out of the concrete by axial tensile forces (Fig. 5.28).
In this way concentrations of loose asperities are formed, which contribute in their own way to the transmission of forces across the crack (Fig. 5.29). This mechanism is likely to be rather complicated. Not only yielding of matrix material occurs, but also sliding friction at the contact points between the aggregate particles and rolling friction, due to which the particle shape may have an influence. Furthermore the volume of loose particles increases with continuing extraction of the reinforcing bars.

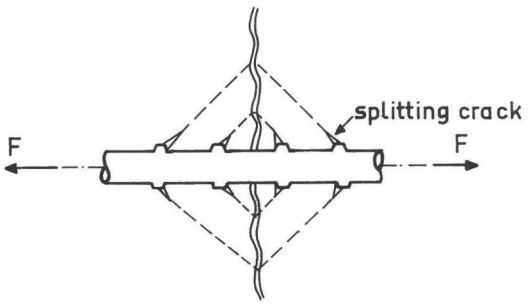

Fig. 5.28 Deterioration of the concrete by splitting forces around the bar

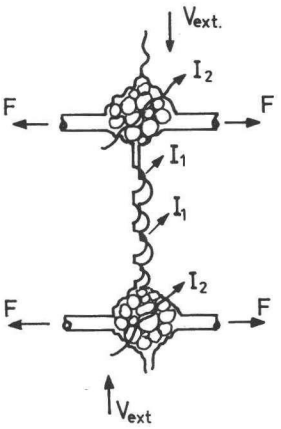

Fig. 5.29 Two mechanisms of aggregate interlock in a crack, crossed by reinforcement

The differences in crack structure can also be observed after opening of the specimens. Fig. 5.30 shows a crack face of a specimen, tested with external restraint bars: only a small amount of fine material was found to be torn off the crack faces. So the interlocking forces must indeed have been transmitted via particles embedded in the concrete. Fig. 5.31 shows a crack face of a specimen, reinforced with two stirrups ϕ 8 mm, after opening of the crack. A considerable amount of loose particles was released. After removal of remaining particles, crater-shaped holes around the bars were revealed. It is likely that these holes were mainly formed before yielding of the bars, during the actual shear test, and only to a minor extent during crack opening after the tests, since the greatest increase in stress in the steel, and attendant slip of the reinforcing bars, combined with splitting of the adjacent concrete, occurs before yielding.

In order to investigate the hypothesis that local disturbance of the crack structure is responsible for the difference in behaviour

between reinforced and unreinforced cracks, an additional series of 4 specimens was cast. These specimens were made of mix 1, with f'_{cc} = 36.1 N/mm^2, and were again reinforced with 2, 4, 6 and 8 stirrups ϕ 8 mm: around the stirrup legs soft sleeves were secured to both sides of the crack over a distance of 20 mm. These sleeves eliminated local splitting forces and thus the activation of the additional mechanism of aggregate interlock (Fig. 5.29). The effect of the sleeves on the restraint stiffness, calculated as earlier with the finite difference method, proved to be inconsiderable (Fig. 5.32). If the behaviour hypothesis were correct, these specimens would behave in the same way as the unreinforced specimens with external restraint bars. Indeed it appeared that the crack opening path was dependent on the restraint stiffness of the reinforcement. The results of the tests are represented in Fig. 5.33 (dashed lines).

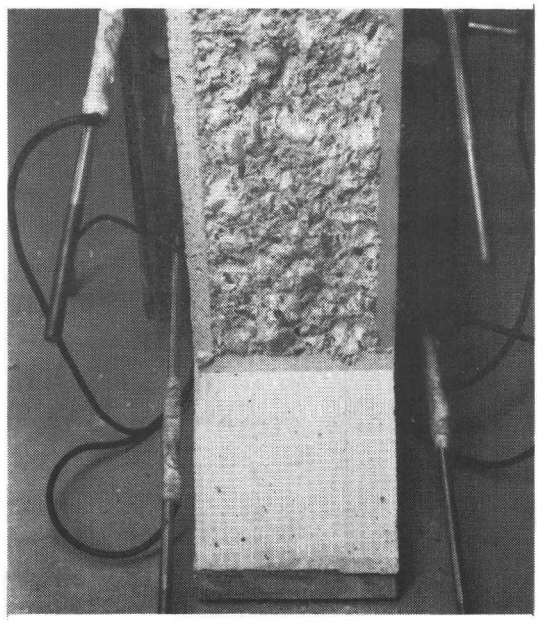

Fig. 5.30 Crack face of a specimen tested with external restraint bars

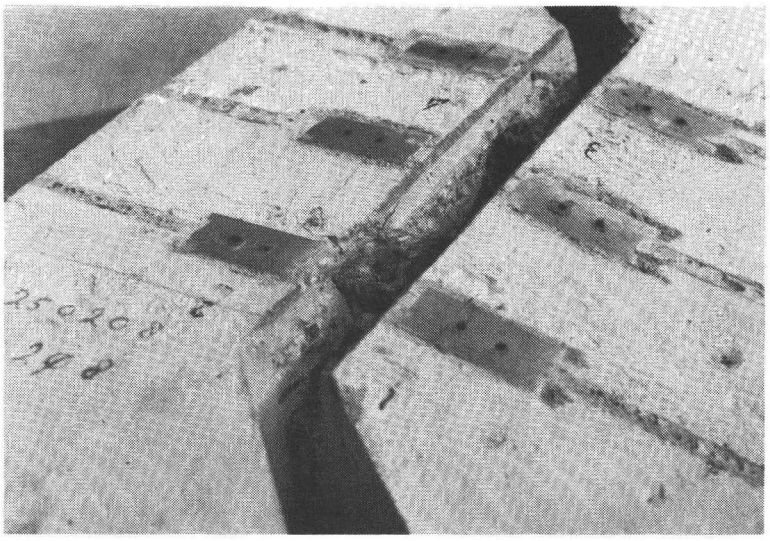

Fig. 5.31 Crack face of a specimen, reinforced with 2 stirrups ϕ 8 mm, showing crater-shaped holes around the reinforcing bars (after removal of loose material)

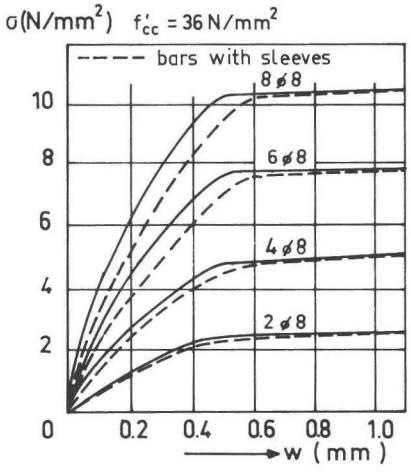

Fig. 5.32 Effect of sleeves on the restraint stiffness for specimens with 2, 4, 6 and 8 stirrups ϕ 8 mm, and f'_{cc} = 36 N/mm² (calculated)

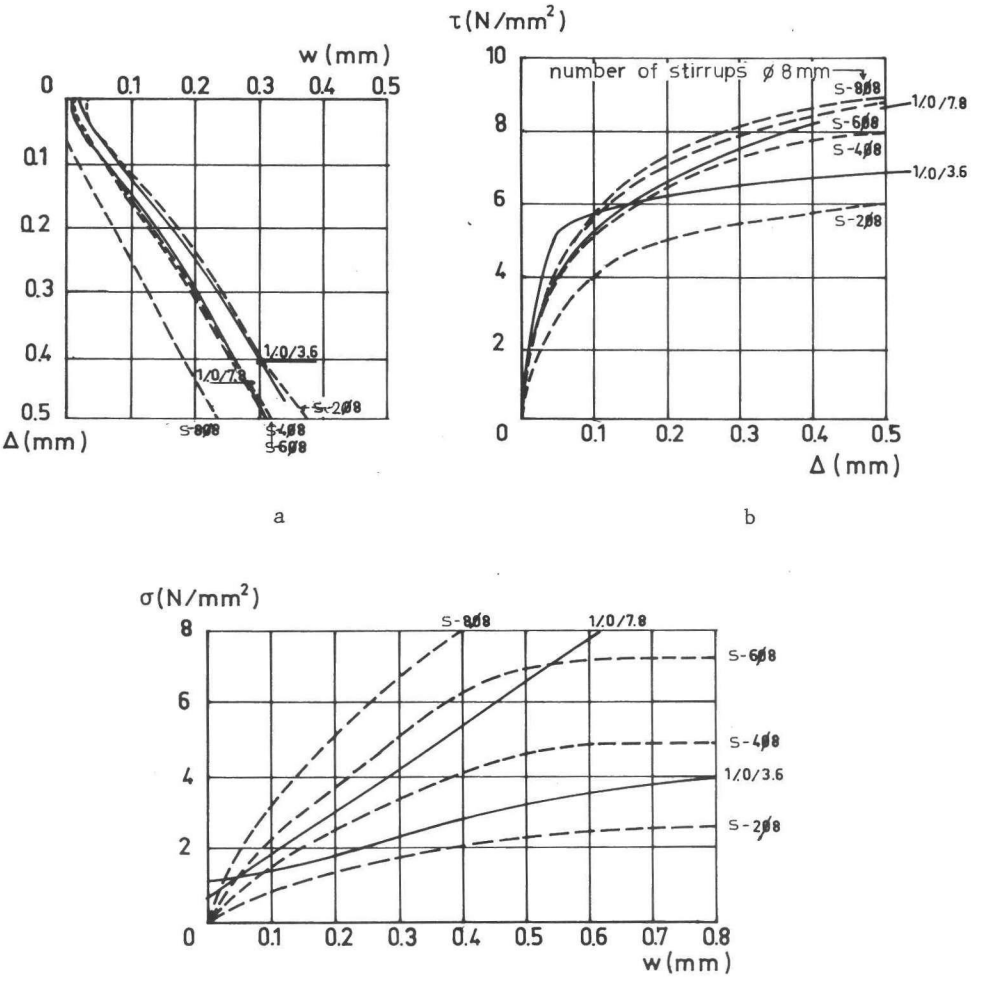

Fig. 5.33 Comparison between the results of the tests on specimens with reinforcing bars, provided with short sleeves, and two specimens with external restraint bars: (a) crack opening path (b) shear stress-shear displacement relation, (c) restraint stiffness

A direct comparison can be made with the results of two tests with external restraint bars, carried out earlier (solid lines). All

the specimens were of the same concrete quality. Fig. 5.33.c shows a comparison between the (measured) restraint stiffness of the unreinforced specimens with the (calculated - using Fig. 5.32) restraint stiffness of the reinforced specimens. The specimen with 6 stirrups (s - 6 ϕ 8) had a stiffness against crack opening approximately equal to that of specimen 1/.0/7.8. (Fig. 5.33.c). It is seen that the crack opening path (Fig. 5.33.a) and the τ-Δ relation (Fig. 5.33.b) are also almost the same. Furthermore the stiffness against crack opening of specimen 1/.0/3.6 is intermediate between those of the specimens s - 2 ϕ 8 and s - 4 ϕ 8 (for w > 0.1 mm and Δ > 0.13 mm). In this case, too, the positions of the w-Δ relation (Fig. 5.33.a and the τ-Δ relation (Fig. 5.33.b) are in agreement with what could be expected on the basis of the stiffness against normal crack opening.

In spite of the apparently complex character of the mechanism of transmission of forces around the reinforcing bars, the experiments on reinforced specimens reveal two characteristic modes of behaviour.

1. The mechanism is not active for low values of the reinforcement ratio (see for instance Fig. 5.26 and 5.27). It seems that if the "natural" crack opening direction does not exceed a certain critical value the loose particles around the bars do not lock and as such do not influence the behaviour.
2. If locking of the loose particles occurs, struts with relatively high stiffness are apparently formed, since for all reinforcing percentages greater than about 0.6% the crack faces are forced to follow the same crack opening path.

5.2.3 Quantitative analysis of the behaviour of reinforced cracks

In the previous section it was shown that the mechanism of transmission of forces across reinforced cracks is not simply a function of aggregate interlock (as established for unreinforced cracks), dowel action and axial restraint stiffness of the embedded reinforcement. It appeared that aggregate interlock can be subdivided

into two parts: aggregate interlock type I, transmitting forces via embedded particles, and aggregate interlock type II, representing the forces which act between the crack faces via concentrations of loose particles around the reinforcing bars.
The overall behaviour is, as a result, a function of four components, three of which can adequately be described as a function of the displacements w and Δ: dowel action, axial restraint stiffness and aggregate interlock type I. Hence it is obvious to study the role of aggregate interlock type II as the missing link in the polygon of forces.
The equilibrium of one half of a test specimen is represented in Fig. 5.34.

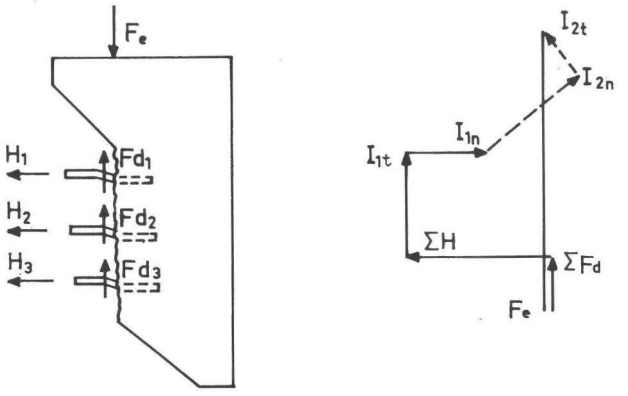

Fig. 5.34 Equilibrium of forces in a reinforced crack, in which two types of aggregate interlock are distinguished

The forces, which are indicated by solid lines, are known for any displacement combination (w, Δ): the external shear force F_e was measured by a load cell, the dowel force ΣF_d can be calculated with equation (5.16), the axial restraint forces H, of the reinforcement normal to the crack plane, can be obtained from Figs. 5.23.a-d, and the shear and normal forces resulting from aggregate interlock type I can be calculated with equation (5.10) and (5.11). Since

aggregate interlock type II seems to be narrowly related to the crack opening path, which is nearly constant for all concrete types, it is resolved into a component normal and a component tangential to this path (I_{2n} and I_{2t}).
The components I_{2n} and I_{2t} have been calculated for all specimens of the basic series (Table 4.II), for a great number of displacement combinations (w, Δ). It appeared that for low amounts of reinforcement (2 stirrups ϕ 8 mm, ρ_o = 0.56%), both components were very small (this agrees with the observations in Fig. 5.26 and 5.27). For increasing amounts of reinforcement the value I_{2n} increased considerably, but the value I_{2t} remained relatively unimportant, irrespective of the amount of reinforcement.
This implies that approximately equilibrium of forces is obtained if the polygon of forces is simply closed by a line, normal to the crack opening path (Fig. 5.35.a).

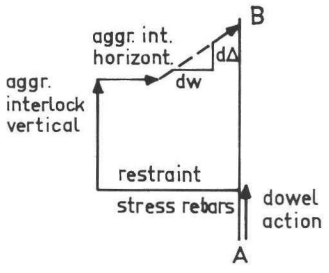

Fig. 5.35.a Polygon of forces

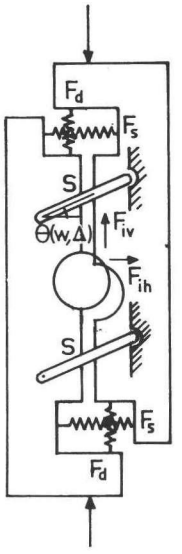

Fig. 5.35.b Schematic representation of forces in a reinforced crack

Considering all crack opening paths of the basic series (Fig. 4.12),

it was deduced that for low and intermediate concrete strengths ($20 < f'_{cc} < 40$ N/mm^2) the relation

$$\Delta = 1.40\ w^{1.2} \tag{5.17}$$

and for high concrete strength ($f'_{cc} = 56$ N/mm^2) the relation

$$\Delta = 1.87\ w^{1.4} \tag{5.18}$$

describe the results with adequate accuracy.
Schematically the mechanism of force transmission is shown in Fig. 5.35.b.
Aggregate interlock type II is represented by the infinitely stiff compression struts S, which are defined to be always perpendicular to the critical crack opening path, given by the equations (5.17 and 5.18). The struts S permit no crack opening steeper than the critical crack opening path, but are not stressed if the natural crack opening path is less steep.
In the following, the experimental results are compared with those predicted on the basis of the system of Fig. 5.35.
First, it has to be established whether the compression struts are activated or not. This is done as shown in Fig. 5.25; the relation between the equivalent restraint stress and the crack width is taken from Fig. 5.23, and the value Δ is then determined. The combination (w, Δ) reveals whether the critical crack opening path is exceeded or not. If not, the value τ can be assessed with the diagram, as a function of w and Δ, and the total external shear stress is obtained by adding a dowel term, according to equation (5.16).
If the critical crack opening path is indeed exceeded, the struts S are activated and the crack faces are forced to follow this path. In this case the external shear stress is constructed, using the principle represented in Fig. 5.35.a. The polygon of forces can be constructed for every value of w, starting from point A. For a value w the accompanying value Δ can be calculated with equation (5.17) or equation (5.18). The dowel contribution is obtained from equation (5.16). The normal restraint stress, caused by the rein-

forcement, can be taken from the diagrams in Fig. 5.23. The vertical and horizontal components of aggregate interlock (type I) are assessed, using the relations (5.10) and (5.11). The direction of the normal on the crack opening path is obtained from (5.17) or (5.18). Consequently the external shear stress is found as AB. This calculation has been carried out for a great number of specimens (Fig. 5.36.a-v).

In general, satisfactory agreement with the experimental results is obtained. In some of the more heavily reinforced specimens the calculated lines reach a higher peak value than the experimental ones, which can be explained by the occurrence of spalling regions at the top and bottom of the crack, observed during testing, which weaken the ultimate resistance (Fig. 5.36.c, h, j, k, p). Indeed, the specimens with lower concrete strength are more susceptible to this strength reduction. (As discussed earlier, this effect was theoretically demonstrated by Schwing [69]).

Only in one of the specimens the struts S were not found to be stressed (Fig. 5.36.r-v). If the influence of the stresses transverse to the bars on the bond characteristics could be taken into account, this would probably even increase the accuracy of the approximation, since slightly higher values for τ would be obtained for values $w < 0.4 - 0.5$ mm.

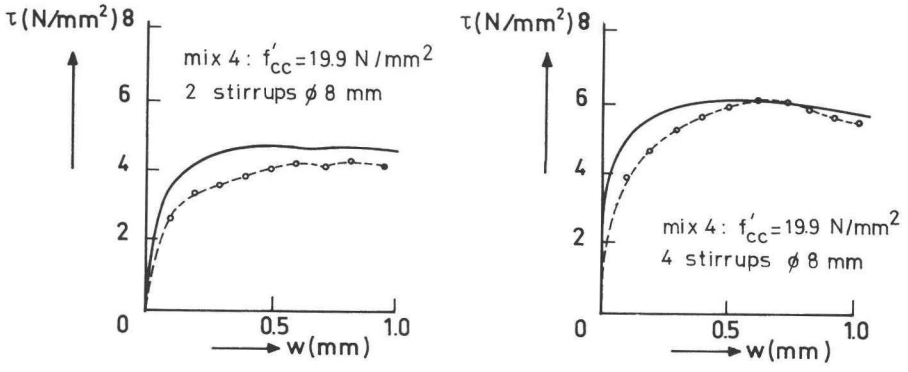

Fig. 5.36.a-b

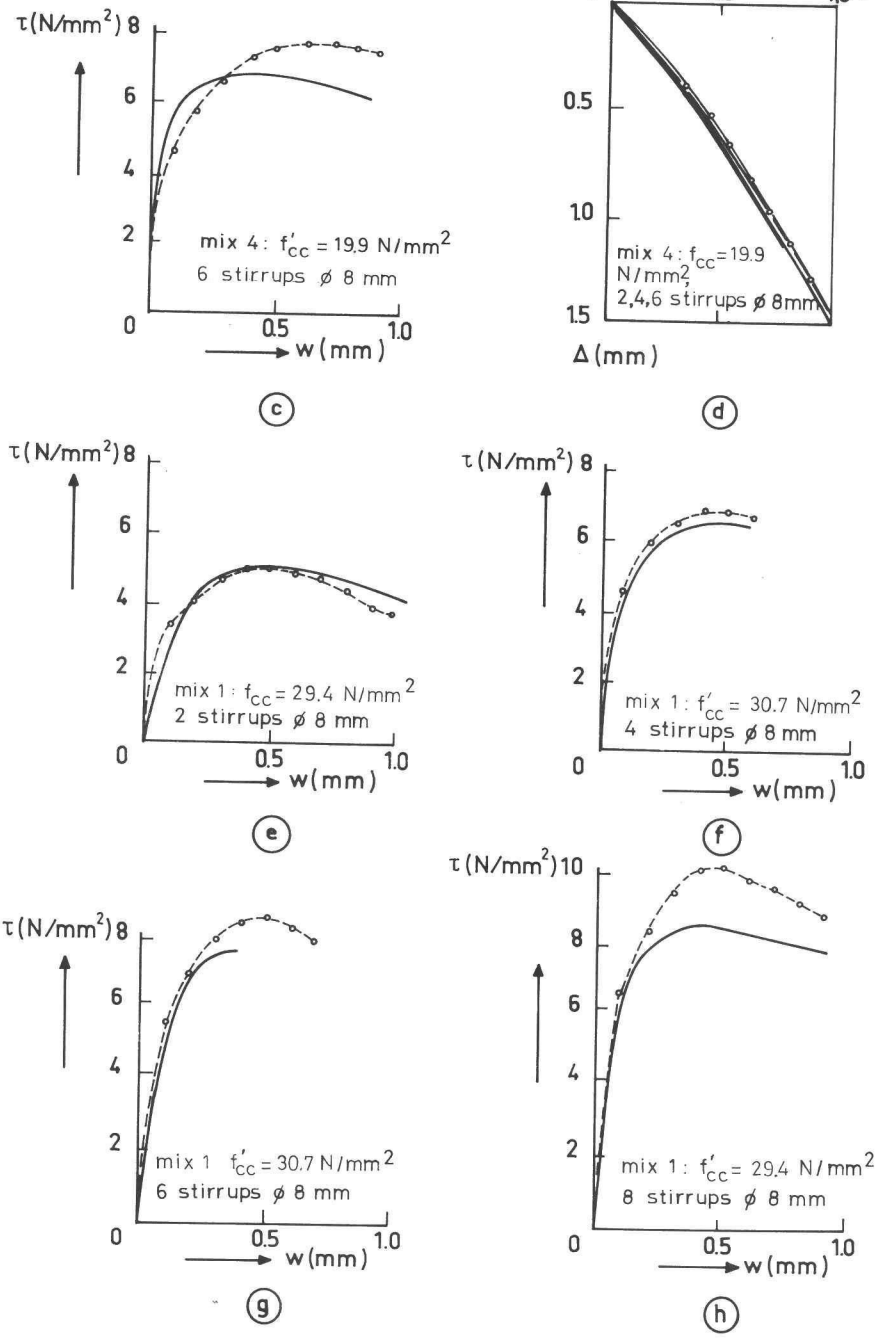
τ(N/mm²) 8
6
4
2
0
0.5
1.0
w (mm)
mix 4: f'cc = 19.9 N/mm²
6 stirrups ø 8 mm
c
w (mm)
0
0.5
1.0
0.5
1.0
1.5
mix 4: fcc=19.9 N/mm²
2,4,6 stirrups ø 8mm
Δ (mm)
d
τ(N/mm²) 8
mix 1: fcc= 29.4 N/mm²
2 stirrups ø 8 mm
e
τ(N/mm²) 8
mix 1: f'cc = 30.7 N/mm²
4 stirrups ø 8 mm
f
τ(N/mm²) 8
mix 1 f'cc = 30.7 N/mm²
6 stirrups ø 8 mm
g
τ(N/mm²) 10
8
mix 1: f'cc= 29.4 N/mm²
8 stirrups ø 8 mm
h

Fig. 5.36.c-h

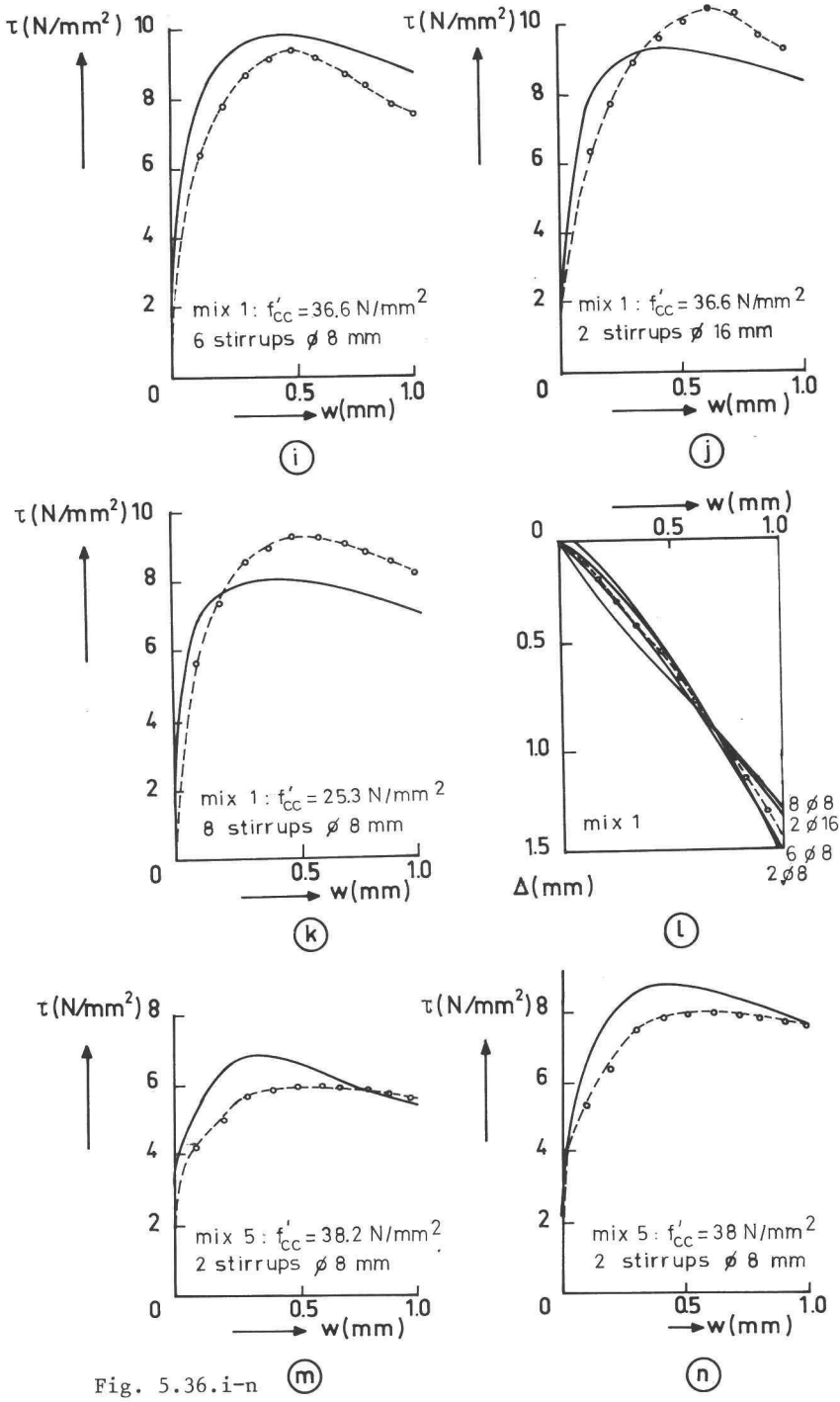
τ(N/mm²) 10
8
6
4
2
0
0.5
1.0
w(mm)
mix 1: f'cc = 36.6 N/mm²
6 stirrups ø 8 mm
(i)
τ(N/mm²) 10
mix 1 : f'cc = 36.6 N/mm²
2 stirrups ø 16 mm
(j)
τ(N/mm²) 10
mix 1 : f'cc = 25.3 N/mm²
8 stirrups ø 8 mm
(k)
w(mm)
0.5
1.0
1.5
Δ(mm)
mix 1
8 ø 8
2 ø 16
6 ø 8
2 ø 8
(l)
τ(N/mm²) 8
mix 5 : f'cc = 38.2 N/mm²
2 stirrups ø 8 mm
(m)
τ(N/mm²) 8
mix 5 : f'cc = 38 N/mm²
2 stirrups ø 8 mm
(n)

Fig. 5.36.i-n

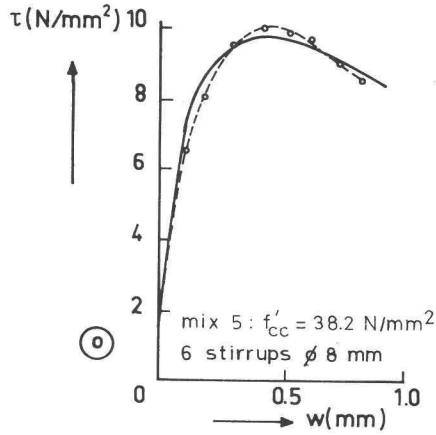
τ(N/mm²) 10
8
6
4
2
0
0.5
1.0
w(mm)
mix 5 : f'cc = 38.2 N/mm²
6 stirrups ø 8 mm
o

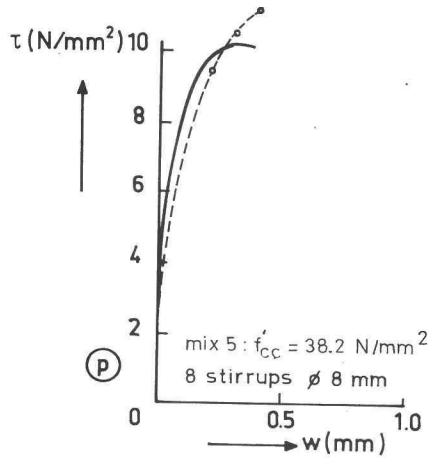
τ(N/mm²) 10
8
6
4
2
0
0.5
1.0
w(mm)
mix 5 : f'cc = 38.2 N/mm²
8 stirrups ø 8 mm
p

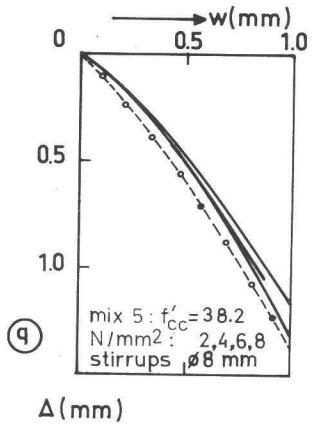
w(mm)
0
0.5
1.0
0.5
1.0
mix 5 : f'cc = 38.2
N/mm² : 2,4,6,8
stirrups ø 8 mm
q
Δ(mm)

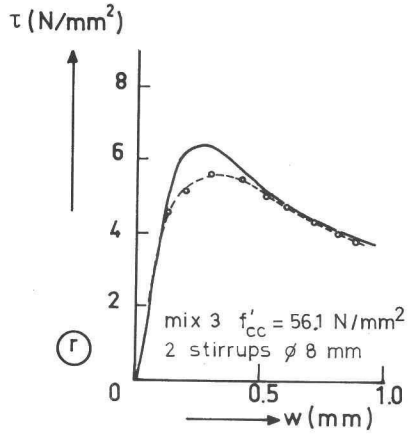
τ(N/mm²)
8
6
4
2
0
0.5
1.0
w(mm)
mix 3 f'cc = 56.1 N/mm²
2 stirrups ø 8 mm
r

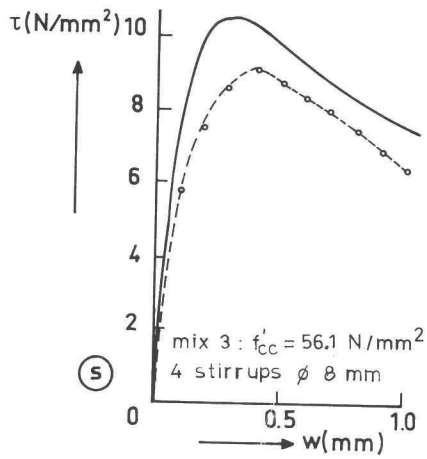
τ(N/mm²) 10
8
6
4
2
0
0.5
1.0
w(mm)
mix 3 : f'cc = 56.1 N/mm²
4 stirrups ø 8 mm
s

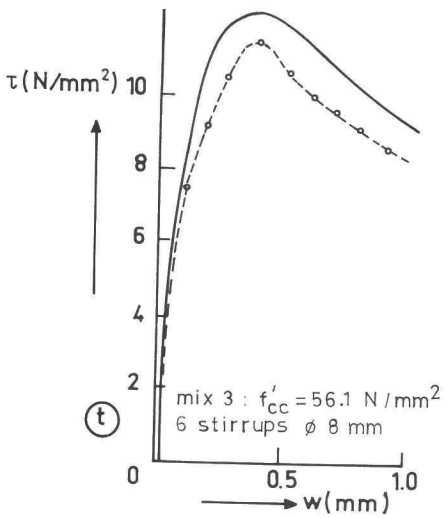
τ(N/mm²) 10
8
6
4
2
0
0.5
1.0
w(mm)
mix 3 : f'cc = 56.1 N/mm²
6 stirrups ø 8 mm
t

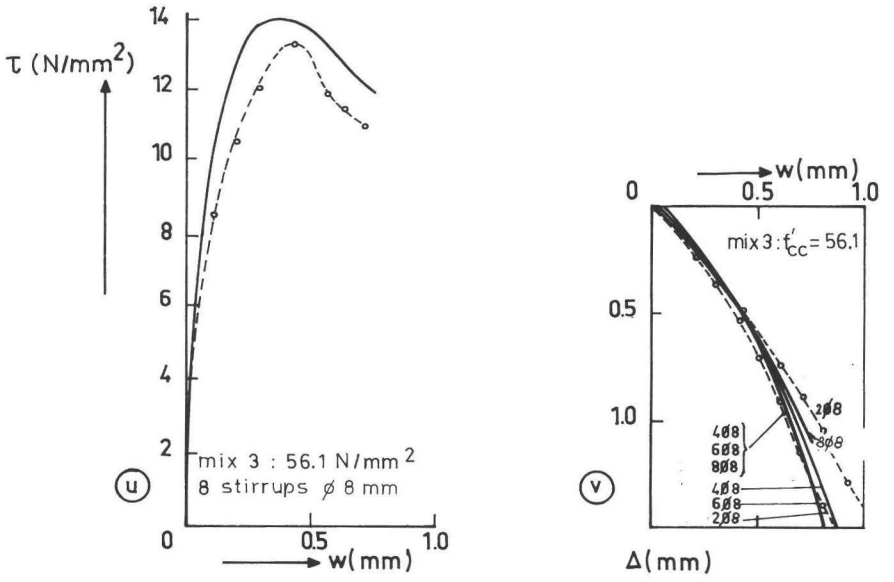

Fig. 5.36 Comparison between calculated relations (dotted lines) and experimental relations (solid lines)

5.2.4 Specimens with reinforcing bars inclined to the crack plane

It can be shown that the behaviour of specimens with reinforcing bars inclined to the crack plane is not essentially different from that of specimens with reinforcement perpendicular to the crack plane. In order to construct the τ-w and Δ-w relations it is necessary to calculate the restraint stress normal to the crack plane, and the dowel action of the bars. The restraint stress normal to the crack plane is, in the case of inclined bars, not only a function of the crack width w, but also of the shear displacement Δ (Fig. 5.37).

For a displacement (w, Δ) the total pull-out slip of the reinforcing bar is equal to $w_{*} = w \sin\theta + \Delta \cos\theta$. The total steel force $F_{s,\theta}$ in the direction θ can be calculated by using Fig. 5.23, replacing w by w_{*} and multiplying σ by the crack area A_c (σ is related to A_c in Fig. 5.25), and is subsequently resolved into a restraint force normal to the crack plane, equal to $F_{s\theta}.\sin\theta$, and a shear force parallel to the crack plane, equal to $F_{s\theta}.\cos\theta$.

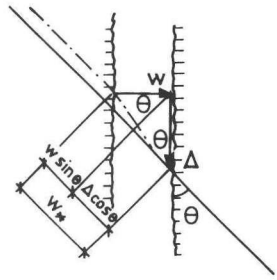

Fig. 5.37 Pull-out slip for an inclined reinforcing bar

For the dowel action of the inclined bars an expression suggested by Mattock [50] has been used, which related this force to the dowel action of a bar perpendicular to the crack, according to the formula

$$F_{d,\theta} = F_{d,90} \cdot \sin^2\theta \qquad (5.19)$$

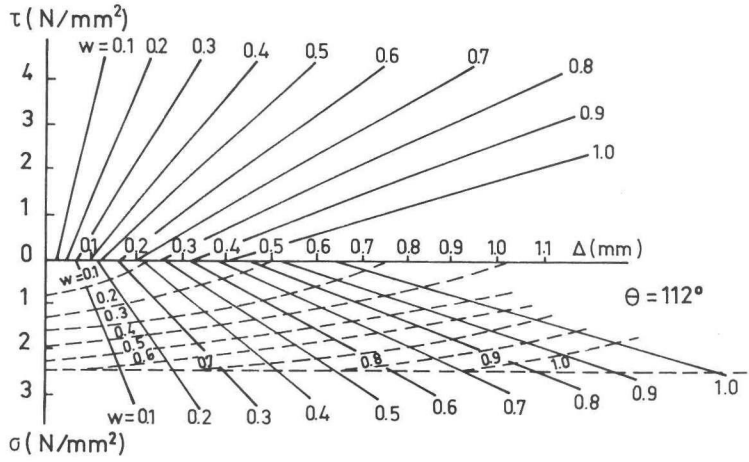

Fig. 5.38 Interaction diagram for f'_{cc} = 34 N/mm^2 and 2 stirrups ϕ 8 mm inclined to the crack plane with θ = 112^o

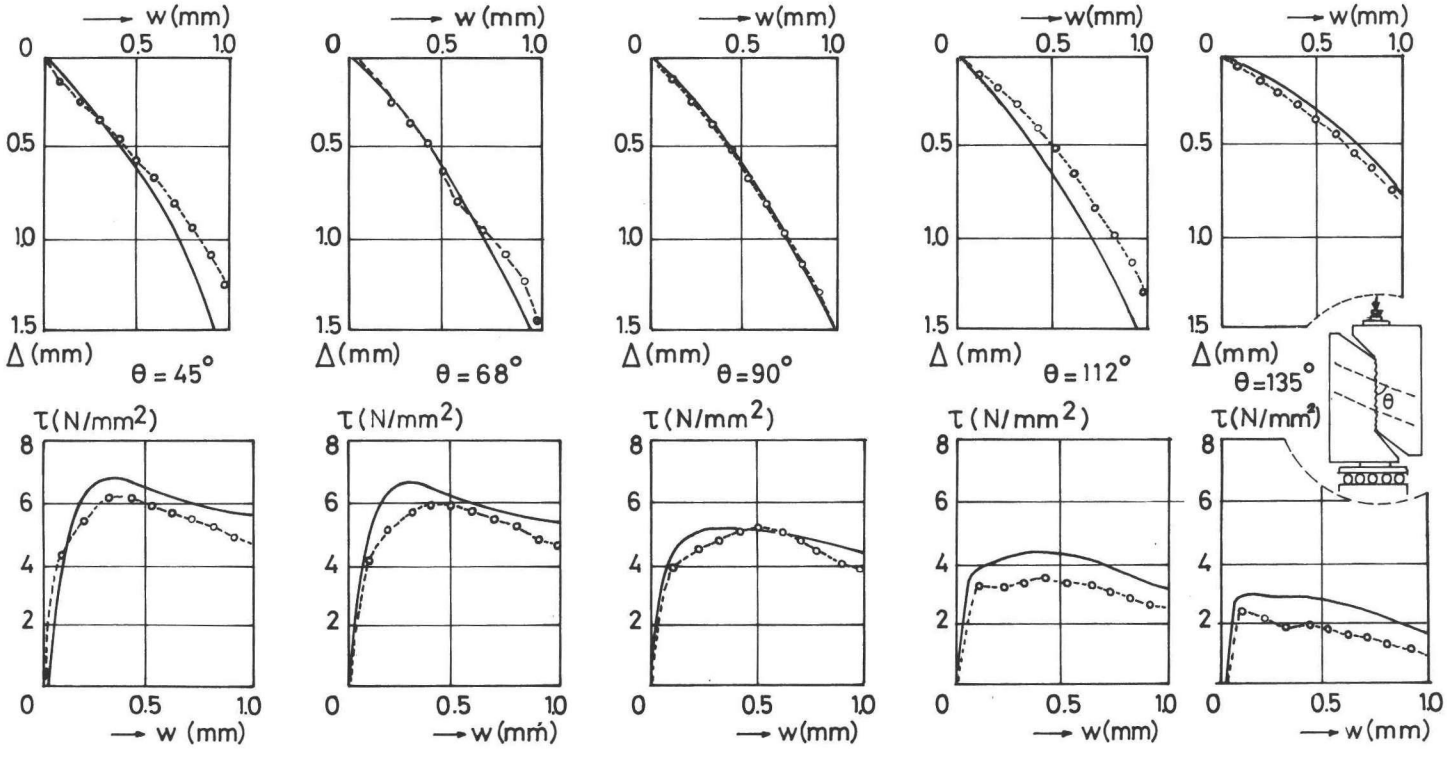

Fig. 5.39 Comparison between calculated (dotted) and experimental (solid) τ-w and w-Δ relations for specimens with inclined bars

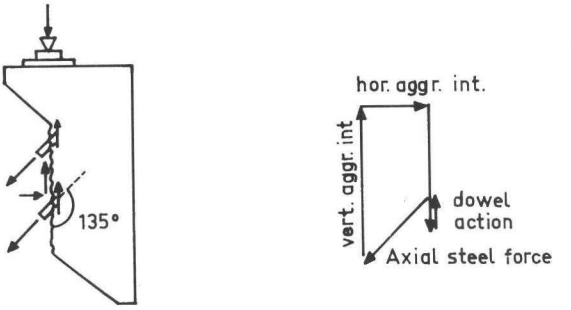

Fig. 5.40 Equilibrium in a crack with reinforcement inclined with $\theta = 135^{o}$

The τ-w and w-Δ curves can be constructed, requiring equilibrium in the direction normal to the crack. The stress normal to the crack, due to aggregate interlock, is formulated as a function of w and Δ in equation (5.10) and equation (5.11). The restraint stress normal to the crack, due to the tensile force in the reinforcement, is calculated, as described previously, also as a function of w and Δ (dashed lines in Fig. 5.38). Combinations of (w, Δ) for which equilibrium is obtained can be graphically estimated with interactions diagrams, an example of which is given in Fig. 5.38. The corresponding value of τ due only to aggregate interlock can be read in the upper part of the diagram. To obtain the total shear force, this value has to be increased by a term resulting from the axial steel force and a term resulting from dowel action. Furthermore it has to be checked whether the critical crack opening path is not exceeded. The results of these calculations are represented in Fig. 5.39. The agreement between calculated and experimental results is satisfactory. In the calculation it was found that even for $\theta = 135^{o}$ the reinforcement was subjected to a tensile stress. In the case of $\theta > 90^{o}$ this axial tensile force itself has a negative influence on the shear resistance, but acts positively by providing a restraint stiffness against crack opening and, as such, activating aggregate interlock (Fig. 5.40).

5.2.5 Hypothesis for the behaviour of reinforced cracks subjected to general combinations of external loads or imposed displacements

In the previous section it was shown that the behaviour of the test specimens could be described by defining two types of aggregate interlock: type I, interlock over embedded particles, and type II, interlock over concentrations of loose particles around the bars, forcing the crack to follow a certain constant crack opening path. The first type can be denoted as the micro-roughness, and the second as the macro-roughness of the crack plane. For the tests carried out, the macro-roughness seemed to be a characteristic property, since a high degree of repeatability of crack opening paths was observed. However, nearly all specimens had an initial crack width of less than 0.04 mm, and all specimens were subjected only to (external) shear forces. Due to these restrictions the information obtained was limited. It may for instance be wondered what crack opening path would be followed, if the initial crack width were greater, or, if the external shear force were combined with an axial tensile force. It seems not unlikely that also in other points of the w, Δ plane critical crack opening directions exist due to locking of loose particles. At present little evidence is available to support this supposition. Besides a few tests carried out with slightly greater initial crack widths, represented in Fig. 4.8 and 4.9, only a series, carried out by Mattock [51] was found in the literature, giving complementary results. In that investigation comparable precracked specimens, with reinforcing ratios of 0.4 - 2.3%, were subjected to an external shear load. During precracking the crack width reached an average maximum value of 0.28 mm. When the line loads were removed, a residual crack width of about 0.23 mm remained, this being the average width of the crack in the shear plane before the shear transfer test.

Fig. 5.41 shows the crack opening path (supposing that for all specimens w_o = 0.23 mm) for this series, with $f'_{ccyl} \approx 28$ N/mm^2 (which agrees with a cube crushing strength of about $f'_{cc} = 35$ N/mm^2), and D_{max} = 19 mm. It is seen that after a short vertical branch an

approximately constant slope is followed (other tests, on other types of concrete did not exhibit the vertical branch; see also Fig. 2.36.b and [83, p. 85], so that also here a characteristic crack opening path seems to exist.

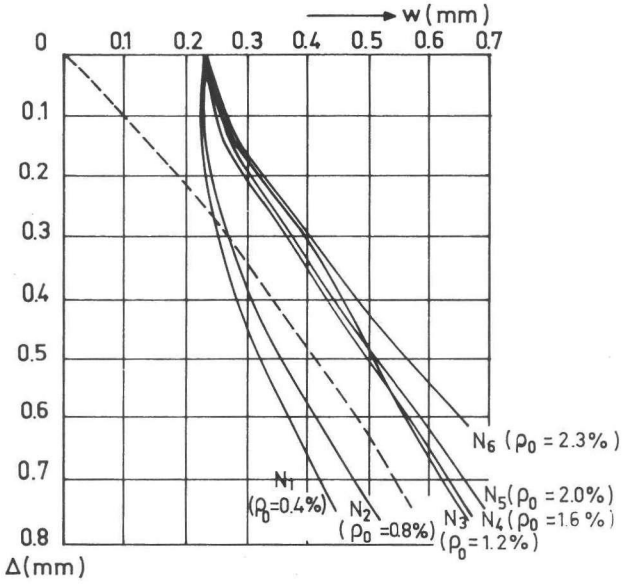

Fig. 5.41 Crack opening paths for specimens, tested by Mattock [51], for gravel concrete with $f'_{cc} \approx 35$ N/mm^2, $D_{max} = 19$ mm, $0.4\% < \rho_o < 2.3\%$ and $\bar{w}_o = 0.23$ mm

The average crack opening path obtained in the present author's own tests for intermediate concrete strengths is indicated by a dashed line in Fig. 5.41. It may be assumed that at every point of the w, Δ plane a critical crack opening direction exists, which cannot be exceeded, and that the critical directions can be represented by the definition of a continuous vector field. An example is given in Fig. 5.42, in which the expression

$$\frac{d\Delta}{dw} = w^{0.18} (1.65 + 2.10\ w) - 1.5\ \Delta \qquad (5.20)$$

is used as a definition formula for the critical crack opening direction.

This formula is so constructed that both for the present author's own tests, and for Mattock's, a fitting crack opening path is obtained (see also Fig. 5.42).

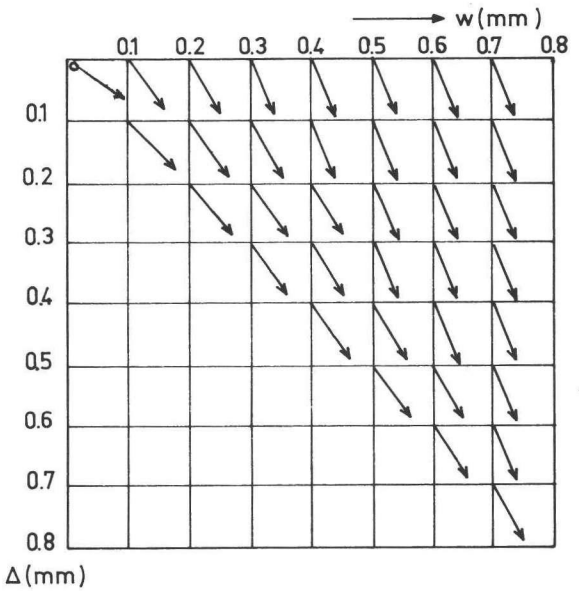

Fig. 5.42 Vector field according to equation (5.20), so defined that both for Mattock [51] and the present author's own tests a good approximation of the experimental crack opening path is obtained

It can be demonstrated that also Mattock's test results [51] can be reasonably well described using the procedure described in section 5.2.3, with the formulas (5.10), (5.11), (5.16) and Figs. 5.23.a-d, if equation (5.20) is used to define the critical crack opening path. A comparison between calculated and experimental relations for these tests is represented in Fig. 5.43.

Since, however, only a few test results are available, further experiments on reinforced specimens are necessary, focusing on the existence of critical crack opening paths for a wider range of w, Δ-values. Aspects of load history should also be taken into account.

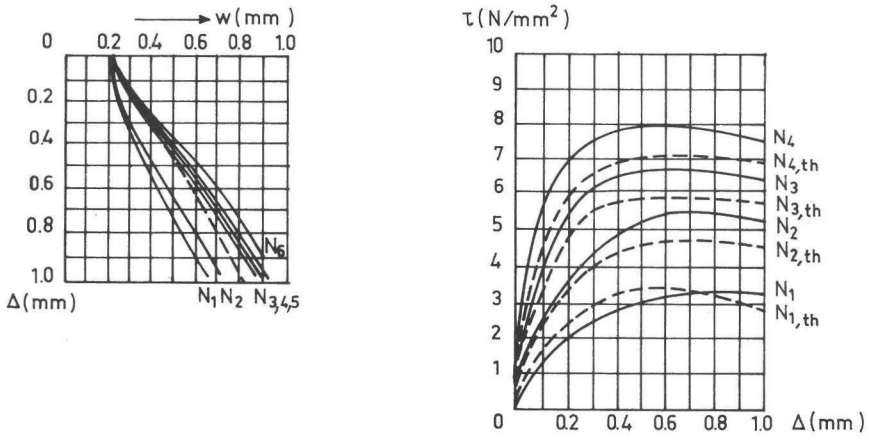

Fig. 5.43 Comparison between experimental values of tests by Mattock [51] (solid lines) with calculated relations (dashed lines)

6 A MATHEMATICAL FORMULATION OF THE RELATION BETWEEN STRESSES AND DEFORMATIONS OF CRACKED REINFORCED CONCRETE, TAKING INTO ACCOUNT THE CRACK PROPERTIES

6.1 The stress-displacement relation for a single crack

A distinction has to be made between the two cases of a crack in plain concrete and a crack in reinforced concrete. The experiments demonstrated that in the case of reinforced cracks the crack opening direction may be confined to a certain limit value. To simulate the behaviour displayed by the cracks a compression strut has been introduced (Fig. 5.35), which is activated only if the shear displacement tends to exceed the limit value.

a. The unreinforced crack.

For the sake of succinct formulation a modified notation is used for the stresses and displacements, referring to the directions n (normal to the crack) and t (tangential to the crack) (Fig. 6.1).

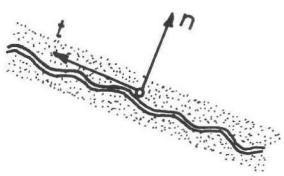

Fig. 6.1 Principal directions n and t

δ_n and δ_t represent the displacements in normal and tangential directions ($\delta_n > 0$: δ_n = crack width, earlier denoted as w), δ_t = shear displacement (earlier denoted as Δ). The associated stresses are σ_{nn} (normal stress) and σ_{nt} (shear stress). The relations between σ_{nn}, σ_{nt} and δ_{nn}, δ_{nt} can be expressed as:

$$\begin{Bmatrix} d\,\sigma_{nn} \\ d\,\sigma_{nt} \end{Bmatrix} = \begin{bmatrix} B_{nn} & B_{nt} \\ B_{tn} & B_{tt} \end{bmatrix} \begin{Bmatrix} d\,\delta_n \\ d\,\delta_t \end{Bmatrix} \text{ or}$$

$$\{d\,\sigma\} = \left[B^{cr,p}\right] \{d\,\delta\} \tag{6.1}$$

where B_{nn}, B_{nt}, B_{tt} and B_{tn} are the crack stiffness coefficients: the superscripts cr,p refer to crack and plain concrete. With the equations (5.10) and (5.11) simplified expressions have been given for the relations between σ_{nn}, σ_{nt} and δ_{nn}, δ_{nt}. In a generalized way these functions are represented by

$$\sigma_{nn} = f_n\,(\delta_n, \delta_t)\ ,\ \sigma_{nt} = f_t\,(\delta_n, \delta_t) \tag{6.2}$$

Differentiation of (6.2) results in expressions for the crack stiffness coefficients:

$$B_{nn} = \frac{\partial f_n}{\partial \delta_n}\ ,\ B_{nt} = \frac{\partial f_n}{\partial \delta_t}\ ,\ B_{tn} = \frac{\partial f_t}{\partial \delta_n}\ ,\ B_{tt} = \frac{\partial f_t}{\partial \delta_t} \tag{6.3}$$

Detailed formulations for these expressions are given in Appendix III. These relations are valid for increasing values of δ_n and $|\delta_t|$, as generally encountered in the case of monotonically increased loading. A path-dependent formulation, taking into account plastic deformations and friction between particles and matrix, would be possible on the basis of the data presented in the Chapters 3 and 5, but would require more complicated expressions. Considering the values of the crack stiffness coefficients, it can be expected that the crack stiffness matrix is not positive definite. However, the unstable behaviour is usually stabilized by the restraint provided by the reinforcement and the boundary conditions (Bazant, Gambarova [3]).

b. The reinforced crack.

A distinction has to be made between the case where the crack

opens freely and the case where crack opening is confined to a limit direction due to secondary effects caused by local modifications of the crack structure around the reinforcing bars due to splitting forces. In Fig. 5.35 it was shown that in the case of a confined crack opening it is possible to simulate the behaviour by the introduction of hinged struts with high stiffness. The direction of these struts depends on the actual combination of displacements (δ_n, δ_t) (Fig. 6.2).

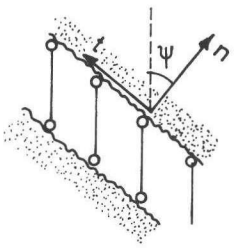

Fig. 6.2 Compression struts as an expedient to simulate the behaviour of reinforced cracks

The relation between stresses and displacements is now a function of two mechanisms: the compression struts (aggregate interlock type II) and the particle-matrix interaction, as formulated in the previous section (6.1.a) (aggregate interlock type I). In the next formulation the influence of dowel action is neglected. The average stresses, caused by the very stiff compression struts, are represented by

$$\{d\,\sigma^{str}\} = \left[B^{str}\right] \{d\,\delta^{cr}\} \qquad (6.4)$$

where the superscript str refers to strut and cr refers to crack. Since the struts are inclined to the crack, the matrix $\left[B^{str}\right]$, which is by definition related to the crack direction (n, t), has to be obtained by the transformation

$$\left[B^{str}\right] = \left[R^{str}\right]^T \left[B^{str}_{\psi}\right] \left[R^{str}\right] \tag{6.5}$$

with $$\left[R^{str}\right] = \begin{bmatrix} M^2 & 2MN \\ -MN & M^2-N^2 \end{bmatrix}$$

and $$\left[B^{str}_{\psi}\right] = \begin{bmatrix} E_{str} & 0 \\ 0 & 0 \end{bmatrix}$$

where $M = \cos \psi$, $N = \sin \psi$ and ψ is the angle between the direction normal to the crack and the direction of the struts. The direction of the struts depends on the combination of displacements: $\psi = \psi(\delta_n, \delta_t)$ (Appendix III).
A sufficiently high stiffness could be attributed to the struts, for example, $E_{str} = 10^{20}$ ($\approx \infty$).
The stresses in the crack as a result of the particle-matrix interaction have earlier been formulated in equation (6.1).
A summation of the stresses caused by both effects yields

$$\{d\,\sigma^{cr}\} = \left[B^{cr,r}\right] \{d\,\delta^{cr}\} \tag{6.6}$$

with $$\left[B^{cr,r}\right] = \left[B^{cr,p}\right] + \left[B^{str}\right] \tag{6.7}$$

where the superscript cr,r refers to crack in reinforced concrete. If the struts are subjected to tensile forces, the matrix B^{str} is defined to be $\left[B^{str}\right] = \left[0\right]$.

6.2 The relation between stresses and displacements in cracked reinforced concrete

The relation between stresses and displacements in cracked reinforced concrete is formulated in a way similar to that previously proposed by Bazant and Gambarova [3]. A slight modification is applied, enabling the introduction of tension stiffening effects.
A cracked concrete element is considered, reinforced with steel bars in one direction. The concrete is intersected by a system of

parallel cracks of average spacing s; the angular deviation between the bars and the crack normal is equal to Θ (Fig. 6.3).

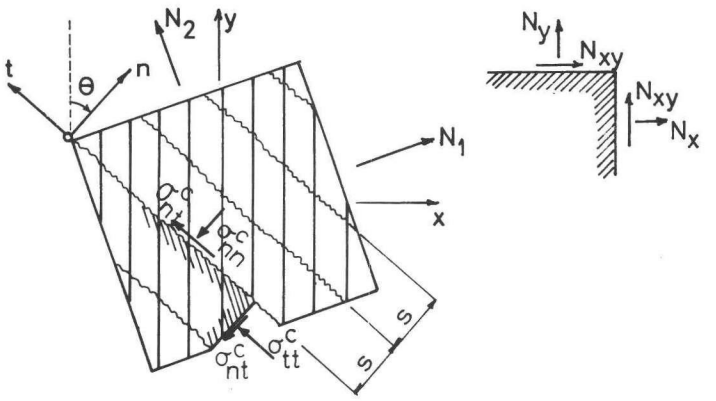

Fig. 6.3 Reinforced concrete element intersected by cracks

It is assumed that the element is sufficiently large compared to the spacing of bars and cracks and that the internal forces vary gradually and smoothly, so as that they could be assumed to be almost uniform over a distance of several bar and crack spacings. By inversion of the crack stiffness matrix $\left[B^{cr,r}\right]$ from equation (6.7), we obtain:

$$\begin{Bmatrix} d\,\delta_n \\ d\,\delta_t \end{Bmatrix} = \begin{bmatrix} F_{nn} & F_{nt} \\ F_{tn} & F_{tt} \end{bmatrix} \begin{Bmatrix} d\,\sigma_{nn} \\ d\,\sigma_{nt} \end{Bmatrix} \tag{6.8}$$

or $$\{d\,\delta^{cr}\} = \left[F^{cr,r}\right] \{d\,\sigma^{cr}\}$$

where $\left[F^{cr,r}\right]$ is the flexibility matrix of the crack and $\left[F^{cr,r}\right] = \left[B^{cr,r}\right]^{-1}$.

The average strains resulting from the "smeared out" cracks are:

$$\varepsilon_{nn}^{cr} = \frac{\delta_{nn}}{s(\varepsilon)} \quad , \quad \gamma_{nt}^{cr} = 2\,\varepsilon_{nt}^{cr} = \frac{\delta_{nt}}{s(\varepsilon)} \tag{6.9}$$

The superscript cr indicates that only deformations directly related to the crack displacements are considered. $s(\varepsilon)$ is the mean crack spacing attended by a strain condition $\{\varepsilon\}$. The mean crack spacing $s(\varepsilon)$ depends on a number of influencing factors:

- the bond-slip relation, depending on the profiling of the reinforcing bars, the concrete quality and the stresses in the surrounding concrete;
- geometrical effects, such as the bar diameter, bar distance and concrete cover;
- the concrete tensile strength (low strength results in many cracks), which is also influenced by the stresses in the surrounding concrete due to external forces;
- the angle between reinforcing bars and crack direction: in general the mean crack width is a function of the introduction length l_b of the bond stresses. If the cracks are perpendicular to the direction of the reinforcement, the average crack spacing is about $s = 1.5\ l_b$. If the angle between cracks and reinforcement deviates from 90^o, the average crack spacing is reduced as a function of this deviation (Fig. 6.4).

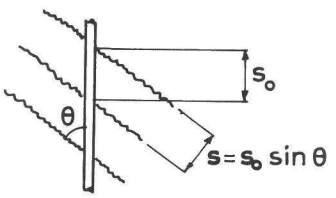

Fig. 6.4 Crack spacing related to the orientation of the reinforcement

Extended reviews and discussions on crack spacing have been given by, among others, Leonhardt [42], Eibl and Ivanyi [16] and

Geistefeld [24].
A combination of the equations (6.8) and (6.9) results in:

$$\begin{Bmatrix} d\,\varepsilon^{cr}_{nn} \\ d\,\varepsilon^{cr}_{tt} \\ d\,\gamma^{cr}_{nt} \end{Bmatrix} = \begin{bmatrix} F_{nn}\, s(\varepsilon)^{-1} & 0 & F_{nt}\, s(\varepsilon)^{-1} \\ 0 & 0 & 0 \\ F_{tn}\, s(\varepsilon)^{-1} & 0 & F_{tt}\, s(\varepsilon)^{-1} \end{bmatrix} \begin{Bmatrix} d\,\sigma^{c}_{nn} \\ d\,\sigma^{c}_{tt} \\ d\,\sigma^{c}_{nt} \end{Bmatrix} \quad (6.10)$$

which may be briefly written as

$$\{d\,\varepsilon^{cr}\} = \left[D^{cr} \right] \{d\,\sigma^{c}\} \quad (6.11)$$

Here the superscript c refers to the concrete between the cracks. The last equation indicates that the stresses in the concrete are equal to those in the cracks. The average strains of the cracked reinforced concrete element ε_{nn}, ε_{tt} and γ_{nt} can be obtained as the sums of the strains of the solid concrete between the cracks ε^{c}_{nn}, ε^{c}_{tt} and γ^{c}_{nt} and the strains due to the cracks ε^{cr}_{nn}, ε^{cr}_{tt}, γ^{cr}_{nt}; so

$$\{d\,\varepsilon\} = \{d\,\varepsilon^{cr}\} + \{d\,\varepsilon^{c}\} \quad (6.12)$$

where $\{d\,\varepsilon\} = (d\,\varepsilon_{nn},\ d\,\varepsilon_{tt},\ d\,\gamma_{nt})^{T}$, T denoting the transpose, and $\{d\,\varepsilon^{cr}\}$, $\{d\,\varepsilon^{c}\}$ are the analogous column matrices for strains due to cracks and to concrete between the cracks. The strains in the concrete between the cracks are related to the stresses by the incremental stress-strain relation

$$\{d\,\varepsilon^{c}\} = \left[D^{c} \right] \{d\,\sigma^{c}\} \quad (6.13)$$

where D^{c} is the tangent flexibility matrix of concrete.
Substitution of (6.11) and (6.13) into (6.12) yields

$$\{d\,\varepsilon\} = \left[D \right] \{d\,\sigma^{c}\} \qquad \left[D \right] = \left[D^{cr} \right] + \left[D^{c} \right] \quad (6.14)$$

where D is the flexibility matrix of cracked concrete as a whole. Equation (6.14) being known, the influence of the reinforcement can be insterted. It is assumed that the average strains of the reinforcement are equal to those of the cracked concrete. The effect of tension stiffening is implied in the stress-strain relation of the steel. The averaged stresses are:

$$\{d\ \sigma^s\} = \left[C^s \right] \{d\ \varepsilon\} \tag{6.15}$$

where the superscript s refers to steel. Since the cracks are in general inclined with respect to the reinforcing bars, the matrix $\left[C^s \right]$, which is by definition related to the axes n and t, must be obtained by the transformation:

$$\left[C^s \right] = \left[R^s \right]^T \left[C^s_\theta \right] \left[R^s \right],$$

$$\left[R^s \right] = \begin{bmatrix} P^2 & Q^2 & 2\,PQ \\ Q^2 & P^2 & -2\,PQ \\ -PQ & PQ & P^2-Q^2 \end{bmatrix} \tag{6.16}$$

with

$$\left[C^s_\theta \right] = \begin{bmatrix} \frac{\rho_\theta E_s}{\alpha(\varepsilon)} & 0 & 0 \\ 0 & 0 & 0 \\ 0 & 0 & 0 \end{bmatrix} \tag{6.17}$$

where $P = \cos\theta$, $Q = \sin\theta$, θ is the angle between the reinforcing bars and the direction normal to the crack (Fig. 6.3). $E_s(\varepsilon)$ is the tangential spring stiffness of the reinforcing steel, ρ_θ is the reinforcing ratio in the bar direction and $\alpha(\varepsilon)$ is a factor taking account of the effect of tension stiffening. This factor $\alpha(\varepsilon)$ is closely related to the mean crack spacing $s(\varepsilon)$.

Finally the stresses due to the cracked concrete and to the steel bars must be added:

$$\{d\,\sigma\} = \{d\,\sigma^{c}\} + \{d\,\sigma^{s}\}$$

Because, according to equation (6.14):

$$\{d\,\sigma^{c}\} = [\,D\,]^{-1}\,\{d\,\varepsilon\}$$

this results in

$$\{d\,\sigma\} = [\,C\,]\{d\,\varepsilon\} \quad \text{with } [\,C\,] = [\,C^{s}\,] + [\,D\,]^{-1}$$

where $[\,C\,]$ is the tangential stiffness matrix of cracked reinforced concrete, referred to the axes n and t. This matrix $[\,C\,]$ must of course be further transformed to the element co-ordinates.

7 RETROSPECTIVE VIEW

The aim of the investigation was to study the phenomenon of aggregate interlock as an individual mechanism and its role in co-operation with other components in reinforced cracks.

The analysis of the first item resulted both in an adequate insight into the physical backgrounds of the mechanism and in a simple mathematical formulation. The results apply for a great variety of concrete mixes. However, due to limitations in time and costs not all aspects could be taken into account:

- Particle shape:

  The results have been obtained for concretes with natural rounded aggregate particles, for which a simplification to spheres may be considered reasonable. In a number of countries crushed aggregate is also used. To see whether the same relations apply also to these types of concretes, or whether modifications are necessary, other tests would be of interest.

- The orientation of the crack plane with respect to the direction of casting:

  It was shown by the mathematical model describing the mechanism of aggregate interlock that the stress-displacement relations for cracks are affected by the quality of the matrix. The yielding strength of the matrix, as defined in the model, is an average value for a heterogeneous material. Effects of anisotropy of this material have not been taken into account. However, anisotropy may occur, due to the influence of the direction of casting: as a result of water gain and sedimentation under coarse aggregate particles a soft and spongy layer can form, with a variable thickness. Hence, it may make a difference whether the orientation of the layer is as represented in Fig. 7.1.a or as in Fig. 7.1.b. It would be interesting to see whether this difference has a significant influence.

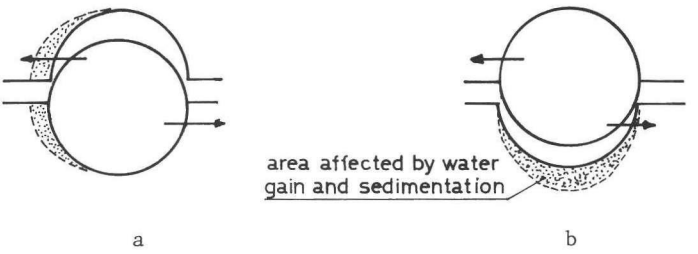

Fig. 7.1 Effect of water gain and sedimentation on the stiffness characteristics of a crack

- Matrix/particle strength ratios:

  In the experiments the particle strength was generally higher than the matrix strength. Even in the case of a concrete strength of $f'_{cc} = 60$ N/mm^2 in the tests, only a limited number of particles were found to have fractured. However, if the relation particle strength/matrix strength would be lower than in this investigation, the crack faces would be less profiled and the total contact area could be significantly reduced. Tests have also been carried out on cracked specimens made of lightweight concrete [84, 85] in which the crack intersected all lightweight particles but avoided the sand particles. In spite of the fact that the sand was distributed according to a Fuller curve, the results obtained by calculation with the theoretical model (only taking account of the sand particles) were too low. This is probably caused by the rough surface of the broken lightweight particles, the influence of which was neglected.

In the tests on reinforced cracks it appeared that for a wide range of reinforcement ratios the crack opening path was not influenced by the restraint stiffness against crack opening in normal direction. The divergence of the crack opening paths was small, in spite of considerable variations in concrete strength and reinforcement ratio. Hence, the results obtained in this part of the investigation do not cover all possibilities of crack opening which can be expected in cracked reinforced concrete in practical situations.

To improve the provisional model for the behaviour of reinforced cracks, as proposed in this study, further experimental evidence is needed. Above all, what is required are the results of tests on reinforced cracks subjected to combinations of shear and tension normal to the crack.

8 SUMMARY

As a result of the increasing difficulties in structural design associated with the increase in scale and complexity of new structures and their loading conditions in recent years, added impetus has been given to the development of numerical calculation techniques. Above all, the non-linear finite element methods, which are still being refined, may become powerful tools in future design. These methods, however, can only show to full advantage if the material characteristics to be inserted are adequately known. One of the characteristics affected by lack of information concerns the mechanism of transmission of forces across cracks whose the faces are subjected to shear displacements. This mechanism is achieved by interaction of several components: axial and transverse stiffness (dowel action) of the reinforcement and direct transfer of forces between the rough concrete crack faces, generally denoted by the term "aggregate interlock". Since aggregate interlock appeared to be the missing link in this system with regard to the available knowledge, a research program was carried out, focusing on this subject.

First, "pure" aggregate interlock, i.e., aggregate interlock in cracks which are not intersected by reinforcement, was studied. To obtain an insight into this mechanism a theoretical model was developed, which was subsequently compared with experimental results. The theory is based on the assumption that concrete can be conceived as a "two-phase" material which is composed of a collection of aggregate particles with high strength and stiffness (phase I), and a matrix material consisting of hardened cement paste with fine sand with lower strength and stiffness (phase II). A crack in this composite material generally intersects the matrix, but not the aggregate particles, because the contact layer between particles and matrix is of relatively low quality. The transmission of forces during shear displacement of the crack faces is effected via local contact areas between the particles protruding from one of the crack faces and the matrix in the opposite crack face. The

interdependence between forces and displacements of the crack faces is closely related to the deformation of the matrix material. The most probable distribution and orientation of the contact areas were determined by a statistical analysis. For this analysis the aggregate particles were simplified to spheres, protruding for an arbitrary part of their diameter from one of the crack faces. For the distribution of the aggregate particle diameters a Fuller curve was chosen, frequently used in the design of concrete mixes, which has the advantage of being characterized by a simple mathematical formulation. The coefficient of friction between particles and matrix at overriding, and the stress at which plastic deformation of the matrix occurs, were used as "adjusting parameters" in the model. The validity of the theory has been verified by a number of experiments in which the concrete quality, the particle sizes and the external restraining stiffness against crack opening had been varied. It was shown that the experimental results could be adequately described by the theoretical model. By means of a parameter study carried out with the model, the mechanism of transmission of forces was further analyzed, focusing on the role of the individual particle fractions, the scale of the aggregate particles and the influence of the grading curve. It was demonstated that the behaviour of cracks subjected to cyclic loading, as known from the literature, can be explained by the model. It was also shown that the concrete quality has a great influence on the "crack stiffness".

The second part of the investigation was concerned with the question whether the relations for cracks in plain concrete, derived in the first part, are directly applicable to cracks in reinforced concrete, in which the resistance to crack opening is internally provided and in which the role of dowel action has to be considered. Therefore a number of experiments were carried out, in which the reinforcement ratio, the bar diameters and the concrete quality were varied. It emerged that the relations previously found for cracks in plain concrete could not be directly applied to cracks in reinforced concrete. It was demonstrated that this must be due

to local modifications caused in the crack structure in the immediate vicinity of the reinforcing bars crossing the crack by splitting forces transmitted through the ribs of the bars into the concrete. It was observed that due to this additional mechanism a preferred direction for crack opening exists, which exhibited only minor differences for the various concrete types tested. It was shown how the relation between forces and displacements for cracks in reinforced concrete can be formulated on the basis of the experimental results.

Finally it was indicated how the relation between stresses and deformations for cracked reinforced concrete can be formulated, taking account of the characteristics of the behaviour of single cracks.

SAMENVATTING

Vooral de laatste jaren worden voor verschillende doeleinden constructies vereist met een steeds complexer karakter, waaraan vooral schaalvergroting en bijzondere functionele eisen debet zijn. Bij het ontwerpen van dit soort constructies kan vaak niet meer worden teruggegrepen naar bestaande ontwerpmethoden en rekenregels, omdat deze meestal geldig zijn voor betrekkelijk eenvoudige gevallen. In verband met het voorgaande zijn de laatste jaren sterke impulsen gegeven aan de ontwikkeling van nieuwe rekentechnieken. Vooral de ontwikkeling van de niet-lineaire elementenmethode opent in dit opzicht brede perspectieven. Een dergelijke methode komt echter slechts dan goed tot zijn recht, als nauwkeurige materiaalkarakteristieken kunnen worden ingevoerd.
Eén van de mechanismen waarvan te weinig bekend was betreft de overdracht van krachten tussen scheurvlakken indien deze aan parallelverplaatsingen onderhevig zijn. De krachtsoverdracht kan plaatsvinden via een interactie tussen de axiale veerstijfheid en de deuvelwerking van de wapening, en "aggregate interlock", d.w.z. de krachtsoverdracht tussen de ruwe beton-scheurvlakken. Omdat gebrek aan kennis voornamelijk het laatste onderdeel betrof is hiernaar een onderzoek verricht.

In de eerste plaats is onderzoek gedaan naar de krachtsoverdracht bij "zuivere aggregate interlock", d.w.z. aggregate interlock in ongewapende scheurvlakken. Om een inzicht te krijgen in dit mechanisme is een theoretisch model ontwikkeld, dat vervolgens aan experimenten is getoetst. De theorie gaat er van uit dat beton kan worden beschouwd als een zogenaamd twee-fasen materiaal, dat is opgebouwd uit een verzameling toeslagkorrels met grote sterkte en stijfheid (fase I) en een matrixmateriaal, bestaande uit cementsteen met fijne toeslagkorrels, dat een lagere sterkte en stijfheid bezit (fase II). Een scheur door dit materiaal doorsnijdt in het algemeen wel de matrix, maar niet de korrels, omdat de aanhechtingslaag tussen korrels en matrix van relatief lage kwaliteit is. De krachtsoverdracht bij tegengerichte parallelverplaatsing der

beide scheurvlakken komt tot stand ter plaatse van de contactvlakken tussen de korrels aan de ene zijde van de scheur en de matrix aan de andere zijde. De relatie tussen de krachten en de verplaatsingen der scheurvlakken ten opzichte van elkaar hangt samen met de mate waarin het matrixmateriaal wordt vervormd. De meest waarschijnlijke verdeling der contactvlakken is met een statistische berekening bepaald. Hierbij zijn de toeslagkorrels tot bollen geschematiseerd, die voor een willekeurig deel van hun afmetingen uit het scheurvlak kunnen steken. Voor de opbouw van de korrelgrootte-verdeling is een Fullerkromme aangehouden, die bij het samenstellen van beton vaak wordt gehanteerd en het voordeel heeft door een eenvoudige mathematische formulering te worden gekarakteriseerd. De wrijvingscoëfficiënt ter plaatse van het korreloppervlak en de spanning waarbij het matrixmateriaal plastisch gaat vervormen zijn als "instelparameters" in het model opgenomen. De geldigheid van de theorie is getoetst aan een aantal experimenten, waarbij de betonkwaliteit, de korrelgrootte en de uitwendige stijfheid tegen openen van de scheur werden gevarieerd. Vastgesteld werd dat de experimentele resultaten zeer goed door het mathematische model kunnen worden beschreven. Door een parameterstudie, uitgevoerd met behulp van het model, werd het mechanisme van krachtsoverdracht in scheuren nader geanalyseerd, waarbij aandacht werd besteed aan de bijdrage van afzonderlijke korrelfracties aan de krachtsoverdracht, de invloed van de schaal van het korrelmengsel en de invloed van de verdelingsfunctie van het toeslagmateriaal. Aangetoond werd dat het gedrag van scheurvlakken onder wisselbelasting, zoals bekend uit de literatuur, in overeenstemming is met de aannamen van het model en hieruit kan worden verklaard. Vastgesteld werd dat de betonkwaliteit een grote invloed heeft op de krachtsoverdracht in scheuren.

In het tweede deel van het onderzoek werd nagegaan of de gevonden wetmatigheden direct toepasbaar zijn op scheuren in gewapend beton, waarin de weerstand tegen scheuropening inwendig wordt geleverd en waarbij rekening gehouden moet worden met de deuvelwerking van de wapeningsstaven. Hiertoe zijn een aantal proevenseries uitge-

voerd waarin onder meer het wapeningspercentage, de staafdiameters en de betonkwaliteit werden gevarieerd. Hieruit bleek dat de relaties, gevonden voor ongewapend beton niet zonder meer mogen worden gebruikt voor gewapend beton. Aangetoond kon worden dat dit toegeschreven moet worden aan vernietiging van de scheurstructuur ter plaatse van de kruising met de wapeningsstaven, door splijtkrachten die via de ribben van het staal in het beton worden ingeleid. Vastgesteld werd dat door het optreden van dit mechanisme een voorkeursrichting voor scheuropening ontstaat, die voor de verschillende betonsoorten en kwaliteiten slechts zeer geringe verschillen vertoont. Aangegeven werd op welke wijze de kracht-verplaatsingsrelatie voor scheuren in gewapend beton, op grond van de beschikbare gegevens, geformuleerd kan worden.

Tot slot is aangegeven hoe de relatie tussen spanningen en vervormingen voor gescheurd gewapend beton kan worden geformuleerd, rekening houdend met de gevonden karakteristieken voor het scheurgedrag.

9 REFERENCES

1. ACI-Committee 349: "Criteria for reinforced concrete nuclear power containment structures", ACI-Journal, Vol. I, January 1972, pp. 2-28.

2. BAUMANN, T.: "Tragwirkung orthogonaler Bewehrungsnetze beliebiger Richtung in Flächentragwerken aus Stahlbeton", Deutscher Ausschuss für Stahlbeton, Heft 217, Wilhelm Ernst and Sohn, Berlin, 1972.

3. BAZANT, Z.P., GAMBAROVA, P.: "Rough cracks in reinforced concrete", Preprint 3579, ASCE-Convention, Boston, April 1979.

4. BAZANT, Z.P., TSUBAKI, T.: "Optimum slip-free limit design of conrete reinforcing nets", Journal of the Structural Division, Proc. ASCE, Vol. 105, February 1979, ST 2, pp. 327-346.

5. BRAESTRUP, M.W.: "Plastic analysis of shear in reinforced concrete", Report No. 70, Afdelingen for Baerende Konstruktioner, Technical University of Denmark, Copenhagen, 1970.

6. BLAAUWENDRAAD, J., LEYTEN, S.F.C.H., VAN MIER, J.G.M.: "Comparison of plastic prediction with STANIL Analysis", Final Report IABSE, Colloquium "Plasticity in reinforced concrete", Copenhagen, 1979.

7. BRONDUM-NIELSEN, T.: "Optimum design of reinforced concrete shells and slabs", Report No. R. 44, Structural Research Laboratory, University of Denmark, Copenhagen, 1974, pp. 190-200.

8. BRUGGELING, A.S.G., BRUNEKREEF, S.H., WALRAVEN, J.C.: "Partially prestressed concrete - Theory and experiments", Heron, Vol. 23, No. 1, 1978, pp. 18-35.

9. CEB-Bulletin d'Information, No. 88, p. 123.

10. CEB-FIP: Model Code for Concrete Structures, 3-thd edition 1978.

11. CEDOLIN, L., DEI POLI, S.: "Non-linear plane stress analysis of reinforced concrete by the finite element method", Costruzioni in cemento armato, Studi e Rendiconti, Politecnico di Milano, Vol. VIII, 1977, pp. 3-33.

12. CEDOLIN, L., DEI POLI, S.: "Finite element studies of shear critical reinforced concrete beams", Journal of the Engineering Mechanics Division, EM 3, June 1977, pp. 395-410.

13. CERVENKA, V.: "Inelastic finite element analysis of reinforced concrete panels under in-plane loads", Doctor Thesis, University of Colorado, 1970.

14. CORDON, W.A., GILLESPIE, H.A.: "Variables in concrete aggregates and Portland cement paste which influence the strength of concrete", ACI-Journal, Proceedings Vol. 60, No. 8, August 1963, pp. 1029-1055.

15. EBBINGHAUS, P.: "Herleitung eines Verfahrens zur Berechnung von Stahlbetonscheiben unter Berücksichtigung der Rissentwicklung", Dissertation, RWTH Aachen, 1975.

16. EIBL, J., IVANYI, G.: "Studie zum Trag- und Verformungsverhalten von Stahlbeton", Deutscher Ausschuss für Stahlbeton, Heft 260, Berlin, 1976.

17. ELEIOTT, A.F.: "An experimental investigation of shear transfer across cracks in reinforced concrete", M.S. Thesis, Cornell University, Ithaca, June 1974.

18. FENWICK, R.C., PAULAY, T.: "Mechanisms of shear resistance of concrete beams", Journal of the Structural Division, ASCE, Vol. 94, No. ST 10, Proc. Paper 2325, 1968, pp. 2325-2350.

19. FINNEY, E.: "Structural design considerations for pavement joints", ACI-Journal, Proceedings, Vol. 53, No. 1, 1956, pp. 17-30.

20. FINNEY, E.A., FREMONT, W.O.: "Progress report on load-deflection tests dealing with length and size of dowels", Proceedings, Highway Research Board, Vol. 27, 1947, p. 171.

21. FRANKLIN, H.A.: "Non-linear analysis of reinforced concrete frames and panels", Dissertation, University of California, Berkeley, 1970.

22. FRIBERG, B.F.: "Load and deflection characteristics of dowels in transverse joints of concrete pavements", Highway Research Board, Proceedings, Vol. 18, Part I, 1940, pp. 154-173.

23. FRIBERG, B.F.: "Design of dowels in transverse joints of concrete pavements", Transactions, ASCE, Vol. 105, 1940, pp. 1078-1080.

24. GEISTEFELD, H.: "Stahlbetonscheiben in gerissenem Zustand - Berechnung mit Berücksichtigung der rissabhängigen Schubsteifigkeit im Materialgesetz", Dissertation, TU Braunschweig, 1976.

25. GOTO, Y.: "Cracks formed in concrete around deformed tension bars", ACI-Journal, Proceedings, Vol. 68, No. 4, April 1971, pp. 244-251.

26. GRINTER, L.E.: "Design of reinforced concrete road slabs", Texas Engineering Experimental Station Bulletin, No. 39, Texas 1931.

27. GROOTENBOER, H.J.: "Finite element analysis of two-dimensional reinforced concrete structures, taking account of non-linear physical behaviour and the development of discrete cracks", Thesis, Delft University of Technology, The Netherlands, 1979.

28. HAND, F.R., PECKNOLD, D.A., SCHNOBRICH, W.C.: "Non-linear layered analysis of RC plates and shells", Journal of the Structural Division, ASCE, Vol. 99, ST 7, Proc. Paper 9860, July 1973.

29. HOBBS, D.W.: "Strength and deformation properties of plain concrete subject to combined stress. Part 3: Results obtained on a range of flint gravel aggregate concretes", Technical Report, Cement and Concrete Association, No. 42.497, July 1974.

30. HOUDE, J., MIRZA, M.S.: "A finite element analysis of shear strength of reinforced concrete beams", ACI-Special Publication "Shear in reinforced concrete", SP-42, Vol. I, pp. 103-128.

31. ISENBERG, J., ADHAM, S.: "Analysis of orthotropic reinforced concrete structures", Journal of the Structural Division, Proceedings of the ASCE, Vol. 96, ST 12, December 1970, pp. 2607-2624.

32. JIMENEZ, R., PERDIKARIS, P., GERGELY, P., WHITE, R.N.: "Interface shear transfer and dowel action in cracked reinforced concrete subject to cyclic shear", Methods of Structural Analysis, Proceedings of the ASCE Conference, Madison, August 1976, pp. 457-475.

33. DE JOSSELIN DE JONG, G.: "Aeolotropie van gestructureerde materialen", Cement XXVI, No. 4, 1974, pp. 166-176.

34. KLEIN, D., KRISTJANSSON, R., LINK, J., MEHLHORN, G., SCHAEFER, H.: "Zur Berechnung von dünnen Stahlbetonplatten bei Berücksichtigung eines wirklichkeitsnahen Werkstoffverhaltens", Forschungsbericht No. 25, Institut für Massivbau, TU Darmstadt, 1975, pp. 1-28.

35. KOCH, R.: "Verformungsverhalten von Stahlbetonstäben unter Biegung und Längszug im Zustand II auch bei Mitwirkung des Betons zwischen den Rissen", Dissertation, Stuttgart, 1976, P. 59.

36. KREFELD, W., THURSTON, C.W.: "Contribution of longitudinal steel to shear resistance of reinforced concrete beams", ACI-Journal, Proc. Vol. 63, March 1966, pp. 325-344.

37. KRISNAMOORTHY, C.S., PANEERSELVAM, A.: "A finite element model for non-linear analysis of reinforced concrete framed structures", The Structural Engineer, August 1977, No. 8, Vol. 55.

38. KUPFER, H., HILSDORF, H.K., RUSCH, H.: "Behaviour of concrete under biaxial stresses", ACI-Journal, Proceedings Vol. 66, No. 8, August 1969, pp. 656-666.

39. KUYT, B.: "Zur Frage der Netzbewehrung von Flächentragwerken", Beton- und Stahlbetonbau, Vol. 59, No. 7, 1964, pp. 158-163.

40. LAIBLE, J.P., WHITE, R.N., GERGELY, P.: "Experimental investigation of seismic shear transfer across cracks in concrete nuclear containment vessels", ACI-Special Publication SP-53-9, pp. 203-226.

41. LEITZ, H.: "Eisenbewehrte Platten bei algemeinem Biegungszustand", Die Bautechnik, Vols. 16 and 17, 1923.

42. LEONHARDT, F.: "Vorlesungen über Massivbau", Vierter Teil, Nachweis der Gebrauchsfähigkeit, Springer Verlag, Berlin, Heidelberg, New York.

43. LIN, C.S., SCORDELIS, A.C.: "Non-linear analysis of RC shells of general form", Journal of the Structural Division, ASCE, ST 3, March 1975, pp. 523-537.

44. LOCHER, F.W., WISCHERS, G.: "Aufbau und Eigenschaften des Zementsteins", Zement Taschenbuch 1976/77, NCH Nederlandse Cement Handelsmij B.V., s-'Gravenhage, pp. 43-59.

45. LOE, J.A.: "Dowel bar joints for airfield pavements", Journal of Institution of Civil Engineers, London, Vol. 1, October 1952, p. 625.

46. LOOV, R.: "The determination of stresses and deformations of reinforced concrete after cracking", Proceedings of the Southamton 1969 Civ. Eng. Materials Conference, pp. 1257-1260.

47. LUESCHE, M.: "Beitrag zum Bruchmechanismus von auf Druck beanspruchtem Normal- und Leichtbeton mit geschlossenem Gefüge", Schriftenreihe der Zementindustrie, Heft 39/1972, Verein Deutscher Zementwerke e.v., Düsseldorf, p. 27.

48. MARCUS, H.: "Load carrying capacity of dowels at transverse pavement joints", Proceedings, ACI-Journal, Vol. 23, October 1951, pp. 169-184.

49. MARTIN, H.: "Zusammenhang zwischen Oberflächenbeschaffenheit, Verbund und Sprengwirkung von Bewehrungsstählen unter Kurzzeitbelastung", Deutscher Ausschuss für Stahlbeton, Heft 228, Berlin, 1973.

50. MATTOCK, A.H.: "Shear transfer in concrete having reinforcement at an angle to the shear plane", ACI-Special Publication SP-42, "Shear in reinforced concrete", Vol. I, pp. 17-42.

51. MATTOCK, A.H.: "Effect of aggregate type on single direction shear transfer strength in monolithic concrete", Report SM 74-2, Department of Civil Engineering, University of Washington, Seattle, Washington, August 1974.

52. MUELLER, P.: "Plastische Berechnung von Stahlbetonscheiben und -Balken", Bericht Nr. 83, Institut für Baustatik und Konstruktion, ETH-Zürich, July 1978.

53. NIELSEN, M.P., BRAESTRUP, M.W., JENSEN, B.C., FINN BACH: "Concrete plasticity: Beam shear - Shear in joints - Punching Shear", Specialpublikation udgivet af Dansk Selskab for Bygningsstatik, Lyngby, October 1978.

54. NGO, D., SCORDELIS, A.C.: "Finite element analysis of reinforced concrete beams", ACI-Journal, Vol. 64, No. 3, March 1967, pp. 152-163.

55. NILSON, A.H.: "Non-linear analysis of reinforced concrete by the finite element method", ACI-Journal, September 1968, pp. 757-766.

56. NOAKOWSKI, P.: "Einfluss der Profilierung und des Betons auf die Verbundqualität von Stahl in Beton", Aus unseren Forschungsarbeiten III, Lehrstuhl und Institut für Massivbau, Technische Universität München, Dezember 1973, pp. 89-91.

57. NOAKOWSKI, P.: "Berechnung der bezogenen Rippenfläche", Aus unseren Forschungsarbeiten III, Lehrstuhl und Institut für Massivbau, Technische Universität München, Dezember 1973, pp. 92-94.

58. PARK, R., PAULAY, T.: "Reinforced concrete structures", Wiley Intersience Publication, New York, 1975, pp. 319-338.

59. PAULAY, T., PARK, R., PHILLIPS, M.H.: "Horizontal construction joints in cast in place reinforced concrete", ACI-Special Publication SP-42, "Shear in reinforced concrete", Vol. II, pp. 599-616, 1974.

60. PAULAY, T., LOEBER, P.J.: "Shear transfer by aggregate interlock", ACI-Special Publication SP-42, "Shear in reinforced concrete", 1974, Vol. I, pp. 1-16.

61. REGAN, P.E.: "Shear in reinforced concrete - an experimental study", Report Imperial College, London, 1971, pp. 93-110.

62. REHM, G.: "Ueber die Grundlagen des Verbundes zwischen Stahl und Beton", Deutscher Ausschuss für Stahlbeton, Heft 138, Berlin, 1961.

63. REHM, G., MARTIN, H., NOAKOWSKI, P.: "Einfluss der Profilierung und des Betons auf die Verbundqualität von Stahl in Beton - Ausziehversuche an gefrästen Stählen", Bericht Nr. 2203 des Lehrstuhls und Instituts für Massivbau der TU München, 1970.

64. REINHARDT, H.W.: "Ansprüche des Konstrukteurs an den Beton", Beton 27, 1977, Nr. 5, pp. 195-199.

65. SCHAEFER, H.: "Zur Berechnung von Stahlbetonplatten", Dissertation, TU Darmstadt, 1976.

66. SCHIESSL, P.: "Beschränkung der Rissbreiten bei Zwangsbeanspruchung", Betonwerk + Fertigteiltechnik, Heft 6/1976.

67. SCHIMMELPFENNIG, K.: "Bruchsicherheitsberechnung von Stahlbeton-Druckbehältern", Deutscher Ausschuss für Stahlbeton, Heft 257, Berlin, 1976.

68. SHAH, S.P., CHANDRA, S.: "Critical stress, volume change and microcracking of concrete", ACI-Journal, Proceedings, Vol. 65, No. 9, September 1968, pp. 770-781.

69. SCHWING, H.: "Zur wirklichkeitsnahen Berechnung von Wandscheiben aus Fertigteilen", Dissertation, TU Darmstadt, 1975.

70. STANTON, J.F.: "An investigation of dowel action of the reinforcement of nuclear containment vessels and their non-linear dynamic response to earthquake loads", M.S. Thesis, Cornell University, January 1977.

71. STAUDER, W.: "Ein Beitrag zur Untersuchung von Stahlbetonscheiben mit Hilfe finiter Elemente unter Berücksichtigung eines wirklichkeitsnahen Werkstoffverhaltens", Dissertation, TU Darmstadt, 1976.

72. SUIDAN, M., SCHNOBRICH, W.C.: "Finite element analysis of reinforced concrete", Journal of the Structural Division, Proceedings of the ASCE, Vol. 99, No. ST 10, October 1973, pp. 2109-2122.

73. SWAMY, R.N., ANDRIOPOULOS, A.D.: "Contribution of aggregate interlock and dowel forces to the shear resistance of reinforced beams without web reinforcement", ACI-Special Publication SP-42, 1974, Vol. I, pp. 129-166.

74. SWOBODA, G.: "Rissuntersuchungen in Stahlbetonbalken und Scheiben mit Hilfe des L.S.T.-Element", Der Bauingenieur, Vol. 50, 1975, No. 12, pp. 465-468.

75. TAYLOR, H.P.J.: "Investigation of the forces across cracks in reinforced concrete beams in shear by aggregate interlock", Technical Report No. 42.447, Cement and Concrete Association, November 1970.

76. TAYLOR, H.P.J.: "Fundamental behaviour in bending and shear of reinforced concrete", Thesis, London, 1971.

77. TAYLOR, H.P.J.: "The fundamental behaviour of reinforced concrete beams in bending and shear", ACI-Special Publication SP-42, "Shear in reinforced concrete", 1974, Vol. I, pp. 43-78.

78. THUERLIMANN, B.: "Shear strength of reinforced and prestressed concrete beams - CEB Approach", and "Torsional strength of reinforced and prestressed concrete beams - CEB Approach", Lecture, ACI Symposium Philadelphia, 1976.

79. TIMOSHENKO, S., LESSELS, J.M.: "Applied elasticity", Westinghouse Technical Night School Press, East Pittsburg, Pa, 1925.

80. WALRAVEN, J.C.: "Aeolotropie van gewapend beton", Cement XXVI, No. 6, 1974, pp. 256-258.

81. WALRAVEN, J.C.: "Spannungs - Dehnungsverhalten von gerissenem Beton", Heron, Vol. 21, No. 2, 1976, pp. 29-40.

82. WALRAVEN, J.C.: "The influence of depth on the shear strength of lightweight concrete beams without shear reinforcement", Report No. 5-78-4, May 1978, Stevin Laboratory, Delft University of Technology, The Netherlands.

83. WALRAVEN, J.C.: "Mechanisms of shear transfer in cracks in concrete - A survey of literature", Report No. 5-78-12, December 1978, Stevin Laboratory, Delft University of Technology, The Netherlands.

84. WALRAVEN, J.C., VOS, E., REINHARDT, H.W.: "Experiments on shear transfer in cracks in concrete. Part I: Description of results", Report No. 5-79-3, January 1979, Stevin Laboratory, Delft University of Technology, The Netherlands.

85. WALRAVEN, J.C.: "Experiments on shear transfer in cracks in concrete. Part II: Analysis of results", Report No. 5-79-10, Stevin Laboratory, Delft University of Technology, The Netherlands, November 1979.

86. WEAVER, J., CLARK, A.J.: "The effect of dowel bar misalignment in the joints of concrete roads", Technical Report No. 42.448, Cement and Concrete Association, November 1970.

87. WISCHERS, G.: "Aufnahme und Auswirkungen von Druckspannungen auf Beton", Beton, 1978, Nr. 2, pp. 63-67 and Nr. 3, pp. 98-103.

88. WEISS, R.: "Ein Haufwerkstheoretisches Model der Restfestigkeit geschädigter Betone", Dissertation, TU Braunschweig 1978, pp. 37-47.

89. WHITE, R.N., HOLLEY, M.J.: "Experimental studies of membrane shear transfer", Journal of the Structural Division, ASCE, August 1972, pp. 1835-1665 and Discussions: July 1973, pp. 1664-1665 and April pp. 816-818.

90. WHITE, R.N., GERGELY, P.: "Final report on shear transfer in thick walled reinforced concrete structures under seismic loading", Report No. 78-2, Department of Structural Engineering, Cornell University, Ithaca, New York, May 1978.

91. YUZUGULLU, O., SCHNOBRICH, W.C.: "A numerical procedure for the determination of the behaviour of a shear wall frame system", ACI-Journal, Proceedings, Vol. 70, No. 7, July 1973, pp. 474-479.

92. ZIENKIEWICS, O.C., PHILLIPS, D.V., OWEN, P.R.J.: "Finite element analysis of some concrete non-linearities - Theory and examples", Proceedings of the Seminar "Concrete structures subjected to triaxial stresses", May 1974, Bergamo, Italy.

10 NOTATION

a_x	projection of a contact length in a Z-plane on the X-axis
a_y	projection of a contact length in a Z-plane on the Y-axis
f	free length
f'_{cc}	cube crushing strength
f'_{ccyl}	cylinder crushing strength
f'_{cp}	prism crushing strength
f_R	related rib area of a reinforcing bar, characterizing its profiling
f_{sy}	yielding stress of steel
p	probability
$p(\%)$	percentage of aggregate weight passing a sieve with a certain opening diameter
p_k	probability that an arbitrary point in the concrete is located in an aggregate particle
s	crack distance
$s(\varepsilon)$	crack distance at a strain ε
u	embedment depth of a particle, defined as the distance from the centre of a spherical aggregate particle to the central crack face
u_{max}	maximum embedment depth of a particle for which contact with the opposite crack face still exists.
w	crack width
w_o	initial crack width
y	dowel deflection
A_c	total area of the crack plane
A_s	cross sectional area of reinforcing bar(s)

A_x projection on the Y-plane of the total contact area, obtained over a unit crack area

A_y projection on the X-plane of the total contact area, obtained over a unit crack area

$B_{nn,..}$ crack stiffness coefficients

D diameter of a spherical aggregate particle

D_{max} maximum diameter of a spherical aggregate particle

E_c modulus of elasticity of concrete

E_s modulus of elasticity of steel

F_d dowel force

$F_{d\theta}$ dowel force component parallel to the crack plane provided by bars inclined at an angle θ with this plane

F_s axial steel force

$F_{s\theta}$ axial steel force for bars, inclined at an angle θ with the crack plane

G shear stiffness modulus of uncracked concrete

G_{cr} shear stiffness modulus of cracked concrete

G_f foundation modulus of concrete

R radius of a spherical aggregate particle

R_{max} maximum radius of a spherical aggregate particle

R_{mc} radius of the smallest aggregate particle, providing "maximum contact"

α shear stiffness reduction factor $(= \frac{G_{cr}}{G})$

δ_{nn} crack width

δ_{nt} shear displacement

ε strain

ε_{cr} strain for which cracking occurs

ε_u	ultimate strain
γ	shear deformation angle
μ	coefficient of friction between matrix and aggregate particles
ρ	reinforcement ratio
ρ_o	reinforcement percentage
σ	normal stress
σ_{pu}	normal stress at which plastic deformation of the matrix occurs
σ_s	steel stress
σ_{sx}	steel stress at section x
σ_c	concrete stress
σ_{cx}	concrete stress at section x
τ	shear stress, bond stress
τ_u	ultimate shear stress
τ_{pu}	shear stress at plastic deformation of the matrix during sliding of the crack faces
Δ	shear displacement
Δ_s	slip of steel bar in concrete
ϕ	diameter of a reinforcing bar

All values used in this report are expressed in N, mm, N/mm^2, unless indicated otherwise.

11 APPENDICES

Appendix I

Determination of the contact area for an intersection circle with radius R as a function of the crack width w and the shear displacement Δ.

A contact area can only exist if $R < w$. If $R > w$, three possibilities are distinguished:

1. $\Delta < \Delta_o$; Phase "No contact"; $a_x = 0$; $a_y = 0$

2. $\Delta_o < \Delta < \Delta_b$; Phase "Growing contact";

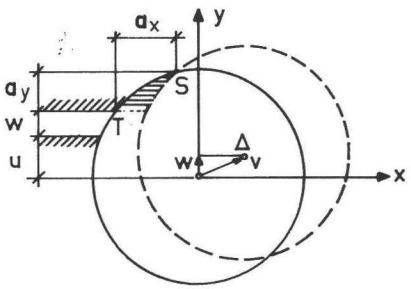

Fig. I.1 Contact components a_x and a_y for $w < R$ and $\Delta_o < \Delta < \Delta_b$

The co-ordinates of S and T can be calculated. To simplify this calculation the xy-axes are rotated through an angle α, so that in the new situation the displacement is not characterized by (Δ, w) but by $(v, 0)$ with $v = \sqrt{\Delta^2 + w^2}$ (Fig. I.2).

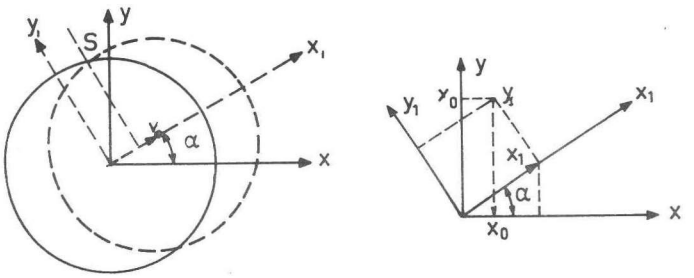

Fig. I.2

The co-ordinates of S can be calculated using Fig. I.2. S must fulfill the conditions

$$x_1^2 + y_1^2 = R^2$$

$$x_1 = \tfrac{1}{2} v$$

which results in

$$y_1 = \sqrt{R^2 - \tfrac{1}{4} v^2}$$

so that:

$$(x_1, y_1) = (\tfrac{1}{2} v, \sqrt{R^2 - \tfrac{1}{4} v^2})$$

The relations between the new and the old co-ordinates are expressed by:

$$x_o = x_1 \cos \alpha - y_1 \sin \alpha$$
$$y_o = x_1 \sin \alpha + y_1 \cos \alpha$$

Hence the co-ordinates of S in the main xy-system are:

$$x_s = \tfrac{1}{2} v \cos \alpha - \sqrt{R^2 - \tfrac{1}{4} v^2} \sin \alpha \qquad \text{(I.1)}$$
$$y_s = \tfrac{1}{2} v \sin \alpha + \sqrt{R^2 - \tfrac{1}{4} v^2} \cos \alpha$$

The co-ordinates of point T can be immediately established (Fig. I.1).

$$y_T = u + w \tag{I.2}$$

$$x_T = -\sqrt{R^2 - (u + w)^2}$$

By subtracting T from S it is found that:

$$a_y = y_s - y_T = \tfrac{1}{2} v \sin\alpha + \sqrt{R^2 - \tfrac{1}{4} v^2}\cos\alpha - u - w \tag{I.3}$$

$$a_x = x_s - x_T = \tfrac{1}{2} v \cos\alpha - \sqrt{R^2 - \tfrac{1}{4} v^2}\sin\alpha + \sqrt{R^2 - (u+w)^2}$$

Furthermore v and α are related to w and Δ by:

$$v \sin\alpha = w$$

$$v \cos\alpha = \Delta \tag{I.4}$$

$$v = \sqrt{w^2 + \Delta^2}$$

So $$\sin\alpha = \frac{w}{\sqrt{w^2 + \Delta^2}} \text{ and } \quad \cos\alpha = \frac{\Delta}{\sqrt{w^2 + \Delta^2}} \tag{I.5}$$

Substitution of (I.4) and (I.5) in (I.3) results in:

$$a_y = \sqrt{R^2 - \tfrac{1}{4}(w^2 + \Delta^2)}.\frac{\Delta}{\sqrt{w^2 + \Delta^2}} - \tfrac{1}{2} w - u \tag{I.6}$$

$$a_x = \tfrac{1}{2}\Delta - \sqrt{R^2 - \tfrac{1}{4}(w^2 + \Delta^2)}\,\frac{w}{\sqrt{w^2 + \Delta^2}} + \sqrt{R^2 - (u+w)^2}$$

3. $\Delta_b < \Delta$; Phase "Maximum contact;

It is easily deduced (Fig. I.1) that:

$$a_y = R - (u + w) \tag{I.7}$$

$$a_x = \sqrt{R^2 - (u + w)^2}$$

Appendix II

Construction of the ascending branch of the τ-Δ relationship represented in Fig. 5.16.

The relations between w, Δ, τ and σ, according to Fig. 5.3 are represented in Fig. II.1 for the crack widths w = 0.5, 0.6 and 0.7 mm.

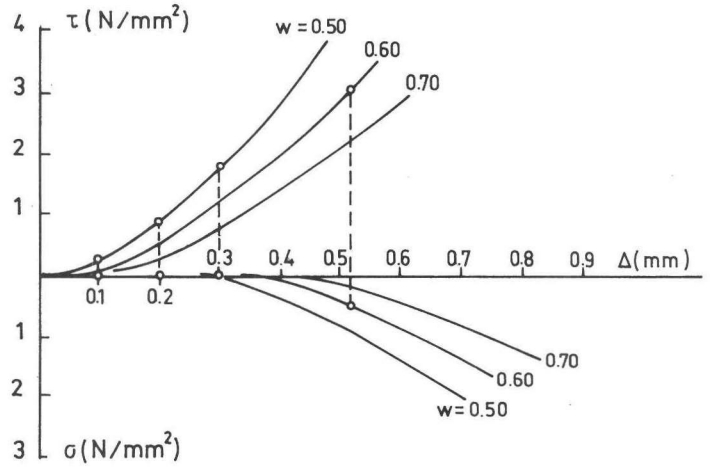

Fig. II.1 τ, σ, Δ, w relations for f'_{cc} = 33.4 N/mm^2 and D_{max} = 32 mm

The initial crack width is w_o = 0.50 mm. It is seen that for w = 0.50 mm and Δ = 0.1, 0.2 and 0.3 mm no increase of crack width can be expected, since no normal stress σ is developed. Furthermore it is known that an increase of crack width of Δw = 0.1 mm results in an increase of the normal stress with $\Delta\sigma$ = 0.5 N/mm^2. So the following points form part of the ascending branch.

w (mm)	Δ (mm)	σ (N/mm²)	τ (N/mm²)
0.50	0.1	0	0.25
0.50	0.2	0	0.85
0.50	0.3	0	1.75
0.60	0.52	0.5	3.10

Calculation of point C in Fig. 5.16

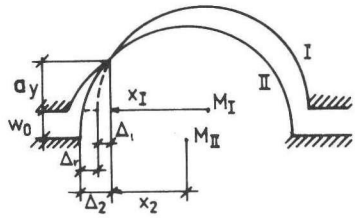

Fig. II.2 Calculation of the residual shear displacement Δ_r after unloading in the first cycle

At peak stress level w_o = 0.6 mm and Δ = 0.52mm. Substituting these values in combination with R = 16 mm in equation (I.6), it is found that a_y = 9.95 mm.
In Fig. II.2 it is seen that

$$\Delta_r = \Delta_2 - \Delta_1$$

Circle I : $x_1^2 + y_1^2 = R^2$, $y_1 = a_y$ $\Rightarrow$ $x_1 = 12.53$ mm $\quad \Delta_1 = R - x_1 = 3.47$ mm

Circle II: $x_2^2 + y_2^2 = R^2$, $y_2 = w_o + a_y$ $\Rightarrow$ $x_2 = 12.12$ mm $\quad \Delta_2 = R - x_2 = 3.88$ mm

So: $\Delta_r = \Delta_2 - \Delta_1 = 3.88 - 3.47 = 0.41$ mm.

Appendix III

Crack stiffness coefficients B_{nn}, B_{nt}, B_{tn}, B_{tt}

The crack stiffness coefficients are described by (see also equation 6.3):

$$B_{nn} = \frac{\partial f_n}{\partial \delta_n} \; , \; B_{nt} = \frac{\partial f_n}{\partial \delta_t} \; , \; B_{tn} = \frac{\partial f_t}{\partial \delta_n} \; , \; B_{tt} = \frac{\partial f_t}{\partial \delta_t}$$

The functions f_n and f_t are described by (see also equation (5.10) and equation (5.11)):

$$f_t = \frac{-f'_{cc}}{30} + \{1.80\ \delta_n^{-0.80} + (0.234\ \delta_n^{-0.707} - 0.20) f'_{cc}\}\delta_t \geq 0$$

$$f_n = \frac{-f'_{cc}}{20} + \{1.35\ \delta_n^{-0.63} + (0.191\ \delta_n^{-0.552} - 0.15) f'_{cc}\}\delta_t \geq 0$$

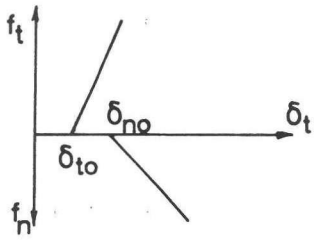

Fig. III.1

Differentiation results in:

$0 \leq \delta_t \leq \delta_{to}$ $\quad B_{nn} = B_{nt} = B_{tn} = B_{tt} = 0$ (or f.i. 10^{-20})

$\delta_{to} \leq \delta_t \leq \delta_{no}$ $\quad B_{nn} = B_{nt} = 0$

$$B_{tn} = \{-1.44\ \delta_n^{-1.80} - 0.165\ f'_{cc}\ \delta_n^{-1.707}\}\ \delta_t$$

$$B_{tt} = 1.8\ \delta_n^{-0.80} + (0.234\ \delta_n^{-0.707} - 0.20) f'_{cc}$$

$\delta_t > \delta_o$

$$B_{nn} = (-0.85\ \delta_n^{-1.63} - 0.105\ f'_{cc}\ \delta_n^{-1.552})\delta_t$$

$$B_{nt} = 1.35\ \delta_n^{-0.63} + (0.191\ \delta_n^{-0.552} - 0.15)f'_{cc}$$

$$B_{tn} = (-1.44\ \delta_n^{-1.80} - 0.165\ f'_{cc}\ \delta_n^{-1.707})\delta_t$$

$$B_{tt} = 1.8\ \delta_n^{-0.80} + (0.234\ \delta_n^{-0.707} - 0.20)f'_{cc}$$

where

$$\delta_{to} = \frac{f'_{cc}}{30\{1.8\ \delta_n^{-0.80} + (0.234\ \delta_n^{-0.707} - 0.20)f'_{cc}\}}$$

$$\delta_{no} = \frac{f'_{cc}}{20\{1.35\ \delta_n^{-0.63} + (0.191\ \delta_n^{-0.552} - 0.15)f'_{cc}\}}$$

where f'_{cc} is the cube crushing strength (cubes 150^3 mm).

The angle ψ between the direction normal to the crack and the axes of the hinged struts (Fig. 6.2), limiting the crack opening direction, can at present only be based on a limited number of test results. Using equation (5.20), which is a provisional formulation, ψ is expresses as:

$$\psi = \arctan\{\frac{1}{\delta_n^{0.18}(1.65 + 2.10\ \delta_n) - 1.5\ \delta_t}\}.$$

Stellingen

1. Het in rekening brengen van de schuifweerstand van scheuren in de formulering van de spannings-vervormingsrelatie van gescheurd gewapend beton door alleen de schuifstijfheid ten opzichte van de ongescheurde fase te reduceren, zoals tot op heden algemeen gebruikelijk, is onjuist: door de structuur van de scheurvlakken treedt dilatatie op, waardoor ook de krachten en de verplaatsingen loodrecht op de scheurrichtingen in beschouwing moeten worden genomen.

2. De veronderstelling van Mattock dat het karakter van aggregate interlock wordt bepaald door het over elkaar schuiven van de fijne toeslagkorrels is onjuist. In de eerste plaats doen vanaf een bepaalde korrelgrootte, afhankelijk van de positie der scheurvlakken, alle fracties aan de krachtsoverdracht mee. In de tweede plaats treedt naast glijding ook deformatie op.

3. Het gedrag van een gewapende scheur onder een schuifbelasting kan niet zonder meer worden verklaard uit de componenten aggregate interlock, deuvelwerking en axiale veerstijfheid van de wapening zoals deze uit afzonderlijke proeven naar voren komen: in samenwerkingsverband kunnen de componenten elkaars krachtsoverdrachtskarakteristieken beïnvloeden.

4. Het feit dat het afschuifdraagvermogen van liggers zonder schuifwapening niet evenredig is met de liggerhoogte kan niet, zoals algemeen wordt aangenomen, worden verklaard uit de schaalgevoeligheid van aggregate interlock.

5. Het gebruik van gemiddelde schuifspanningen ter bepaling van het afschuifdraagvermogen van constructiedelen, zoals in voorschriften gebruikelijk, geeft een onjuist beeld van de werkelijke krachtsoverdracht en kan daarom in de toekomst beter worden vermeden.

6. Om een zinvolle discussie over scheurwijdten in betonconstructies mogelijk te maken, is het noodzakelijk dat voor scheurwijdtemetingen een standaardprocedure wordt afgesproken.

7. In de door de VB '74 voorgeschreven waarden voor de toelaatbare betontreksterkte is een reductiefactor verwerkt, waarmee tijdsafhankelijke effecten in rekening worden gebracht. Gezien het ontbreken van een goede grondslag voor deze factor, alsmede de invloed die deze heeft op het wapenen van veel soorten constructies, is een grondig onderzoek naar het langeduur-gedrag van beton onder trek gewenst.

8. Om de duidelijkheid van voorschriften te vergroten, zouden alle hieraan ten grondslag liggende argumentaties eenvoudig achterhaalbaar moeten zijn.

9. Naarmate de voor het doorrekenen van constructies beschikbaar komende computorprogramma's gecompliceerder worden, groeit het belang van constructief inzicht.

10. Het verminderde aantal verplichte buitenlandse talen op de middelbare scholen zal in de toekomst zowel het verrichten van wetenschappelijk werk bemoeilijken als de plaats van de Nederlander in het internationale overleg ondermijnen.

11. Bij de ontwikkeling van micro-electronische apparatuur ter vergroting van de mogelijkheden van informatieoverdracht dient niet alleen aandacht te worden besteed aan vergroting van het informatie-aanbod, maar ook aan de mogelijkheid van terugmelding.

12. Wanneer een voetbalploeg spreekt over "ons doel", dan wordt hiermee het te verdedigen object bedoeld. Het feit dat dit volledig in strijd is met de betekenis van het begrip "doel" duidt erop dat de voetbalsport een verdedigend karakter heeft.

13. De rassenintegratie zou erbij gebaat zijn als Zwarte Piet niet meer als boeman zou worden afgeschilderd.

Stellingen behorende bij het proefschrift
van J.C. Walraven
Delft, 8 oktober 1980